Thèse de doctorat

Université de Limoges

Université de Limoges

École Doctorale Sciences et Ingénierie pour l'Information, Mathématiques (ED 521)

Pôle Electronique, Axe Systèmes et Réseaux intelligents

Thèse pour obtenir le grade de

Docteur de l'Université de Limoges

Discipline : Electronique des Hautes Fréquences, Photonique et Systèmes

Présentée et soutenue par

Zakaria TAYQ

Le 12 décembre 2017

Intégration et supervision des liens Fronthaul dans les réseaux 5G

Thèse dirigée par Christelle Aupetit-Berthelemot, Luiz Anet Neto et Philippe Chanclou

JURY :

Rapporteurs
Mme Maryline Helard, Professeur, SYSCOM, INSA Rennes (Fr)
M. Didier Erasme, Professeur, LTCI, Telecom ParisTech (Fr)

Examinateurs
M. Xavier Lagrange, Professeur, IRISA, Telecom Bretagne (Fr)
M. Nathan Gomes, Professeur, OCG, University of Kent (UK)
M. Philippe Sehier, Ingénieur R&D, Nokia (Fr)
Mme. Christelle Aupetit-Berthelemot, Professeur, XLIM, Université de Limoges (Fr)
M. Luiz Anet Neto, Ingénieur R&D, Orange Labs (Fr)
M. Philippe Chanclou, Ingénieur R&D, Orange Labs (Fr)

A mes parents

Acknowledgements

The work presented in this manuscript was carried out within the framework of an industrial research training agreement (CIFRE) between Orange Labs (Lannion) and the university of Limoges(Xlim). First of all, I would like to thank these laboratories and in particular Mr. Philippe Chanclou and Mrs Christelle Aupetit Berthelemot for giving me the opportunity to work with them and to have warmly welcomed me in their respective research teams.

I wish to express my gratitude to my supervisors Mr Luiz Anet Neto and Mr Philippe Chanclou for the interest they showed to my work, for their wise advice and for the rigor that they have instilled in me during the last three years. I discovered thanks to them the world of Radio Access Networks and learned a lot from their large expertise. My gratitude goes to Mrs Christelle Aupetit Berthelemot as well for her academical supervision and her multiple reviews. Her pertinent remarks and comments have helped improving the quality of this work.

My thanks to Mrs Maryline Helard and Mr Didier Erasme for their interest in my PhD work by agreeing to be the reporters of this thesis. I also thank Messrs. Xavier Lagrange, Nathan Gomes and Philippe Sehier for doing me the honor of being a part of my jury.

My thanks go naturally to all members of the RAFT team in Orange Labs, particularly Fabienne Saliou, Bertrand Le Guyader, Hugues Le Bras, Kamil Grzybowsky, Naveena Genay, Yann Denis, Zineb Bekfqih and Fabrice Bourgart with whom I enjoyed spending a terrific three years in a very friendly atmosphere. Our multiple interactions allowed me to evolve not only professionally but also personally. Thanks also to the RAFT's PhD candidates, apprentices and interns, namely Sylvain, Thierno, Gael, Justine, Karim, Minqi and Antoine.

I would also like to thank the other PhD students and Orange Labs staff with whom we have sympathized, multiplied activities and helped each other to the point of becoming good friends. I am thinking in particular of Najm, Raouf, Ines, Ghassen, Elias and many others.

Finally, it is with great gratitude that I thank my parents wholeheartedly for all their support and encouragement during my whole studies. I can only dedicate this modest work to them.

Table of contents

General introduction

Radio mobile communications have known a significant evolution over the years with the emergence of a new radio mobile generation every decade. It started in the 80s with 1G which was based on analog voice communications. The 90s knew a wide development of digital voice communications and short message services with 2G. A decade afterwards, the target was to provide data to costumers with the mobile broadband known as 3G. Then, the need of data and multi-media services kept evolving which pushed the launch of 4G in the 2010's. Currently, there are ongoing research, standardization and development activities on the next mobile generation (5G). It is foreseen that this generation will handle higher volumes of data, much more connected devices with diverse service requirements which prompted the need for evolved systems with extended capabilities. The radio access network (RAN) centralization and virtualization, also called Cloud RAN (C-RAN), was identified as a key enabler to the flexibility, scalability and service-oriented management expected in these future systems.

C-RAN proposes the centralization of the base stations intelligence at first. Then the virtualization of theses centralized radio functions allows running them in general purpose processors (GPPs). This will enable having a model resembling to the data centers one which knew a tremendous success over the last years mainly thanks to its flexibility and ease of management. C-RAN promotes a new network segment called "fronthaul" located between the central office where the intelligence (base band unites) is centralized and the antenna sites. The most popular interface carried on these fronthaul links is the CPRI (Common Public Radio Interface) which results from a high-resolution digitization of the radio signals giving high bit-rates time-sensitive signals. Thus, Wavelength Division Multiplexing (WDM) appeared to be the most adequate solution for their transport. Nevertheless, the deployment of such solutions in access networks is having some operational difficulties: namely the burden of wavelengths management due to the use of colored optical transceiver as well as the lack of an optical infrastructure monitoring solution, mandatory for field deployment. Moreover, the current WDM optical transceivers are limited to 25 Gbit/s which can be problematic for 5G interfaces transport. In fact, the CPRI bit-rate scales with the used radio characteristics, namely the signal's bandwidth and the antenna system configuration. In 5G where technologies such as Massive MIMO and mmWaves are expected, the corresponding CPRI signal will have very high bit-rates largely exceeding the reasonable optical transceivers cost for such applications. The community working on the subject has identified some research tracks aiming to cope with this CPRI bit-rate burden. The three main tracks investigated in this thesis are the following: the transport of mobile signals in their native modulation format or other non-binary modulation scheme through analog radio over fiber (A-RoF), the compression of the fronthaul signal thanks to intelligent quantization algorithms, and the transposition of some radio protocol layers from the centralized equipment and the antenna site equipment with different functional splits.

Being very interested by C-RAN, Orange has been conducting WDM based fronthaul field trials without any massive deployment. The main reasons behind their reluctance are the lack of the WDM solutions maturity for access networks (as stated in the previous paragraph, absence of monitoring and wavelengths tunnability) and the questionable sustainability of these network infrastructures with 5G still under investigation and standardization. The objective of this thesis is to contribute in giving Orange insight on this matter through

providing experimental results. These results are derived from European collaborative research projects, namely the COMBO project on “COnvergence of fixed and Mobile BrOadband access/aggregation networks”, the iCirrus project on “intelligent Converged network consolidating Radio and optical access aRound USer equipment” and the 5G-crosshaul project on the integration of a flexible transport network unified for backhaul and fronthaul. Results are derived also from close partnerships with equipment vendors through providing system specifications and evaluating industrial prototypes. “Home-made” experimental setups and simulations are also performed when needed. The ultimate target of this work is to come out with a clear vision on the needed evolutions in the systems and architectures of the transport network enabling to accommodate the future 5G radio interfaces.

After a state of the art on the radio mobile technologies and their corresponding transport networks with an introduction to the Cloud RAN architecture, the fronthaul link and its requirements, in chapter 1, this manuscript deals with four problematics reported in four different chapters, as follows:

- **CPRI-based fronthaul integration:**

As stated before, WDM was identified as the most adequate candidate for the transport of the CPRI interface. Nevertheless, its deployment in access networks still has some difficulties. Notably, the lack of the optical infrastructure monitoring solutions and also the wavelengths management difficulty introduced by the use of colored optical transceivers. Moreover, the lack of easily and quickly available optical fiber is also a problem that could be potentially encountered in fronthaul deployment. The wireless transport of the CPRI signals can therefore resolve this issue.

Chapter II reports a study on the introduction of a control channel in the CPRI signal in order to achieve wavelength tunability and fronthaul infrastructure monitoring using two methods: RF pilot tone and baseband over-modulation. Time multiplexing-based fronthaul aiming to increase the number of transported CPRI links per WDM wavelength is also demonstrated in this chapter. Furthermore, experimental investigation on wireless fronthaul with and without spectral efficiency enhancement is carried out in order to define the impact of introducing a wireless section in the fronthaul link on the end-to-end performances.

- **Mixed Analog and Digital RoF:**

While WDM can handle the CPRI bit-rate burden for LTE, it will surely not be enough to ensure the transport of the 5G interfaces if the current Digital-RoF (D-RoF) approach is maintained. The use of analog RoF to transport these future interfaces has been proposed in order to enhance their spectral efficiency.

In Chapter III, an architecture mixing A-RoF and D-RoF is proposed. It aims to leverage the existing Distributed Antenna System (DAS) infrastructures by pushing back the need of a swap to a WDM solution while guaranteeing, at the same time, full compliance with currently deployed RAN equipment. A real-time demonstration of the proposed architecture is carried out with a single off-the-shelf optical transceiver. Simulations are also performed in order to complete the obtained experimental results with respect to nonlinear conversions in the laser. The target is to define a realistic gain of spectral efficiency that can be obtained in A-RoF compared to D-RoF, while using low cost components suited for access networks equipment.

- **CPRI compression:**

Among the solutions identified to enhance the spectral efficiency of the D-RoF interface, there is the CPRI compression which was the focus in Chapter IV.

Several compression technics have been developed over the years especially for multimedia files size reduction. For this thesis, it has been chosen to concentrate on lossy compression based on quantization. In fact, the CPRI interface is the result of the radio signal digitization with a 15 bits resolution uniform quantization which generates very high bit-rates.

Through real time and offline experimentations, a study is conducted on uniform and non-uniform quantization based on fixed-length coding. The purpose is the optimization of the digitization process to obtain a minimum CPRI bit-rate while maintaining performances compliant to the standard. An experimental investigation of an enhanced compression method based on spectral redundancy removal and “frequency domain quantization” is carried out as well.

- **New functional splits:**

Finally, establishing a new radio functions partitioning between the DU and the RU was identified as a promising solution for 5G. It would imply the emergence of an evolved fronthaul link (known here as “efronthaul”) with relaxed bit-rate and latency requirements. Also with the DU virtualization being targeted in 5G, this new functional split should enable it achievement since the high layer radio functions don’t have strict real-time constraints, thus they don’t need to be implemented in dedicated hardware.

In this context, several options of functional splits have been proposed by standardization bodies. Only two new interfaces have been defined for a high layer split and a low layer split. In Chapter V, a theoretical and experimental study is carried out on a high layer functional split based on a virtualized RAN platform; also its impact on the current access networks (Ethernet backhaul/PON) is evaluated. An analysis of low layer functional split is also reported in this chapter and some adequate solutions for its transport are proposed.

Chapter I. State of the art

I.1. Introduction

Radio mobile technologies have known a tremendous evolution over the past few decades. This implied a need for a continuous progress in their correspondent transport network. This chapter presents a state of the art on the mobile and transport technologies. In section I.2, an overview is given on the different radio mobile generations. The associated distribution network is described in I.3. An assessment of the backhaul technologies as well as the fronthaul requirements and solutions is reported.

I.2. Radio mobile technologies: an overview

The history of radio mobile technologies is relatively recent since the commercial launch of the first mobile network was in 1979 in Japan. Since then, their evolution has not ceased with the emergence of a new radio mobile generation nearly every decade. The 80s knew the appearance of mobile communications with the first generation (1G), which offered analog voice communication. This generation didn't have a considerable success though. In the 90s, the second generation (2G) offered digital voice communication and text messaging. Afterwards, the trend was to provide data to the mobile costumers so 3G emerged in the 2000s offering mobile broadband. Then, the need of data and multi-media services kept evolving which pushed the launch of 4G in the 2010s. Currently, there is an ongoing research and development work on the next mobile generation (5G) which is expected to be launched by 2020. It is foreseen to offer more services and to convey much more traffic. Figure I-1 shows the overall mobile data traffic evolution expected by Cisco. It forecasts a growth to 49 Exabytes per month by 2021, a sevenfold increase over 2016 [1].

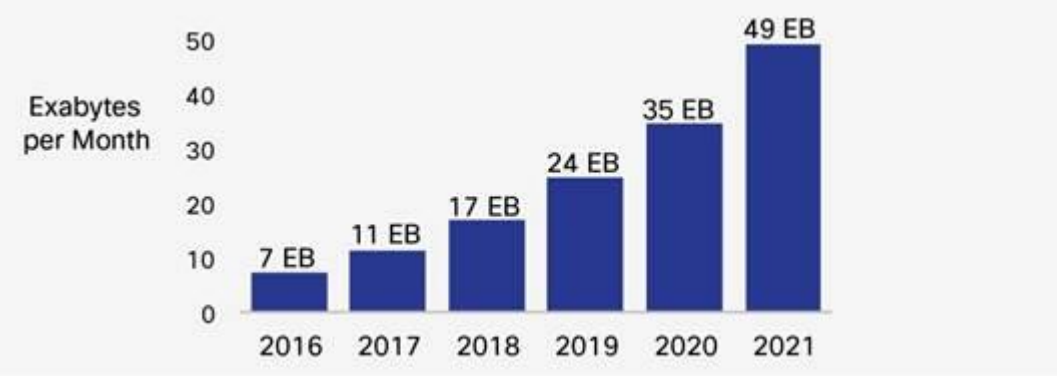

Figure I-1: Cisco mobile data traffic forecast for the period 2016-2021 [1]

I.2.1. Mobile cell definitions

Since the first generation, mobile networks were deployed in the form of cells enabling a seamless communication all over the network. Conceptually, if a cell allows a certain number of simultaneous calls to be made, the total number of calls that can be supported by the network can be controlled by sizing the cells to larger or smaller coverage areas. Consequently, there is a distinction between 3 kinds of cells:

- Macro cells which represent large cells, with a radius ranging from a few hundred meters to several kilometers. They are controlled by macro base stations whose

power is typically around 40 W (46 dBm). Their antennas are placed on high points, such as roofs of buildings or pylons. Usually directional antennas are used for this kind of cells to enable the deployment of several sectors (typically 3 in France) in the same antenna site. [2]

- Micro cells are cells from a few tens to a hundred meters radius, intended to complete the coverage of macro cells in dense or poorly covered areas. The associated base stations are called micro base stations and their power is of the order of 10 W (40 dBm). Their antennas are typically placed under the level of roofs, usually in front of buildings. They are generally omnidirectional antennas allowing the deployment of one sector antenna sites. [2]
- Small cells: defined by the Small Cell Forum [3] as "an umbrella term for operator controlled, low-powered radio access nodes, including those that operate in licensed spectrum, and unlicensed carrier-grade Wi-Fi and mobile. Small cells typically have a range from 10 meters to several hundred meters. Types of small cells include femtocells, picocells, and microcells". Concerning picocells, small cell recommendations ITU-R M.1224 and M.1035 [4] define them as "very small cells with a typical cell radius of less than 50 m. These cells are predominately situated indoor and are intended to give a very high traffic capacity ".

These three radio configurations allow us also to understand that there are three important parameters to consider in provisioning bandwidth/spectrum for the cell sites and also in designing the corresponding transport network:

- The number of Radio Access Technologies (RATs): this corresponds to the type of radio (especially mobile) communication standards and their generations, such as 2G, 3G, 4G, and 5G.
- The number of radio frequency bands allocated within each radio technology. Indeed, it is frequent to transmit some RATs over several radio frequency carriers.
- The number of radio sectors: This is applicable only for cells with sectorial antennas.

I.2.2. GSM

1G was based on analogue modulations using Frequency Division Multiple Access (FDMA) associating each frequency to a user which permitted a very limited number of simultaneous connections. Also, because of the incompatibility between the various proposed systems, 1G was not a success [2].

After the failed attempt to launch an analogue based mobile communication system (1G), the second generation of mobile networks (2G) emerged in the 90s. Several systems were proposed in 2G as well but The Global System for Mobile communications (GSM) was the one deployed in Europe. It offered a voice service with mobility, a Short Message Service (SMS) and low bit-rate data transfer. GSM used FDMA between the cells combined with Time Division Multiple Access (TDMA inside the cell). The transmission rate of GSM is 22.8 Kbit/s. A simplified representation of the GSM architecture is shown in Figure I-2.

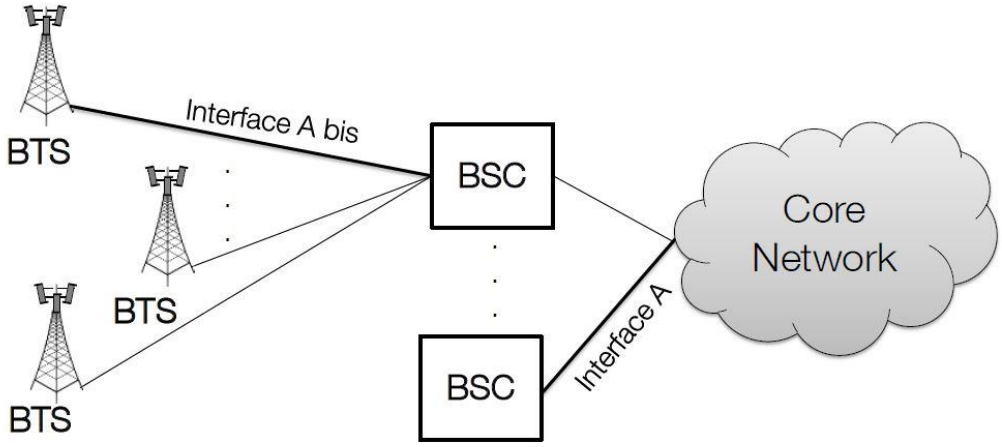

Figure I-2 : GSM architecture [5]

The Base Transceiver Stations (BTS) containing the radio Transmitter and Receiver Modules (TRX) are where the signal processing operations are performed. They are connected via the interface “A bis” to the Base Station Controller (BSC). The latter handles the handovers, the transmitter RF power of the BTSs among some other parameters. It also aggregates/desegregates the traffic before communicating with the Mobile service Switching Center (MSC) located in the core network via the interface A. These interfaces handling the distribution of the radio signals will be discussed in section I.3.

GSM made a huge success and has been deployed in many countries. Nevertheless, the system had many limitations. Mainly, capacity limitations implying calls rejection during peak hours were reported [2]. Also, there were limitations in the access to the data services from the core network that was based on circuit switching introducing much latency. A first enhancement was to connect the GSM access network to the General Packet Radio Service (GPRS) core. Moreover, the Enhanced Data rates for GSM Evolution (EDGE) allowed achieving 240 Kbit/s per cell thanks to an improvement in the radio channel access method [2]. Nonetheless, at the end of the 90s, the throughput offered by 2G started to be unsatisfactory giving the needs in data transmission. This limitation was the reason behind the definition of 3G [6].

I.2.3. UMTS

3G is the result of the telecom industrials will to have a worldwide standard. The motivation is to enable roaming between the countries and decrease the cost of phones and network equipment thanks to the economies of scale. In this context, a group of telecom firms, mainly the ones from the GSM world, formed a consortium called 3rd Generation Partnership Project (3GPP) which released the Universal Mobile Telecommunication System (UMTS) standard. The target of this system was to improve the capacity for the voice services but above all enhance the data services. To this end, UMTS uses the Wideband Code Division Multiple Access (W-CDMA) technology. In the latter, the signal is spread over 3.84 MHz before transmission over a 5 MHz carrier. Each call is associated to a specific code known by the base station and the mobile terminal which allows distinguishing the calls occurring in the same carrier. With this technology, UMTS offers 384 Kbit/s. Its architecture is shown in Figure I-3. The base station in this mobile generation is called Node B. Multiple base stations are controlled by the Radio Network Controller (RNC) through the interface “Iub”. The

interface “Iur” is used for the communication between the RNCs in order to handle handovers among other things. The RNCs are connected to the core network through the interface “Iu”.

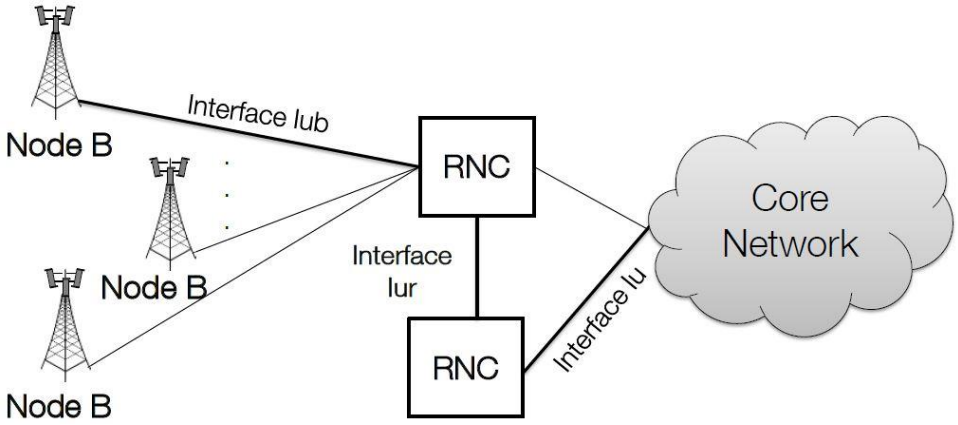

Figure I-3 : UMTS architecture [5]

UMTS knew two major evolutions targeting the improvement of throughput and reducing the latency: The High-Speed Packet Access (HSPA) and the HSPA+.

The main innovation is that HSPA was going from the circuit switching in the air interface, where the radio resources are reserved to each User Equipment (UE) during the call, to the packet switching where the resources are dynamically shared between the active users. This transformation required an upgrade of the transport network to handle packet switching. More information about this subject is brought in section I.3.2.1.

The used modulation is also selected dynamically depending on the quality of the radio channel. The 16QAM modulation is introduced in the downstream in addition to the QPSK originally defined in UMTS. Also, QPSK in introduced in the uplink in addition to BPSK used in the first release. This permitted offering 14.4 Mbit/s radio throughput in the downstream and 5.8 Mbit/s in the upstream.

Further improvements were brought by HSPA+. 64QAM modulation was introduced in the downlink and 16QAM in the uplink. Moreover, the Dual Carrier–HSDPA allowed transmitting data to a user over two 5 MHz carriers simultaneously, thus doubling the throughput. The Multiple Input Multiple Output (MIMO) feature was also introduced to improve the downstream signal. These enhancements permitted HSPA+ to offer a throughput of 42 Mbit/s in the downlink and 11.5 Mbit/s in the upstream.

The proposed performances (throughput, capacity) allowed UMTS and its evolutions to reach a universal success. It has been deployed all over the world. Moreover, new mobile services started emerging (video, TV, mobile applications…) and also more and more terminals were proposed in the market (smartphones, 3G+ dongles…). This has led to a very fast increase of the number of mobile clients and also of the traffic in the networks which brought about the need of a new mobile network generation offering more capacity and more throughput with a reduced latency. [2] [7]

I.2.4. LTE

The fourth generation of mobile networking was proposed in a 3GPP workshop in 2004 as a long-term evolution of the UMTS, hence its name Long Term Evolution (LTE). It was proposed to offer higher capacity per cell, better throughput, reduced latency and more frequency agility. In fact, UMTS constrained the operators to use 5 MHz bandwidth radio

signals which didn't allow an optimized used of the available spectrum. LTE came with a new access method to the frequency resource, as it was the case in each new mobile generation. It actually uses Orthogonal Frequency Division Multiplexing (OFDM), which at that time just reached a level of maturity allowing its integration in UEs. This allowed a better used of the spectrum with a variety of possible bandwidths (1.4 MHz, 3 MHz, 5 MHz, 10 MHz, 15 MHz and 20 MHz) and an enhanced robustness to the radio channel interferences. [8]

As shown in Figure I-4, LTE introduced also a novelty in the network architecture. It removed the radio controller reducing therefore the end-to-end latency. The base station, called "eNodeB", is directly connected to the core network called "Evolved Packet Core" (EPC) through a logical interface called "S1". The control functions of the RNC used in UMTS were integrated in the eNodeB and the coordination between the eNodeBs is done through the "X2" interface. Both S1 and X2 interfaces constitute the mobile backhaul. [8]

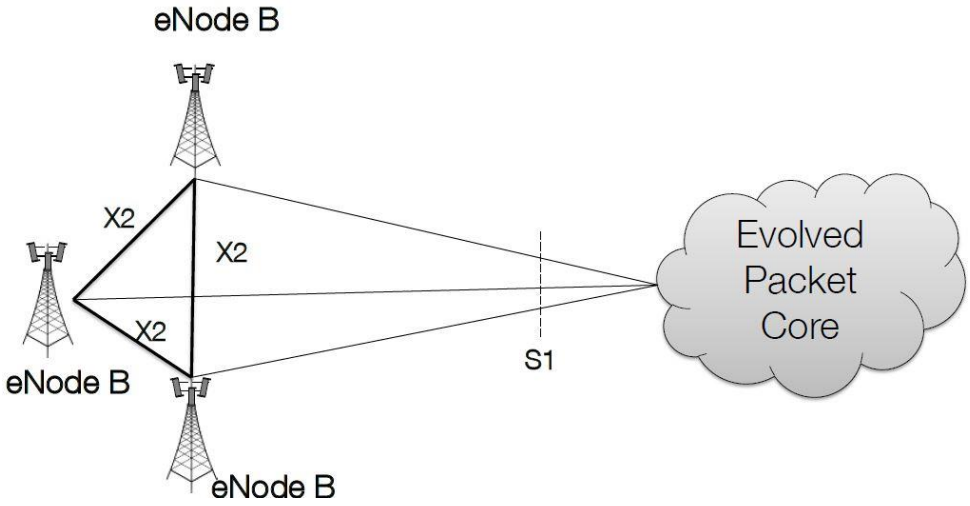

Figure I-4 : LTE architecture [5]

The first version of LTE allowed a theoretical throughput of 100 Mbit/s in the downlink and 50 Mbit/s for 20 MHz bandwidth in Single Input Single Output (SISO) configuration.[8]

After the release 8 and 9 of the 3GPP concerning the LTE standard, the release 10 of the 3GPP brought enhancements targeting a theoretical throughput of 1 Gbit/s in the downlink and 500 Mbit/s in the uplink, this radio version is called LTE advanced (LTE-A). Some radio features were proposed to this end such as link Carrier Aggregation (CA) enabling the transmission over multiple radio carriers simultaneously and Coordinated MultiPoint (CoMP) for a dynamic coordination of transmission and reception over a variety of base stations, the goal being to achieve an improved quality of radio coverage within the whole network.[2]

At first the base station was in a single physical box. Afterwards, it was separated into 2 physical boxes. The first one dedicated to the radio digital processing called Digital Unit (DU) or Base Band Unit (BBU) and the second one to the RF operation called Radio Unit (RU) or Remote Radio Head (RRH). This enabled the evolution from the distributed architecture depicted in Figure I-4 to the centralized architecture explained in the section I.3.4.1. The Chapter II of this thesis was dedicated to eliminate the barriers met in access networks to accommodate such architecture for LTE.

I.2.5. 5G

While LTE was focused on providing broadband connection to mobile costumers, the fifth generation of mobile technology (5G) was intended for much more than that. It is actually positionned to adress the demands and business contexts of 2020 and beyond. It is expected to enable a fully mobile and connected society and to empower socio-economic transformations in many ways including those for productivity, sustainability and well-being [9]. Therefore, in 5G, there is a need to provide, where needed, much greater throughput, much lower latency, ultra-high reliability, much higher connectivity density, and higher mobility range. This would allow providing much more services than voice and data.

The Next Generation Mobile Networks (NGMN), alliance driven by leading operators, published in February 2015 a white paper [9] aiming to communicate their vision on the 5G use cases and also their requirements. Figure I-5 depicts the 5G use case families and related examples proposed in this white paper which shows a large variety of services.

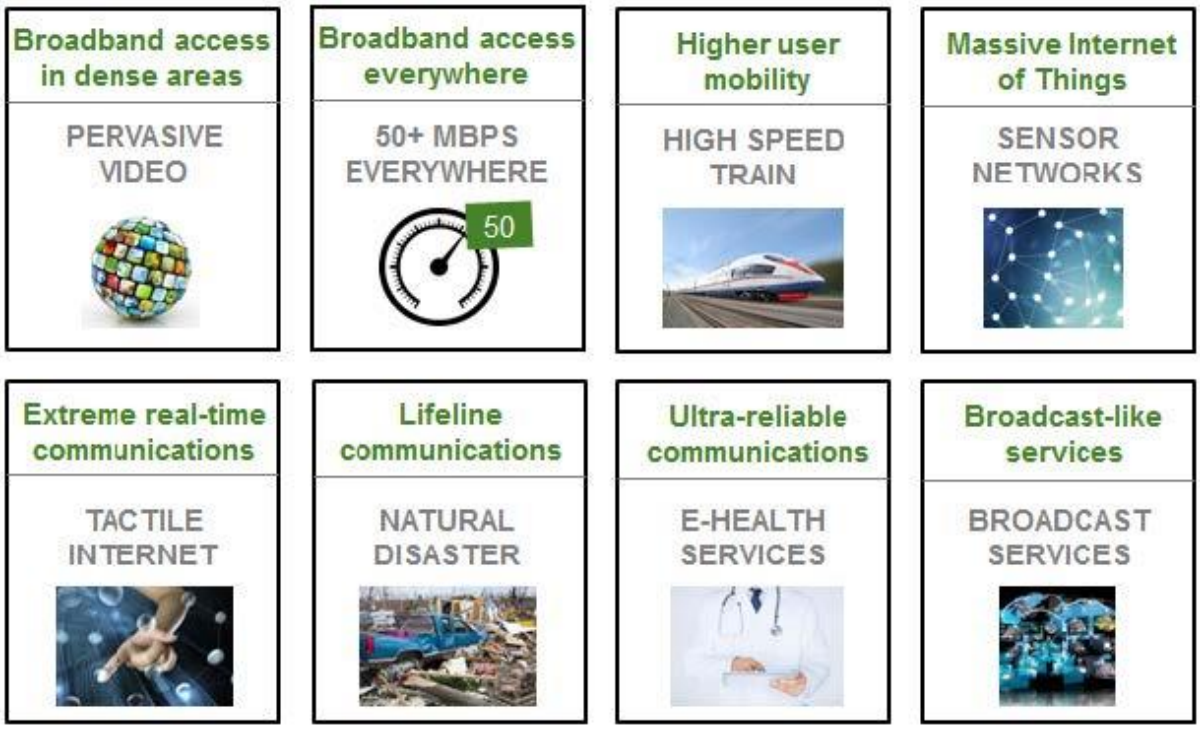

Figure I-5 : 5G use case families and related examples (source: NGMN 5G White paper [9])

Following that white paper, the International Telecommunication Union (ITU) published in September 2015 a recommendation under the reference ITU-R M.2083 [10]. In fact, it gattered the 5G use cases into 3 main pillars and defined the corresponding requirements for the International Mobile Telecommunications (IMT) for 2020 (5G) with respect to the IMT-Advanced (LTE-A). The 3 main pillars of 5G are shown in Figure I-6 and include:

- Enhanced Mobile Broadband (eMBB) which is about delivering multi-media content, services and data with improved performance and an enhanced quality of experience.
- Ultra-Reliable and Low Latency Communication (URLLC) which has use cases with stringent latency and availability requirements. This includes remote medical surgery and wireless control of industrial manufacturing.

- massive Machine Type Communications (mMTC) which affects the connection of a very large number of devices transmitting at a low bit-rate with no specific latency requirement.

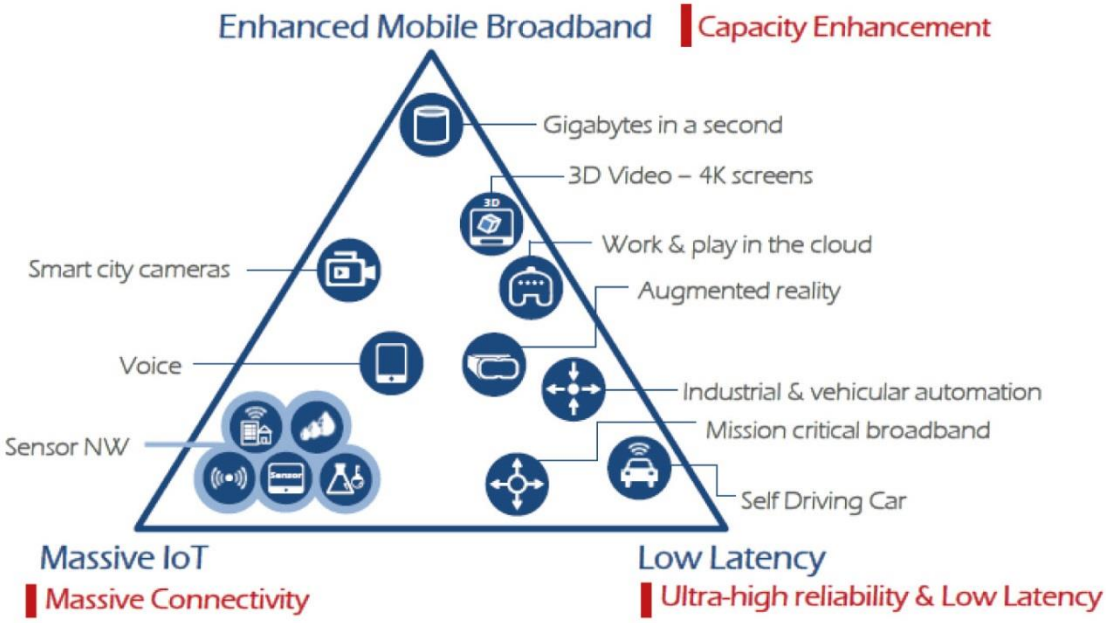

Figure I-6 : The 3 main pillars of 5G (source: ITU-R IMT 2020 requirements [10])

In order to be able to deliver these services, the ITU defined some technical requirements as targets for research and investigation. These requirements are shown in Figure I-7 where IMT-2020 stands for 5G and IMT-advanced for LTE-A.

The peak data rate expected in 5G is 10 Gbit/s but 20 Gbit/s would be supported under certain conditions. 5G would also support different user experienced data rates covering different environments. For instance, a user experienced data rate of 100 Mbit/s is expected to be offered for wide area coverage. For hotspots, up to 1 Gbit/s user experienced data rate is expected to be reached. [10]

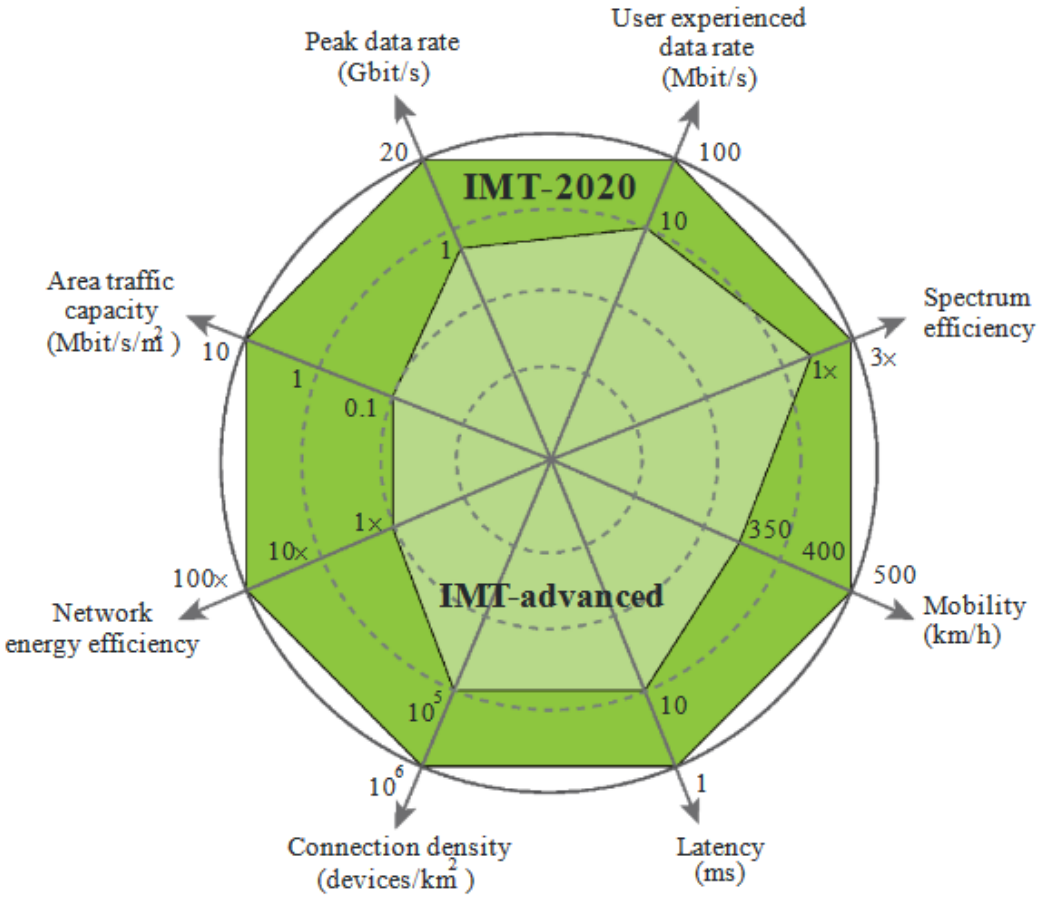

Figure I-7 : Enhancement of key capabilities from IMT-Advanced to IMT-2020 (source: ITU-R IMT 2020 requirements [10])

The spectrum efficiency is expected to be three times higher compared to LTE-A. 5G is expected to support up to 10 Mbit/s/m^2 area traffic capacity in the case of hot spots. [10]

5G shall also provide 1 ms latency which will enable supporting very low latency services. [10]

For the massive machine type communication scenario, 5G is expected to support a connection density of up to 10^6/km^2. [10]

Finally, the 5G radio access network energy consumption should not exceed the consumption of LTE networks deployed today, while delivering the enhanced capabilities. Thus, the energy efficiency should be proportionally improved by a factor at least equal to the expected traffic capacity increase from LTE to 5G. [10]

Consequently, Orange Labs defined 3 keys enablers for 5G radio [11]:

- Massive MIMO: The use of multiple antenna transmitters and receivers is very common in LTE, especially 2x2 MIMO systems which allowed almost doubling the radio throughput thanks to spatial multiplexing. In 5G, the requirement of spectrum efficiently is much higher. In fact, Shannon's capacity equation is a fundamental constraint on the spectral efficiency performance and implies logarithmic dependence of channel capacity on the signal-to-interference and noise ratio (SINR) [10]. Massive

MIMO could improve the SINR through narrow beamforming, pushing the system closer to a noise limited environment, thus enhancing the system's spectral efficiency. Therefore, it is expected that large scale antenna system (up to 128 antennas) will be implemented in 5G base stations [12].

- cm/mm Waves: In order to increase the networks capacity, besides improving the spectral efficacy, there is a need of more spectrum bandwidth. Since the available bandwidth the sub 6 GHz is limited, it was recommended to make advantage of the large available in the cm and mm Waves, notably the 28 GHz band where 500 MHz bandwidth is available [13].
- Network virtualization: In the context of an extreme densification of the network for 5G, an optimized resource allocation and management can be challenging. Using software for radio can provide the flexibility needed especially in the RAN. It was therefore recommended for the 5G [14].

Orange released also the roadmap for 5G deployment which is shown in Figure I-8. The dates are not specified on the figure since they are not public yet, but what should be retained is the fact that there will be 2 phases for the 5G deployment. The first one over the 700 MHz, where 10 MHz bandwidth has been attributed to Orange France at the end of 2015 and the 3.5 GHz band where 300 MHz bandwidth will be divided between the four mobile operators of France. Massive MIMO is expected in the band of 3.5 GHz with a maximum order of 16 antennas at a first moment. Higher MIMO orders are expected to be used in the second phase of deployment (up to 128 antennas) where the use of mmWaves is also expected. In order to achieve the targeted throughput per user in 5G phase 2, it will be probably necessary to deploy small cells.

The greater part of this thesis was dedicated to studying the impact of introducing these elements on the transport networks in general and the access networks in particular and proposing solutions which was done in Chapter III, Chapter IV and Chapter V. A state of the art on the transport networks is reported in the next section.

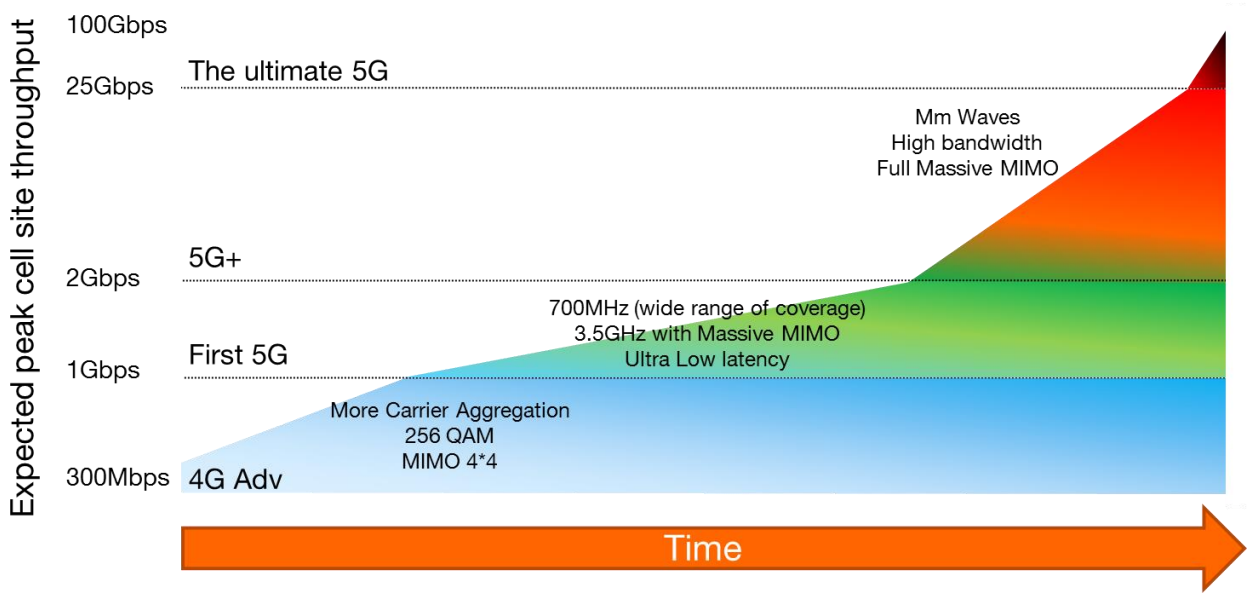

Figure I-8 : Orange roadmap for 5G deployment

I.3. Distribution of radio signals

After reporting the radio mobile technologies evolution and highlighting the radio features expected in the 5G, this section is dedicated to assessing the fixed networks used to transport the previously reported radio interfaces. Namely, the backhaul, midhaul and fronthaul interfaces are discussed in I.3.2, I.3.3 and I.3.4 respectively. But first a general presentation of the fixed network is brought in I.3.1, aiming to locate in the overall network the segments that this thesis focuses on.

I.3.1. The three layers model

Several architectural models have been proposed to describe the network, but the Cisco three hierarchical layers model [15] is usually taken as a reference. In this model, there are three layers as shown in Figure I-9:

- The core layer
- The metropolitan layer
- The access layer

The role of the **core layer** is to link the important points of the network, at the national and international level. This layer constitutes the backbone of the distribution network and presents the longest transmission distances (with the exception of submarine transcontinental cables) and the highest bit-rates. In France in 2016, these links had up to 96 channels modulated at a rate of up to 100 Gbit/s and wavelength multiplexed in a single fiber. Therefore, a bit-rate approaching 10 Tbit/s was transmitted by optical fiber [16] [17]. The signals of each channel are phase modulated in QPSK (Quadrature Phase Shift Keying) at a rate of 32 Gbaud/s, on each of the two polarization axes.

At the lower layer there is the aggregation network, also known as the "**metropolitan network**", which links various major points of the network to a regional scale. The core and metropolitan networks constitute the transport network. This is defined by the ITU-T as "capable to provide the functionalities of transport, multiplexing, switching, management, supervision, and 'survivability' of the optical channels carrying the client signals." [18]

Finally, the **access network** connects the client to the rest of the network. It is characterized by its short distances (typically 20 km) and its very high “capillarity” hence the stringent cost constraint. This segment of the network was originally based on copper to deliver broadband to fixed customers or to connect mobile antenna sites to the rest of the network. Indeed, operators are swapping more and more of their access networks to optical fiber in order enable delivering higher throughputs.

As mentioned above, this thesis is focused on this network segment (access). Within the radio access network, there are different topologies that can be categorized into backhaul, midhaul and fronthaul, which are described thereafter.

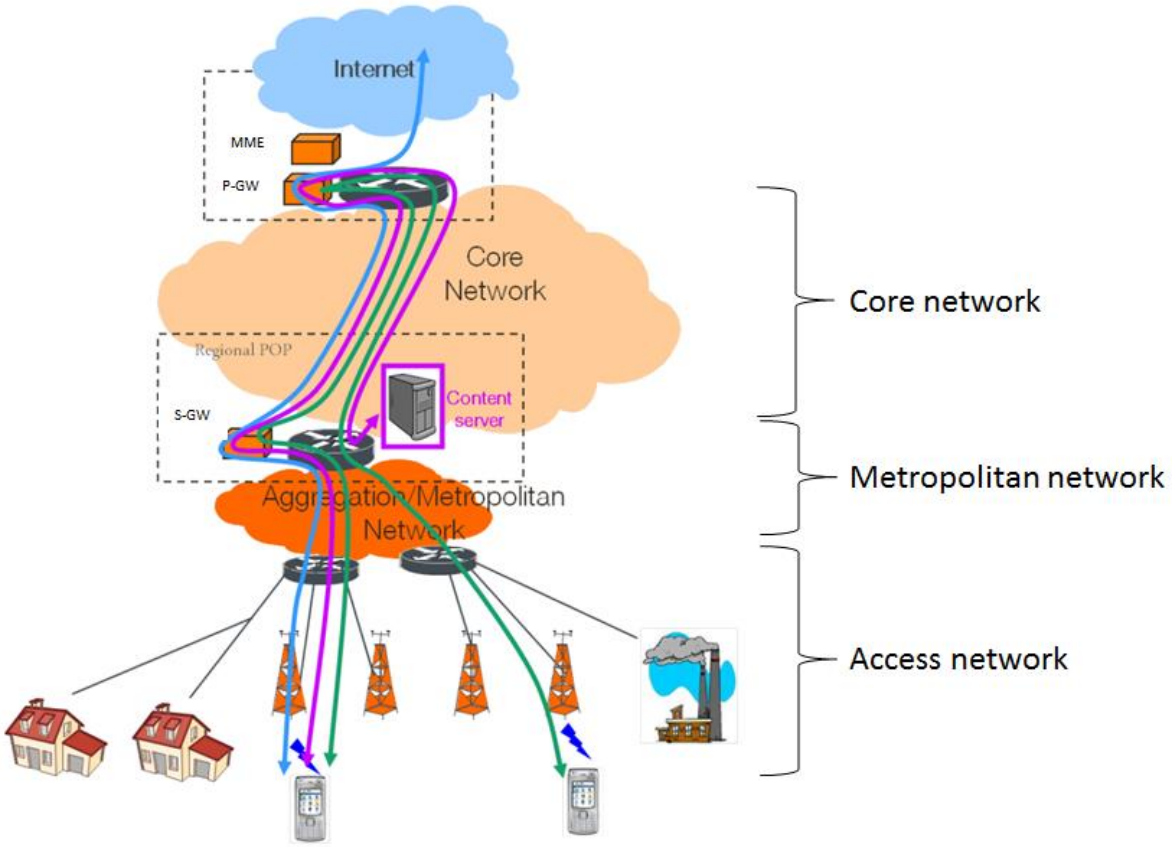

Figure I-9 : Representation of the three hierarchical model of the network

I.3.2. Backhaul

The term Mobile Backhaul [28] refers to the network links between the radio base stations and the network controller/gateway sites for all generation of mobile technologies. The 2G backhaul is based on Time Division Multiplexing technologies particularly the Synchronous Digital Hierarchy (SDH) and the Plesiochronous Digital Hierarchy (PDH) [29]. While the 3G backhaul is achieved with the ATM technology suitable for the circuit switching adopted in UMTS. The data-centric services provided by HSPA and LTE technologies are deployed on packet transport platforms using Ethernet, MPLS and IP. This is because broadband services are based on the packet technology, which provides a solution to overcome issues of cost and scaling. This was reported in the Metro Ethernet Forum (MEF) specifications [30].

The NGMN Alliance has also defined backhaul requirements and made recommendations on how to optimize the transport network [31].

The use of advanced radio features for LTE-A such as radio coordination, higher order MIMO and larger spectrum bandwidths will increase the backhaul traffic. Figure .I-10 shows the introduced backhaul traffic evolution, where “S1” and “X2” are the logical interfaces explained in the previous section. And the deployment of 5G will certainly bring further traffic per link.

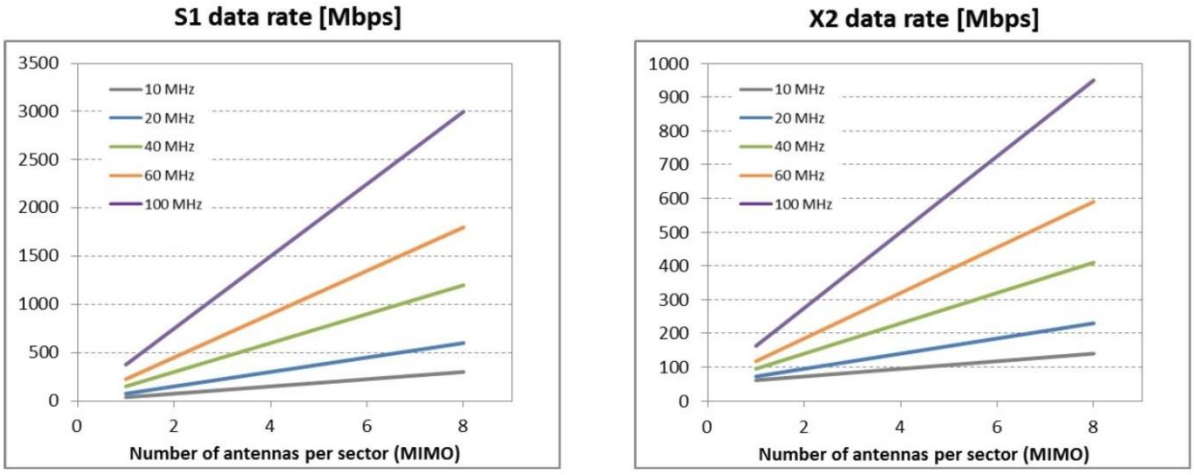

Figure .I-10 : LTE-A backhaul traffic [33]

For the dimensioning of the backhaul link capacity, the sum of LTE S1 and X2 peak sector traffic per site have to be taken into account [33]. According to NGMN backhaul dimensioning rules, backhauling with peak data rate of one sector is sufficient for a site due to statistical gains [32], this is referred to as statistical multiplexing.
In addition to deploying point-to-point backhaul links, operators leverage their fixed networks originally deployed for residential clients to deploy mobile base station, namely the xDSL networks discussed in I.3.2.1 and the FTTx networks reported in I.3.2.2.

I.3.2.1. xDSL

Digital Subscriber Line (DSL) was largely deployed for this purpose, especially the Asymmetric DSL (ADSL) and the Very-high-bit-rate DSL (VDSL). Their popularity is mainly due to the fact that they take advantage of the very widespread Public Switched Telephone Network (PSTN). Therefore, tremendous amount of investment is saved in this way for the benefit of the operators.

The ADSL performance may reduce depending on the line quality; usually, the most significant factor in line quality is the distance from the Digital Subscriber Line Access Multiplexer (DSLAM) to the customer's equipment. ADSL only supports short distances, typically less than 5 km. If more reach is required, the data rate has to be sacrificed. Table I.1 shows the specifications of the main xDSL technologies [19].

Giving the large availability of these networks, the fixed entity of Orange proposes a wholesale offer to the mobile entity as well as to the tier operators for 3G and 4G backhauling via DSL. This wholesale offer is called Core Ethernet Mobile 2 [20].

These technologies are based on the Discrete Multi-Tone (DMT) modulation. In order to offer higher bit-rates, more signal bandwidth is used in each new technology. The higher the signal's bandwidth, the more degradation is induced by the channel and the lower is the reach that can be achievable. The digital signal processing to cancel the noise remain insufficient. The last copper technology (G.fast) can only achieve few hundred meters reach which is unsatisfactory for radio access networks. Thus, the use of copper is becoming irrelevant.

Table I.1: Specifications of xDSL technologies [19]

Technology	Bit-rate (Mbit/s)	Channel	Maximal reach (km)
ADSL	8	Downlink	5.4
	0.64	Uplink	
ADSL2	12	Downlink	5.4
	0.64	Uplink	
ADSL2+	24	Downlink	5.4
	1	Uplink	
VDSL	53	Downlink	1.3
	2.3	Uplink	
VDSL2	100	Downlink	1.3
	32	Uplink	
G. fast	1000 divided between UL and DL	Downlink	0.2
		Uplink	

I.3.2.2. FTTx

Considering the need to deliver more and more content to the fixed costumers and also the extreme increase of the mobile traffic, the use of optical fiber in access networks became inescapable.

Deploying optical fiber can be very costly for the operators, especially in not dense areas and low-density areas. Thus, multiple Fiber-To-The x (FTTx) architectures were developed to enable deploying fiber to different levels of the access network. Some examples are shown Figure I-11.

The short distances in access networks doesn't require optical amplification, thus there is no need for active elements in this stratum. Giving its low cost, Passive Optical Network (PON) was a good candidate to replace xDSL, partly since it forms a mass market since each customer will potentially have a very high speed optical fiber connection at home.

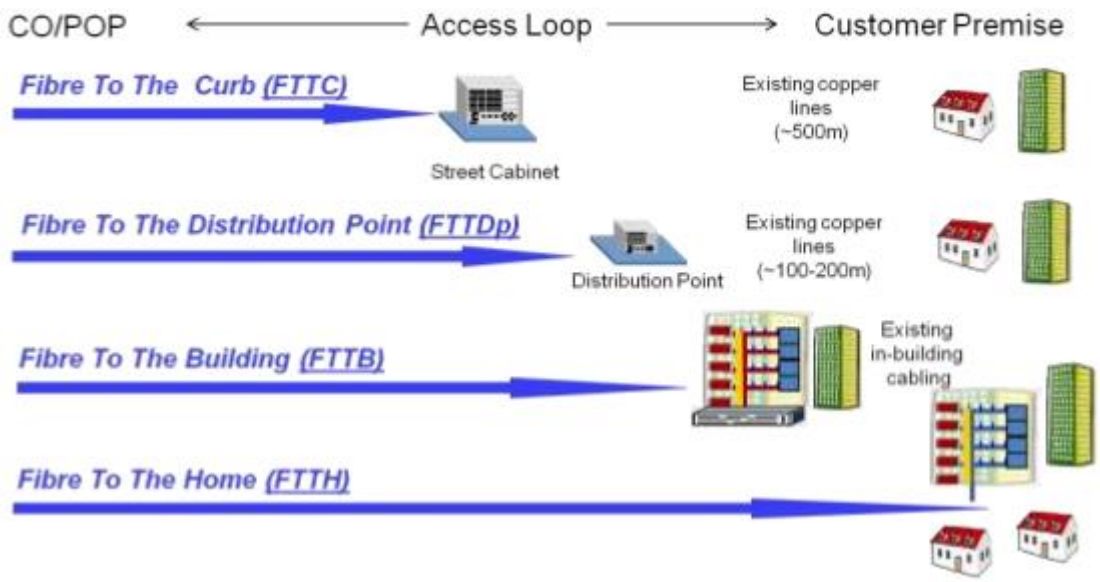

Figure I-11 : Examples of FTTx architectures [21]

The first PON technology was in 1995 with the APON (PON based on the ATM Asynchronous Transfer Mode). In 1999, BPON (Broadband PON) technology emerged enabling transmissions at 622 Mbit/s in the downstream and 122 Mbit/s in the upstream. However, it is only with the GPON, which first part of the standard (G.984 [22]) came out in 2003, that the advent of PON technologies for mass markets was reached.

This technology is based on a point-to-multipoint architecture where each Optical Network Unit (ONU), associated to a costumer, receives the entire signal from the Optical Line Termination (OLT) as shown in Figure I-12. Thus, GPON requires sharing Information which takes place in the time domain as follows:

- In the downstream, the optical transmitter located at the OLT transmits continuously data, of which each time range is intended for a different ONU. This is called Time Division Multiplexing (TDM). Then the GPON protocol, upon reception of the totality of the signal transmitted by the OLT, determines which part of the signal corresponds to the ONU.
- In the upstream, TDM cannot be used considering the GPON point-to-multipoint architecture. The reception at the OLT would actually be quiet challenging giving the continuous data transmission by the entire ONUs simultaneously. Consequently, the transmission at the ONU takes place for a brief moment (around 10µs) with a periodicity of 125 µs: this is generally called burst mode transmission. The role of the OLT is to orchestrate the ONUs bursts, so that it receives them successively, despite the possible distance difference between the OLT and the different ONUs. This is called Time Division Multiplexing Access (TDMA).

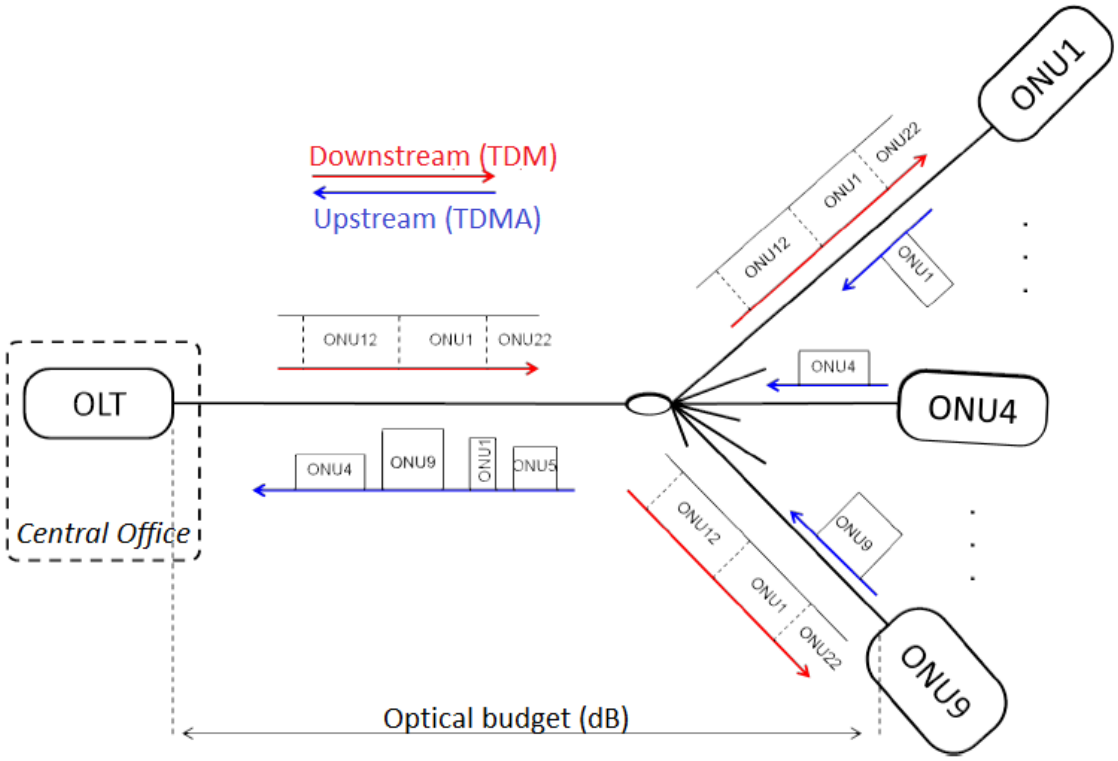

Figure I-12 : Simplified architecture of the point to multipoint architecture used in GPON

The bursts management by the OLT is achieved according to some bandwidth allocation mechanisms. The easier to implement is the Fixed Bandwidth Allocation (FBA) which relies on a definitive and a priori bandwidth allocation [23]. Nevertheless, it doesn't permit an optimized use of the offered bandwidth, especially when some customers are not using their entire bandwidth. On the other hand, Dynamic bandwidth Allocation (DBA) [23] [24] allows a better use of the PON resources by permitting to take advantage of the unused bandwidth by other customers and also to attribute different service profiles to the traffic which allows a better Quality of Service (QoS). More elements about the PON resource allocation are brought in Chapter V.

The most common use case, provided in the first amendment of ITU-T G.984.2, considers a bit-rate of 2.5 Gbit/s in the downstream and 1.25 Gbit/s in the upstream. The corresponding optical budget must match with the B+ class based on a range of 13dB to 28dB, the optical budget being a metric frequently used in optical communication, it represents the difference between output power level of the source and the receiver sensitivity. Therefore, it should be noted that the GPON is designed to reach a maximum range of 20km (with the possibility of reach extension by amplification) and to be able to serve up to 64 ONU using the B+ optical budget class [25].

In practice, GPON allows to propose commercial offers with up to 500 Mbit/s in the downstream and 200 Mbit/s in the upstream for each residential customer (for instance the "Livebox Jet" offer of Orange). In France, the FTTH market is mainly held by Orange with nearly one million subscribers in 2015 (around 67% of the French market), and a target of 21.6 million subscriber by 2022. The use of GPON for mobile backhauling was studied by Orange and some deployments were achieved in some of its African affiliates for the 3G

network. Using GPON for the mobile network can be more interesting in 5G where much higher base stations density is expected to be deployed which will be discussed in Chapter V.

In fact, in order to face the increasing need of bandwidth and also to anticipate the future 5G deployment, the ITU standardized more evolved PON technologies, namely XG-PON [26], XGS-PON [27] and NG-PON2 [59]. The offered bit-rates and commercial availability of these technologies are shown in Table I.2.

Table I.2 : ITU PON technologies

Technology	Multiplexing	Downstream bit-rate (Gbit/s)	Upstream bit-rate (Gbit/s)	Availability for deployment
G-PON	TDM	2.5	1.25	Yes
XG-PON	TDM	10	2.5	Yes
XGS-PON	TDM	10	10	S2 2017
NG-PON2	TWDM	40	40	not before 2020

I.3.3. Midhaul

The term midhaul has been defined by the MEF as the carrier Ethernet network between radio base station sites (especially when one site is a small cell site) [34]. The MEF reference scenario in Figure I-13 shows that the midhaul is considered as a backhaul extension between a small cell base station and its master macrocell base station [36]. Two other scenarios are also considered:

i) The midhaul between two digital unit (DU) pools
ii) The midhaul between two DU pools through a network controller (not illustrated in Figure I-13).

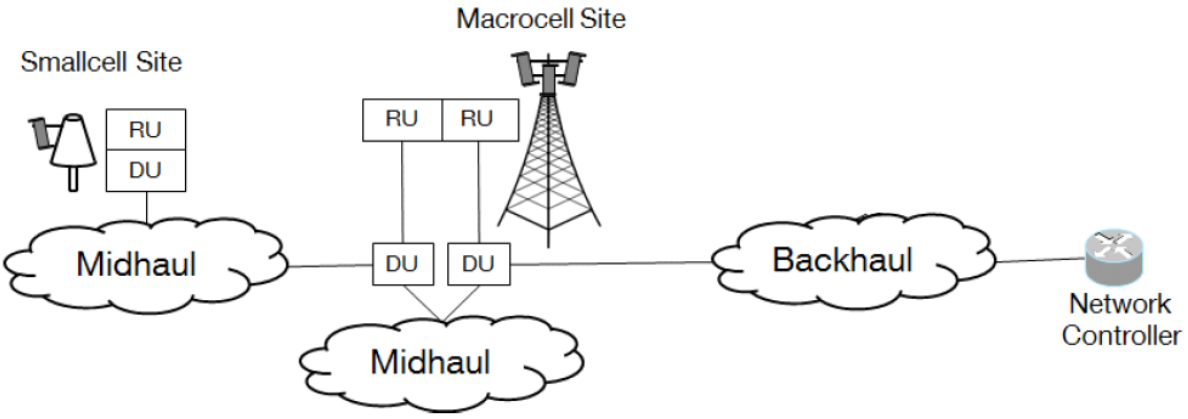

Figure I-13 : Mobile midhaul network according to MEF [34]

I.3.4. Fronthaul

The fronthaul is the nascent network segment following the separation of the signal processing part from the RF part of the radio base station targeting the RAN centralization. It was defined by MEF [34] as a connection from the radio Base Station site to a remote radio unit.

Fronthaul actually carries the very high bit-rate digitized radio signals between the DU and RU over one of the following interfaces:

CPRI – Common Public Radio Interface [35]
CPRI started in April 2003 as cooperation between five radio equipment vendors and by the end of that year the first CPRI specification was released. Today the work is maintained by Ericsson, Huawei, NEC, NSN and Alcatel-Lucent. This initiative has the objective of defining a publicly available specification that standardizes the protocol interface between DU and RU, which, in turn, will allow interoperability of equipment from different vendors. Currently CPRI is, by far, the predominant standard for implementing the interface between the DU and the RU. However, because of proprietary additions by equipment manufacturers, interoperability is not feasible [36]. A new specification (eCPRI 1.0) was just released at the end of August 2017 aiming to enhance the interface in order to support 5G; this new version will be further discussed in Chapter V.

OBSAI – Open Base Station Architecture Initiative [37]

OBSAI is an industry initiative that brings together base station vendors, module and component manufacturers. It aims to create an open market for cellular base stations, thus substantially reduce the development effort and costs associated with creating new base station product ranges.

The complete set of OBSAI specifications covers the areas of Transport, Clock/Control, Radio and Base Band, as well as interfaces and conformance test specifications. OBSAI was first established in 2002 and nowadays more than 140 companies have joined the initiative [36].

ORI – Open Radio equipment Interface [38]
ORI is originated in a European Telecommunication Standards Institute (ETSI) Industry Specification Group (ISG) that was created in May 2010 to develop an interface specification envisioning interoperability between the base station elements. An open interface enables operators to purchase the DU and RU from different vendors, helping to avoid “lock-in” to a specific supplier and permitting a more rapid response to operational demands and market opportunities.
The interface defined by the ORI ISG is based on the CPRI interface. However, some functions are removed, and others are added with the objective of making the interface fully interoperable. ORI also proposes Digital IQ compression which be discussed in Chapter IV. The ORI group has more than twenty members including leading equipment vendors and several network operators [36].

Despite some differences between CPRI, OBSAI and ORI, some key common aspects can be highlighted:

- All base stations are split into two parts connected through the fronthaul interface.
- The most adopted physical medium for the fronthaul is optical fiber.

- The fronthaul interface is typically implemented with Small Form-factor Pluggable (SFP) or Enhanced Small Form Factor Pluggable (SFP+) optical interfaces that constitute the “de facto” connectivity in all RUs and DUs.
- The fronthaul interface presents a constant bit-rate in uplink and downlink.

In the following we will refer principally to the CPRI interface as it is the most commonly used presently. However, the general principles and requirements can also be applied to ORI and OBSAI.

I.3.4.1. RAN evolutions

To illustrate the C-RAN evolution, Figure I-14 shows a simplified representation of the footprint and functional block arrangements evolution in the RAN equipment.

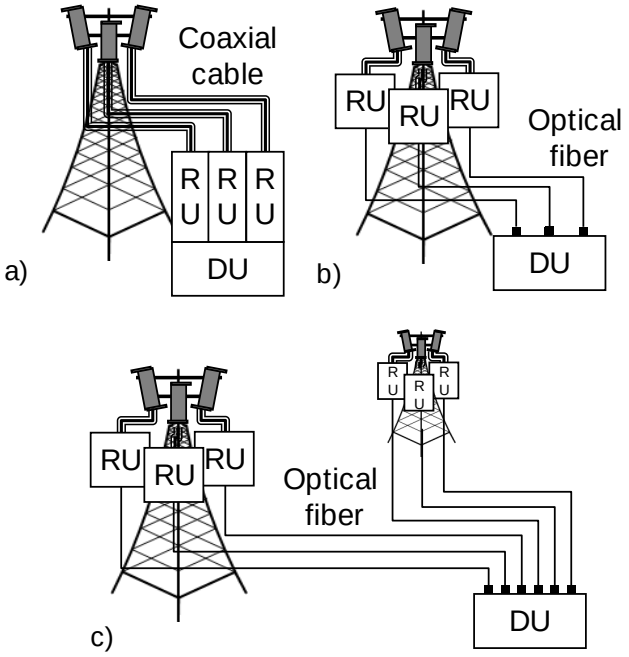

Figure I-14 : RAN evolution

As we have stated in [39], in the most common implementations of 2G and some of the 3G base stations, there is a single unit made up of a radio communication block for transmission and reception connected to a RF power amplifier block with a coaxial cable before reaching the antenna as shown in Figure I-14a. This was not energy efficient since the coaxial cable generated lot of losses.

Thanks to the progress of the processing capabilities of chipsets, it was possible to implement several radio communication blocks inside a single unit. This evolution permitted a rearrangement of the functional blocks. It became possible for a single unit to operate with several RF amplifier blocks (antennas). Since the technologies needed in the radio processing and RF amplifiers are significantly different one from the other, an arrangement based on two different form factors was proposed. The signal processing functions are commonly supported by regular slots on a 19’’ rack. On the other hand, the power consumption and cost of the RF amplifier form factor depend on the RF attenuation of the

coaxial cable reaching the antenna. Therefore, an outdoor form factor was designed to be closer to the antenna.

Concerning the links between the radio units and the outdoor RF unit, the main requirements were to enable for the minimum degradation on the RF signal and to permit transmission over several tens of meters. The combination of DAC & ADC (Digital to Analog Converter and vice versa) and digital transmission over fiber with regular pluggable optoelectronic transceivers allowed meeting these requirements at the expanse of a digitization operation on the time-domain samples of the radio signals. As stated before, this is performed according to some interfaces specification (e.g. CPRI, OBSAI), the resulting bit-rates are reported in the next section. Figure I-14b shows such RAN evolution with separate RU and DU communicating via digital interfaces over optical fiber.

Since the commercial availability of optical transceivers with CPRI-compliant bit-rate and optical budget allowing transmission over tens of kilometers, achieving fronthaul as shown in Figure I-14c became possible. This first phase of the C-RAN architecture is called “Centralized RAN”. It is basically based on the stacking of several DUs in a Central Office which serves several antenna sites. Mainly optical fiber is used to reach the antenna sites within the limit of the maximum round trip time allocated to fronthaul which is explained in the next section. The current LTE RAN equipment is already capable of such centralization. Furthermore, some pooling functions could be implemented in the DUs making the resource allocation more flexible thus optimized. There are four main drivers for the C-RAN architecture [36] [41]:

- First, it facilitates the mobile network deployment. In fact, with the centralization of the digital units, only compact radio units are needed to be deployed. Therefore, the installation will be simplified and less time consuming and the needed footprint is reduced.
- Second, C-RAN will enable the reduction of energy consumption. A study published in [40] shows that up to 50% energy saving can be obtained with C-RAN compared to traditional distributed RAN. This gain comes mainly from avoiding the losses introduced by coaxial feeders and the fact that cooling is no longer needed on antenna sites.
- Third, C-RAN will enable radio performance improvement. In fact, thanks to the very low latency in the “X2” interface (between centralized DUs), radio coordination features can be implemented enabling higher capacities and improved cell-edge performance.
- The last driver is security. It is necessary in distributed RAN to secure the backhaul link by using a secured protocol as IPSec, which adds some overhead to the detriment of the provided bit-rate. In C-RAN, the DUs are located in a physically secured location, thus IPSec is no longer needed.

The last evolution of C-RAN would be DU virtualization. The current RAN equipment is based on dedicated hardware, where the RAN components (hardware + software) are indivisible and provided by RAN vendors. Virtualized RAN (vRAN) will allow operating the virtualized network functions provided by the RAN vendors on generic servers permitting the operators to have more control on their networks. Moreover, as stated in I.2.5, 5G is expected to offer services with different requirements, such as massive Machine-Type Communication (mMTC), Ultra-reliable and low latency communications (URLLC), and extreme Mobile BroadBand (eMBB). Therefore, virtualization is supposed to provide the

flexibility, scalability, and service-oriented management needed for such requirement. This phase of C-RAN is investigated in Chapter V.

I.3.4.2. The fronthaul requirements

I.3.4.2.1. Data-rate

CPRI has a constant bit-rate which goes from 614.4 Mbit/s (CPRI 1) to 24330.24 Mbit/s (CPRI 10) depending on the Radio Access Technology (RAT), the radio carrier bandwidth and the used MIMO option. Here is a method for calculating the CPRI bit-rate [41]:

$$Bit - rate = M \times Sr \times N \times 2(IQ) \times Cw \times C \quad (1)$$

With M being the number of antennas per sector (MIMO option), Sr corresponds to the sampling rate (sample/s/carrier) of the mobile signal, N is the number of bits per sample (bits/sample), 2 (IQ) is a multiplication factor corresponding to I/Q i.e. in-phase (I) and quadrature-phase (Q), Cw is the factor of CPRI control word and C is a coding factor (either 10/8 for 8B/10B coding or 66/64 for 64B/66B coding used for CPRI option 7 and beyond).

For example, for an LTE antenna sector transmitting over a 20 MHz radio band in 2x2 MIMO, the CPRI rate is 2.457 Gbit/s, corresponding to the "CPRI 3" option in the CPRI interface specification. Table I.3 shows some CPRI bit-rates depending on the radio access technology [35]. Here it is worth mentioning that only CPRI option 3 (2457.6 Mbit/s) is implemented for all the deployed RATs in Orange France. Some stuffing was performed in GSM and UMTS DUs to enable using similar transceivers for all technologies, thus decreasing their cost.

Table I.3 : Examples of CPRI bit-rates

RAT	GSM 1T1R	GSM 1T2R	UMTS 1T1R	UMTS 1T2R	LTE 10 MHz 2x2	LTE 10 MHz 2x2	LTE 20 MHz 2x2	LTE 20 MHz 4x4
CPRI bit-rate	12.304 Mbit/s	24.608 Mbit/s	307.2 Mbit/s	614.4 Mbit/s	1228.8 Mbit/s	2457.6 Mbit/s	2457.6 Mbit/s	4915.2 Mbit/s

These bit-rates correspond to the link between one DU and one RU. When designing a fronthaul solution for a macro cell, it should be taken into account the number of section (typically 3), the number of RATs (2G, 3G, 4G, 5G) and number of radio carriers per RAT.

I.3.4.2.2. Performance

According to CPRI specifications, the Bit Error Ration (BER) on the fronthaul link for both user and control plane data must be lower than 10^{-12}. From a global point of view, the fronthaul segment must not degrade the radio performance that is typically quantified in terms of error vector magnitude (EVM) at the RU output. EVM being a vector in the I/Q plane between the ideal constellation point and the point received at the reception. [42] shows methods for EVM calculation, elements are also brought in appendix B.

For instance, for LTE radio signals, the maximum EVM shall not exceed 17.5% for QPSK modulation, 12.5% for 16QAM and 8% for 64 QAM [45]. Experimental BER and EVM measurements are performed in the next chapters.

I.3.4.2.3. Latency

The distance between the RU (antenna site) and the DU (central office) is constrained by the timing requirement of the radio technology. For LTE, the Hybrid Automatic Retransmit reQuest (HARQ) protocol is used as a retransmission mechanism between UE and eNB.

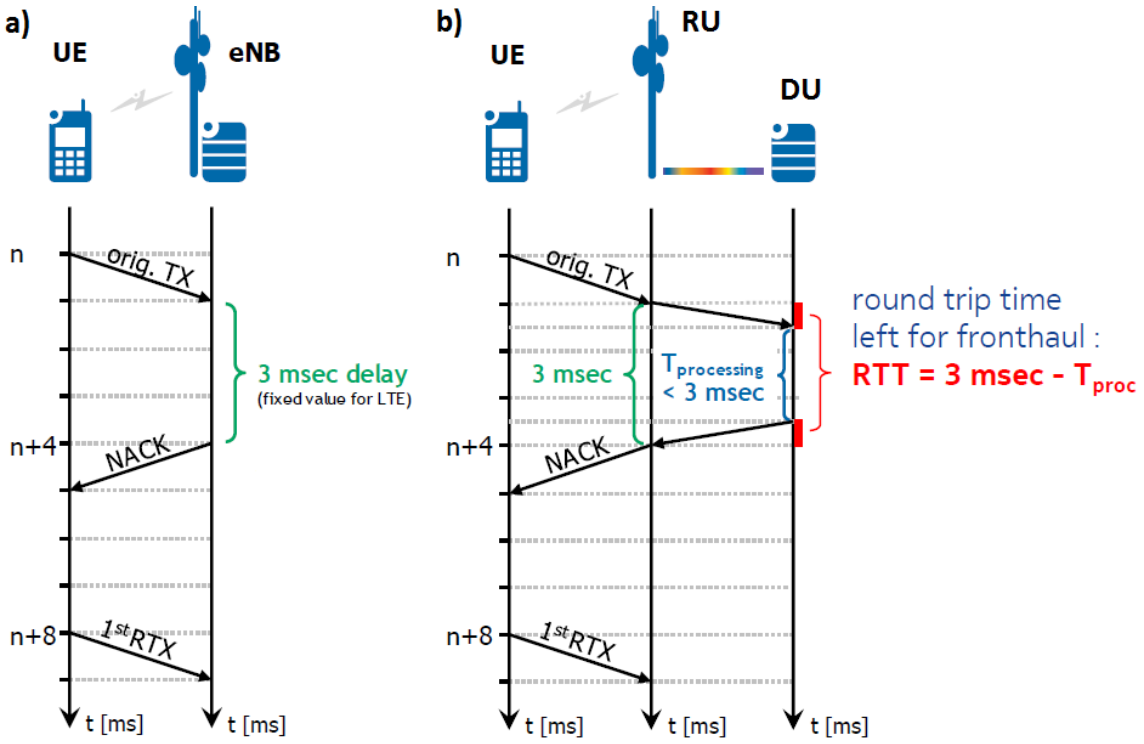

Figure I-15 : Latency analysis in distributed RAN (a) and C-RAN (b) [46]

As shown in Figure I-15, the standard foresees less than 3 ms for DU processing. If the DU is moved away from RU, the additional delay caused by the fiber propagation needs to be considered. To limit the impact of the additional delay on HARQ, the delay needs to be very restricted [47]. Depending on vendor implementation, the Round Trip Time (RTT) is in the range of 150-500 µs [50] [51]. For example, Ericsson considers 150 µs RTT for current LTE Centralized-RAN deployments, to be compatible with LTE-Advanced (CoMP feature) [52].

The index of refraction of optical fibers varies a little depending on the fiber and on the operating wavelength, but has a value around 1.5. This leads to a latency of 5 µs/km in optical fibers.

Therefore, to be compliant with the C-RAN latency recommendation, the fronthaul link should not exceed a distance between 15 km and 20 km depending on the RAN implementation, assuming that no active equipment is introduced in the fronthaul that would add extra latencies.

In 2015, Orange had a total of 20728 mobile antennas deployed, with 19360 in 2G, 17787 in 3G and 4436 in 4G whose deployment is still ongoing.
The topology of the fronthaul link will depend on the antenna site type (number of radio technologies) and the distance between the central office and the antenna site.
Figure I-16 represents an example of the localization of the antenna sites and their corresponding central office for a very dense area (downtown) and a mildly density area (urban area).

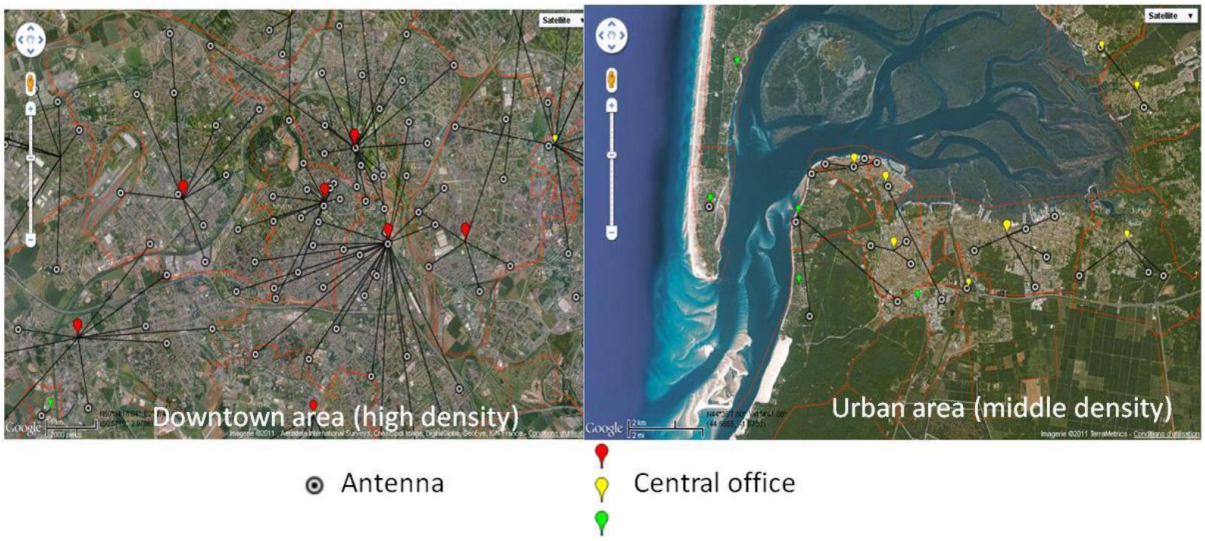

Figure I-16 : Geographical location of antenna sites in very dense (left) and moderately dense (right)

Looking at all metropolitan France, we were able to obtain statistics on the distance as the crow flies between the deployed antennas and their corresponding central offices in Orange France network (cf. Figure I-17).

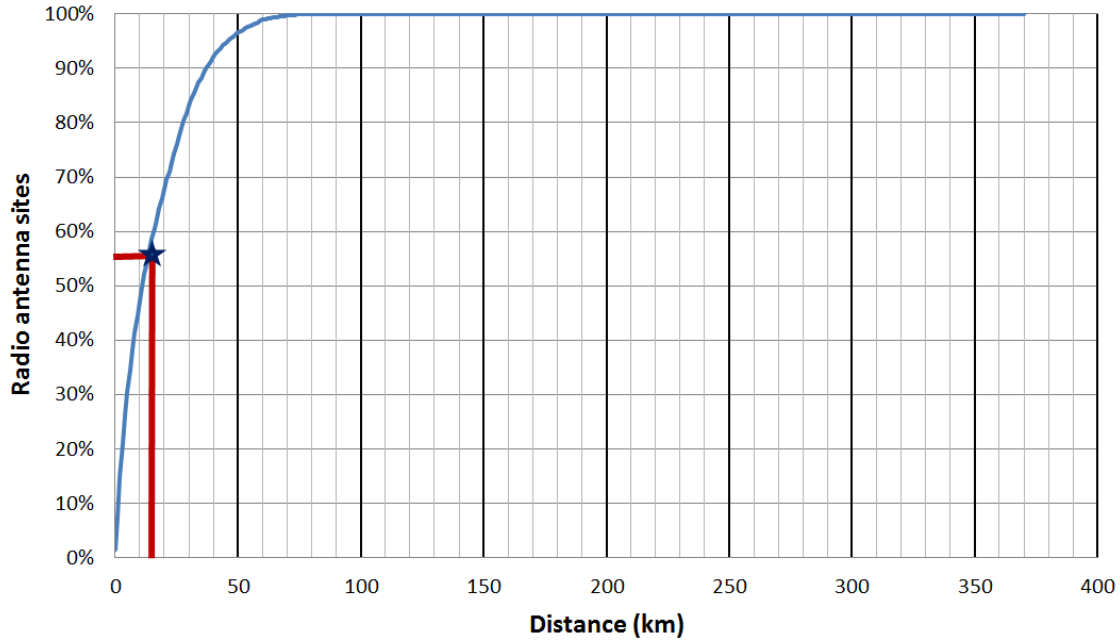

Figure I-17 : Survey of the distance as the crow flies between antenna sites and Central Offices (Orange France network)

It can be seen that 55% of antenna sites are at a distance as the crow flies less than 15 km from a central office. These 15 km, multiplied by a rectification coefficient of 1.3 to adapt the distance between as the crow flies distance and the actual distance in the fiber ducts, we obtain 20 km. This respects the fronthaul constraint specified previously.

If we consider only urban areas that are very dense or mildly dense areas and where it is more beneficial to deploy C-RAN, we obtain the statistics depicted in Figure I-18 (rectification coefficient taken into account):

- Distance between the antennas and the central:
    - 75% of the links have a length <4km
    - 95% of the links have a length <8km
    - 99% of the links have a length <20km
- Number of antenna sites potentially connected to a central office:
    - 20% of central offices would be connected to ≥ 8 antenna sites
    - 45% of central offices would be connected to ≥ 4 antenna sites
    - 70% of central offices would be connected to ≥ antenna sites
    - 30% of central offices would be connected to a single antenna site

Therefore, the existing network in Orange France is compliant with the fronthaul latency constraint with a high number of covered sites per BBU cluster.

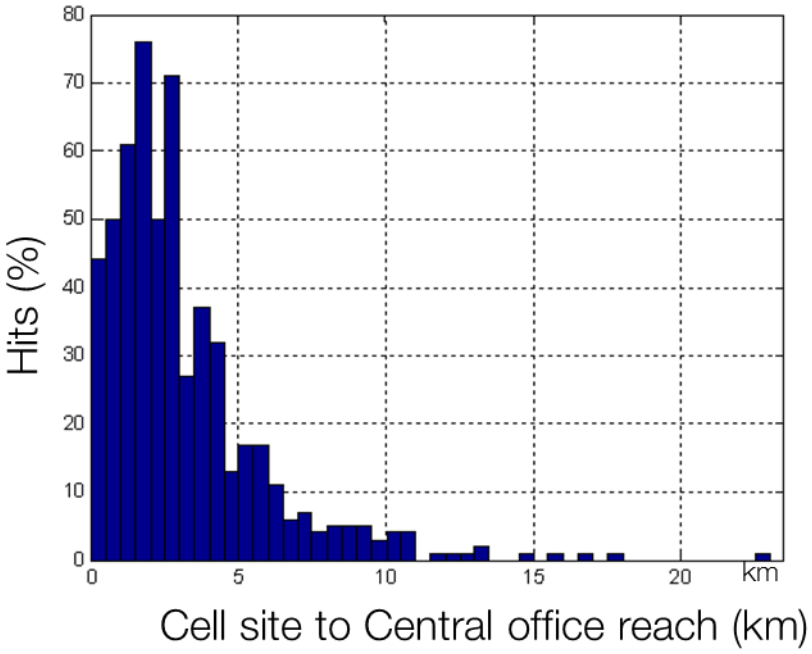

Figure I-18 : Cell site to central office reach in high density areas

I.3.4.2.4. Synchronization

The clock is generally provided to DUs either by GNSS (Global Navigation Satellite System) or by the backhaul link, for instance, by using Synchronous Ethernet [48], increasingly in combination with IEEE1588 [49] for phase/time synchronization. Then, the RU clock for frequency generation is synchronized to the bit clock of the received CPRI signal, thus making the RU a slave of the DU. Consequently, jitter affecting the CPRI signal will also impact on the precision of the clock frequency generation. For LTE, the frequency accuracy requirement over the air interface is ±50 ppb (parts per billion) [45]. Within this overall value, the CPRI link contribution is limited to ±2 ppb. Phase and time synchronization will impose further requirements on the fronthaul link. Moreover, maximum values for tolerated deterministic, random and sinusoidal jitter at the transmitter and at the receiver are specified in [54] [53] and shown in Table I.4. For information, random Jitter is unpredictable electronic timing noise, generally caused by thermal noise, while deterministic jitter is a type of clock timing jitter or data signal jitter that is predictable and reproducible. The unit UI stands for Unit Interval which is the minimum time interval between condition changes of a data

transmission signal, also known as the pulse time. Several measurements on the jitter introduced in the CPRI signal are carried out in Chapter II using the Dual-Dirac model explained in appendix C.

Table I.4 : CPRI specifications on jitter [35]

	Maximum values according to CPRI specification
Deterministic jitter at Transmitter	170 mUI
Total jitter at Transmitter	350 mUI
Deterministic jitter at Receiver	370 mUI
Combined Deterministic and Random jitter at Receiver	550 mUI
Total jitter at Receiver	650 mUI

I.3.4.2.5. Operational requirements

Operational requirements of fronthaul systems include those typical in any telecommunication equipment, for example:

1. Remote in-band manageability, including software upgradeability. A protected local access port, for on-field operation, and local status indications for troubleshooting is required [36].
2. Collection of alarms and events for remote fault prevention/localization.
3. Minimum footprint and standard form factor transceiver.
4. Reduced power consumption.
5. Security mechanisms to prevent unauthorized access and malicious attacks.
6. Remote unit installation in a harsh environment (typically, in outdoor containers or cabinets, under a roof or even on an antenna tower, etc.); as such, compliance of the transport fronthaul equipment with common outdoor environment (-40 to +85 °C) [36].

As a consequence of the previous points, heat dissipation and power consumption of the transport fronthaul equipment at the remote unit should be kept to the minimum.

I.3.4.3. The fronthaul solutions

Giving the bit-rate, latency and jitter constraints of the CPRI interface, Wavelength Division Multiplexing (WDM) was identified as the most appropriate solution for its transport [41].

Coarse WDM (CWDM) [43] offers the possibility to multiplex on a single fiber up to 18 wavelengths, with 20 nm spacing (standardized channels from 1270nm to 1610nm). This solution provides point-to-point colored connectivity with up to 25 Gbit/s per link. It is suitable for fronthauling a macro antenna site with up to 16 RRHs. As shown in Figure I-19, the architecture is based on dual-fiber uplink / downlink transport: 16 CWDM transceivers are inserted in the RUs and 16 are in the DUs. These transceivers are commercially available for transporting CPRI. Up to 10 Gbit/s, they offer operating temperature ranges compatible with outdoor environments: (-40 °C, + 85 °C).

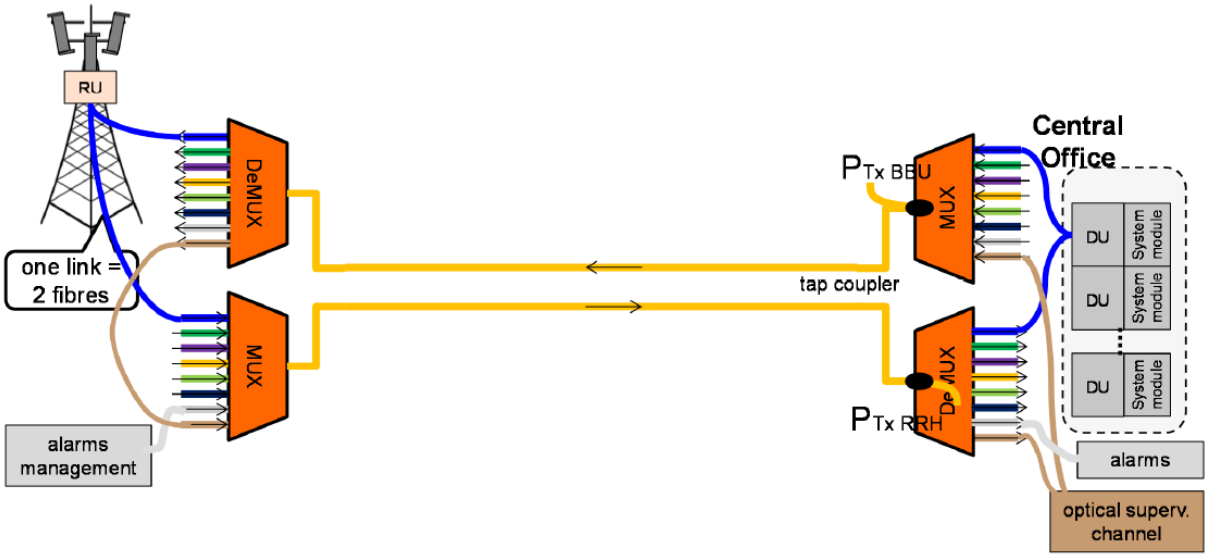

Figure I-19 : CWDM based fronthaul with monitoring

A CWDM channel is dedicated to the fronthaul link supervision and a second channel is dedicated to the antenna site monitoring. In fact, when building a network, it is essential to consider the Operation Administration and Maintenance (OAM) aspects. In particular, links and sites must be monitored in order to detect any kind of problem including faults and performance degradation on the optical layer level. Integrating backhaul and fronthaul segments into fixed access infrastructure can thus raise specific challenges for network operation. Monitoring elements are natively provided by Ethernet in the backhaul network, but no such elements are provided by the CPRI: this is why new monitoring solutions needed to be developed for the fronthaul segment so as to ensure its ultimate integration with fixed access infrastructure.

In the C-RAN architecture the antenna sites and the central office are under the mobile operator's responsibility, whereas the fronthaul link is under the fixed operator's (fiber provider's) responsibility. Precise demarcation points are then needed to separate the responsibilities. A monitoring system must be implemented in such a way that each entity receives alarms about the network segment for which it is responsible. These demarcation points must be outdoor compliant and as simple as possible, preferably without a need for a power supply to reduce expenses and breakdowns. The need for a separation of responsibilities is even more important in wholesale offers where the client requires SLAs (Service Level Agreements) from the infrastructure provider. A first SLA level is the optical link monitoring. Higher SLA levels would address performance monitoring; it could include Key Performance Indicators (KPIs) such as throughput, frame loss rate, latency, jitter and availability.

Antenna site monitoring allows the mobile operator to supervise equipment at antenna sites which are under its responsibility. As shown in Figure I-20, the antenna site alarms are collected by a robot located in the energy cabinet at the antenna site. This robot is connected to the network via IP, which allows remote monitoring of antenna site alarms and remote control of the antenna site power supply. Specifically, linking supervision equipment (sensors, lightning arrester, reclosing device, etc.) to the robot enables the supervision of the antenna sites. In fact, the process takes place in 2 steps. First, three types of alarms can be

generated by the robot in case a sensor triggers: major alarm, minor alarm, lack of power. These alarms are sent to the supervision office via two RUs to secure the process. Second step, once the supervisor is warned, he/she can connect remotely to the robot using this time the wavelength channel dedicated to the antenna site monitoring. He/she can have details about the occurring problem and resolve it remotely if possible.

As stated previously, a second optical channel is dedicated to the fronthaul link supervision. It is accomplished by comparing the inserted optical power in the dedicated channel and the received one, after having introduced a loop back on the RRH side. This solution is simple to implement, reliable and outdoor compliant, but is not compatible with expected evolution to single-fiber architecture.[41]

In fact, thanks to the emergence of bidirectional transceivers, it will be possible to achieve single-fiber CWDM for the fronthaul transport enabling a Capex reduction (with the need to deploy a single fiber instead of two) and the possibility to leverage the existing FTTH infrastructure also based on single fiber. This will also allow a better use of the available ports on the CWDM multiplexor and avoid the uplink/downlink latency imbalance potentially met with the double-fiber CWDM infrastructure.

Different solutions permit the transition to the single fiber architecture. SWSF (Single Wavelength Single Fiber) is a first solution which consists in using the same wavelength for emission and reception thanks to an optical coupler, an isolator placed after the laser diode and a CWDM filter placed before the photodiode.

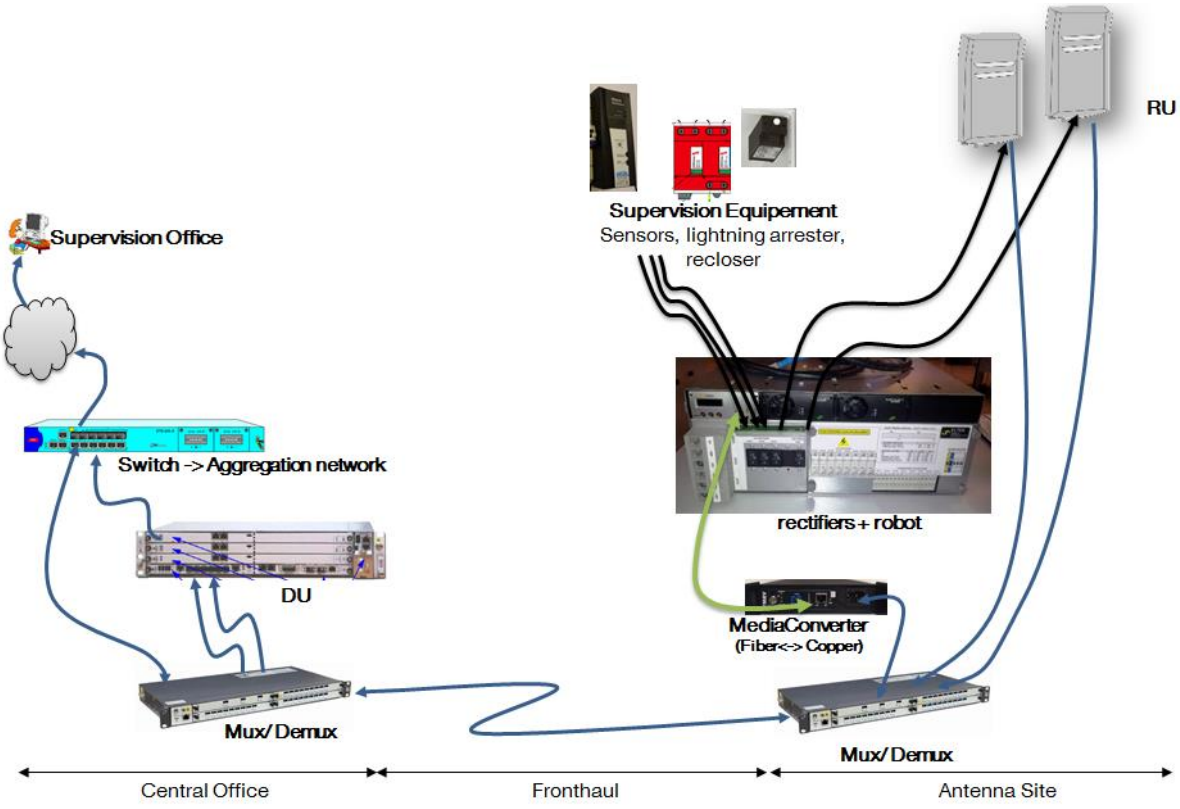

Figure I-20 : Antenna site monitoring

This solution offers low performance due to reflections related to connectors or backscattering of Rayleigh [41]. A second solution is to implement a Reflection Immune Operation (RIO) in an SFP SWSF, which makes it possible to detect parasitic reflections and to cancel them [41]. The third solution called CSC (Cooled Single Channel) is based on the

division of the 20nm CWDM channel into two sub channels, one for the uplink direction and one for the downlink direction [41]. This solution offers the best optical budget compared to other solutions and today commercial products guarantee speeds up to 10 Gbit/s. Nevertheless, the previous monitoring solution (used for double-fiber CWDM) being inadequate for this technology, a new fronthaul monitoring solution is needed. A solution is proposed and experimentally investigated in Chapter II.

Dense WDM (DWDM) [44], which is widely used in core networks, gives better spectral efficiency than CWDM. It offers up to 80 channels with typically 100 GHz (0.8 nm) or 200 GHz (1.6 nm) channel spacing. This small spacing makes this technology fragile to temperature variations since the latter causes wavelength deviations. The existing wavelength control mechanisms are complex and not suited for outdoor environment (-40 °C; +85 °C). DWDM are also known for their high cost which can be reduced by implementing an identical transmitter in each network termination whatever the targeted wavelength, as in this case mass production could be achieved. Solutions for wavelength control and management are yet to be developed. A study on the subject is reported in Chapter II.

The transport of CPRI over other technologies such as Optical Transport network (OTN), Ethernet and PON has been discussed [41], but no actual experimental work confirming its feasibility has been published at the beginning of this thesis. Some state of the art elements, published during the thesis, are provided in the next chapters.

I.4. Conclusion

This chapter reported a state of the art on the evolution of radio mobile technologies and their corresponding transport networks. It also introduced the C-RAN architecture, identified as a key enabler for the future 5G networks. C-RAN promotes the emergence of a new network segment called fronthaul, located between the central office where the DUs are centralized and the antenna sites. Its objective is on one hand to reduce the operational constraints during deployments or field interventions. On the other hand, it targets a radio performance enhancement thanks to a reduced latency between the DUs. Further radio coordination and the flexibility are expected to be brought by virtualization, the ultimate phase of C-RAN.

Consequently, C-RAN has attracted the attention of the major mobile operators all over the world. In fact, China mobile has been deploying C-RAN for over 7 years and showed interesting CAPEX and OPEX savings. China Unicom, HGC and Verizon have been also deploying C-RAN. European operators like Orange, BT Openreach and Telecom Italia, have been conducting C-RAN field trials without any massive deployment. The main reasons behind their reluctance is the immaturity of the WDM solutions for access networks and the lack of visibility on the sustainability of these network infrastructures with the 5G still under investigation/standardization. The objective of this thesis is to contribute in giving Orange insight on this matter.

As explained in the introduction of the manuscript, at the beginning of the thesis when the 5G requirements were not officially specified, the studies were focused on the transport of the CPRI-based fronthaul for LTE networks. Chapter II is mainly dedicated to the assessment of WDM-PON for fronthauling but also to the investigation of the wireless CPRI transport. Once the 5G requirements were defined in 2015, it was perceived that CPRI transport with WDM will be very challenging giving the impact of the 5G radio features of the CPRI bit-rate. Three solutions aiming to cope with this traffic evolution have been investigated. First, transporting

the radio signals in their original waveforms (without digitization) can significantly improve the fronthaul spectral efficiency compared to the CPRI-based fronthaul enabling, potentially, the transport of 5G interfaces. A thorough investigation on this subject is reported in Chapter III. Second, CPRI compression based on uniform and non-uniform quantization can also enhance the CPRI spectral efficiency. Chapter IV describes this solution and experimentally shows the achievable compression rates. Finally, establishing a new radio functions partitioning between the DU and RU was identified as a promising solution for 5G. A study of these new functional split is reported Chapter V.

Chapter II. CPRI-based fronthaul integration

II.1. Introduction

As stated in Chapter I, the use of optical fiber with WDM was identified as the most appropriate solution for the transport of the CPRI interface. Nevertheless, it still has some weaknesses. Notably, the lack of the optical infrastructure monitoring solutions and also the wavelengths management difficulty introduced by the use of colored optical transceivers (mandatory for CWDM). Moreover, still in the C-RAN context, the densification of the mobile network by deploying more and more antennas will significantly increase the energy bill for the mobile operators, particularly because each antenna site is powered separately. A centralization of the energy source could therefore alleviate the energy costs. The lack of easily and quickly available optical fiber is also a problem encountered in the C-RAN densification. The wireless transport of the CPRI signals can therefore resolve this issue. This chapter breaks through all of these barriers to enable successful fronthaul integration. This is done mainly by means of the study and experimental evaluation of industrial prototypes but “home-made” platforms are also built when it is needed.

For fiber-based fronthaul, an assessment of WDM fronthaul is reported in II.2.1; a study is done on the introduction of a control channel in the CPRI interface in order to achieve wavelength tunability and fronthaul infrastructure monitoring using two methods: RF pilot tone and baseband over-modulation. TDM-based fronthaul aiming to increase the number of transported CPRI links per WDM wavelength is also demonstrated in this chapter and the results are reported in II.2.2. Furthermore, a remote powering solution based on the use of hybrid energy/optical fiber cable is introduced in II.2.3. Regarding the wireless-based fronthaul, an experimental investigation is done on wireless fronthaul equipment without spectral efficiency optimization in II.3.1 and with spectral efficiency optimization in II.3.2.

II.2. Fiber-based fronthaul

II.2.1. Wavelength division multiplexing

II.2.1.1. About WDM in the access

The simplest solution to achieve C-RAN is to provide point-to-point fiber links from the DUs to the RUs. Typically, fiber access cables offer 12 to 144 fibers allowing the upgrade of an existing backhaul network to fronthaul by exploiting the unused fibers. The latter are however not always available and new point to point fiber deployment can be very expensive, hence the interest in WDM. Wavelength division multiplexing is actually a multiplexing strategy for optical networks where different flows of traffic are segregated to different wavelengths then multiplexed in a single optical fiber.

Coarse WDM (CWDM) is one of the varieties of WDM which is the most robust for a fronthaul deployment. It is highly reliable, cost effective, compatible with outdoor environments and completely passive (no need for power supply). It offers up to 18 channels with 20 nm spacing according to ITU-T G.694.2 [55]. The classic CWDM architecture needs two fibers, one for the uplink and one for the downlink. Using one fiber for the transmission in both directions was the first improvement. It is achieved by dividing each CWDM channel into two sub-channels of 6.5 nm width each [56]. The wavelength multiplexing and de-multiplexing of these two sub-channels is achieved inside the optical front head of the transceiver. Standard

passive CWDM devices and single fiber infrastructure could be used. This allows the reuse of the same engineering process that is used for FTTH infrastructure which is also based on a single optical fiber. It also solves the issue of unbalanced downstream and upstream latency in fronthaul links.

This sub-channel CWDM version was recently updated with the possibility to have six sub-channels [57] per optical channel based on 300 GHz spacing over the CWDM grid. Six sub-channels allow performing three bidirectional channels. We obtain thus a single fiber CWDM architecture offering up to 54 bidirectional channels. In the case that each sub-channel supports the maximum CPRI rate (option 10, working at 24330.24 Mbit/s), this passive sub-channels CWDM infrastructure will be able to support symmetrical 1,3Tbit/s between antenna sites and the DU hotel.

With such infrastructure, colored transceivers are needed in the DUs and RUs, which makes wavelengths management difficult for mobile operators giving the number of channels. Colorless transceivers are thus welcome. Furthermore, the monitoring of the optical infrastructure is mandatory especially in the case of a wholesale offer on the fronthaul segment, as explained in Chapter I. Such monitoring is not provided in passive WDM. Therefore, there is a need for a monitoring solution for the mono-fiber fronthaul.

In fact, the second Next Generation of Passive Optical Networks (NG-PON2) expects colorless transceivers with Dense WDM (DWDM) wavelengths (0.4 or 0.8 nm channel spacing) [59]. It has two flavors which can be integrated in the same fiber infrastructure: Time and Wavelength Division Multiplexing (TWDM) PON for residential access and PtP WDM for mobile backhauling, fronthauling and business services. Figure II-1 shows the CWDM and PtP WDM wavelengths on the optical spectrum where we can see that their wavelengths are overlapping. Therefore, since Orange started deploying CWDM based fronthaul (in opportunistic mode), it would be feasible to carry out a smooth migration to PtP WDM in case of higher density antenna sites and when this technology achieves maturity.

The wavelength tunability and the transport of monitoring data are expected in PtP WDM with the implementation of an out-of-band control channel as indicated by the ITU-T G.989.2 standard [59]. In fact, this channel, called Auxiliary Management and Control Channel (AMCC), will transmit wavelength assignment and allocation information as well as Operation Administration and Management (OAM) data. It will be inserted in each wavelength for the upstream and downstream. AMCC can be implemented either by a baseband over modulation or by a radio frequency pilot tone (PT) according to the standard.

Such control and management channels are widely used in optical telecommunication. They are low bit-rate signals added on a high-speed modulation channel usually to provide monitoring information and simple OAM services. They have been recommended for PtP WDM by the ITU-T in G.989.2 for such purposes and also to transport the exchanged messages between the OLT and the ONU for the wavelength assignment. The principle of the two possible implementations is shown in Figure II-2.

Figure II-1 : WDM spectrum

The physical transport layer for the over-modulation-based AMCC is realized as a low bit-rate, low-modulation-index baseband amplitude over-modulation over the optical PtP payload signal. As depicted in Figure II-2a, it can be implemented by means of a Semiconductor Optical Amplifier (SOA) or a Variable Optical Attenuator. The modulation index in percent is defined as:

$$m = 100 \times \frac{Pmax - Pmin}{Paverage} \tag{2}$$

with $\mathrm{P_{max}}$, $\mathrm{P_{min}}$, and $\mathrm{P_{average}}$ referring to the maximum, minimum and average power values of the envelope of the over-modulated PtP signal. In the ITU-T recommendation, the AMCC shall have a modulation index of 10%, a nominal line rate of 115 Kbit/s and rectangular pulse shape.

On the other hand, the physical transport layer for the RF-pilot-tone-based AMCC is realized as a low bit-rate, low-carrier-frequency, low-modulation-index amplitude modulation signal which is added to the PtP payload signal in the electrical domain as shown in Figure II-2 (b). The modulation index m in percent is defined as:

$$m = 100 \times \frac{Vpp, AMCC}{Vpp, payload} \tag{3}$$

with $V_{pp,AMCC}$ and $V_{pp,payload}$ referring to the peak to peak voltage values of the AMCC and the PtP signal in the electrical domain. The standard recommends a modulation index of 10%, a nominal line rate of 128 Kbit/s and a carrier frequency at 500 KHz.

Both AMCC implementations are investigated in this section. In subsection II.2.1.2 a real-time investigation is done on the impact of introducing an RF pilot tone on a CPRI signal. Then, an experimental evaluation of PtP WDM industrial prototype based on an “AMCC-like” via a baseband over modulation was carried out. We called it “AMCC-like” because its specifications are slightly different from the ones recommended in the ITU-T in G.989.2. The obtained results are reported in subsection II.2.1.3 and subsection II.2.1.4 shows experimental results of CWDM monitoring provided by smart SFPs based on Remote Digital Diagnostics Monitoring Interface (RDDMI) also performed with a baseband over modulation approach.

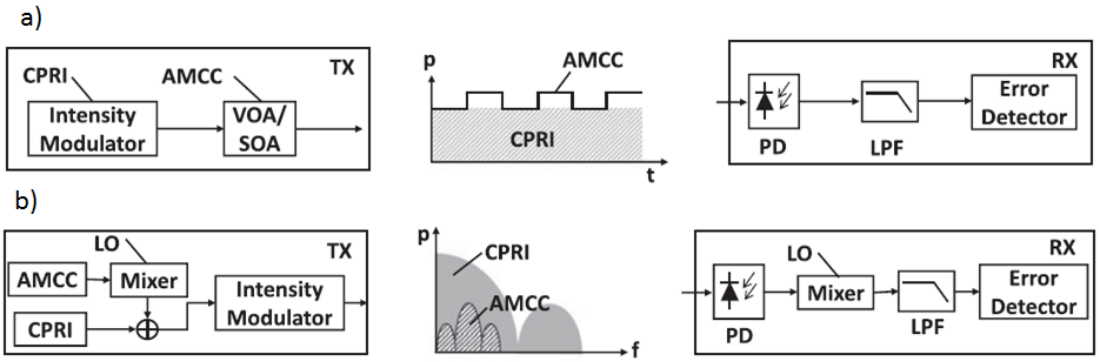

Figure II-2 : Principal of baseband over modulation (a) and RF pilot tone (b) [58]

II.2.1.2. Investigation on RF pilot tones for PtP WDM

II.2.1.2.1. Experimental setup

A first investigation on RF pilot tone based AMCC was done by NTT Labs and published in [60]. In this paper, the authors proposed an offline AMCC implementation for WDM-PON using a Mach-Zehnder Modulator and obtained quite promising results. It was confirmed that it was feasible to insert a 128 Kbit/s pilot tone at 500 KHz with 10% modulation index on a fronthaul link with negligible impact on the CPRI. Following this publication, we carried out an extended study considering the implementation issues. A real-time transmission of AMCC over a 20 km fronthaul link is carried out using a Directly Modulated Laser (DML) of a commercial Small Form factor Pluggable (SFP). Different measurements are performed to verify the performances of the AMCC and to evaluate its impact on the CPRI and radio mobile signal integrity.

Figure II-3 shows the performed experimental setup. At the transmission side, a signal generator is used to generate a 20 MHz LTE carrier using standardized test model E-TM3.1 [61]. This signal is converted to CPRI (sampling + quantization + coding) using an IQ box.

A Pseudo Random Binary Sequence (PRBS) generator is used to emulate the AMCC transmission using a 2^7-1 length sequence. This low frequency signal (128 Kbit/s) is up-converted using a mixer and a Local Oscillator (LO) at 500 KHz. Both AMCC and CPRI signals are separately amplified and gradually attenuated with a Variable Electric Attenuator (VEA) so that the ratio between the signals peak-to-peak voltage can be changed. The signals are then summed up with a power combiner. The obtained signal is fed to a driver then to a Directly Modulated Laser (DML) diode operating at 1590 nm (fixed wavelength) and 0 dBm before transmission over 20 km standard single mode optical fiber. The received optical signal is detected by a pin-photodiode (pin-PD) then amplified with a Trans-Impedance Amplifier (TIA). The used laser, photodiode, driver and TIA are embedded in a commercial SFP module as shown in Figure II-3. The received RF signal is amplified then halved with a power splitter. A part is fed to the RU test equipment composed of an IQ box for CPRI to LTE conversion and a Spectrum Analyzer for LTE analysis. The second part is down converted then low-pass filtered by a 250 KHz filter to remove the CPRI high frequency components and potential harmonics and intermodulation products being generated by non-linear mixers. After filtering, the AMCC signal is amplified before performance evaluation.

In this experimentation, as for the rest of the studies performed in this thesis, the impact of the used wavelengths on the transmission performance is not carried out. In fact, the main phenomenon potentially appearing when carrying the wavelength is the dispersion. Although,

in the fronthaul link, the transmissions are done over 20 km with bit-rates up to 10 Gb/s (in this thesis experimentations). Studies showed that the impact of dispersion in such transmissions is negligible, hence the choice not to carry out studies on wavelength.

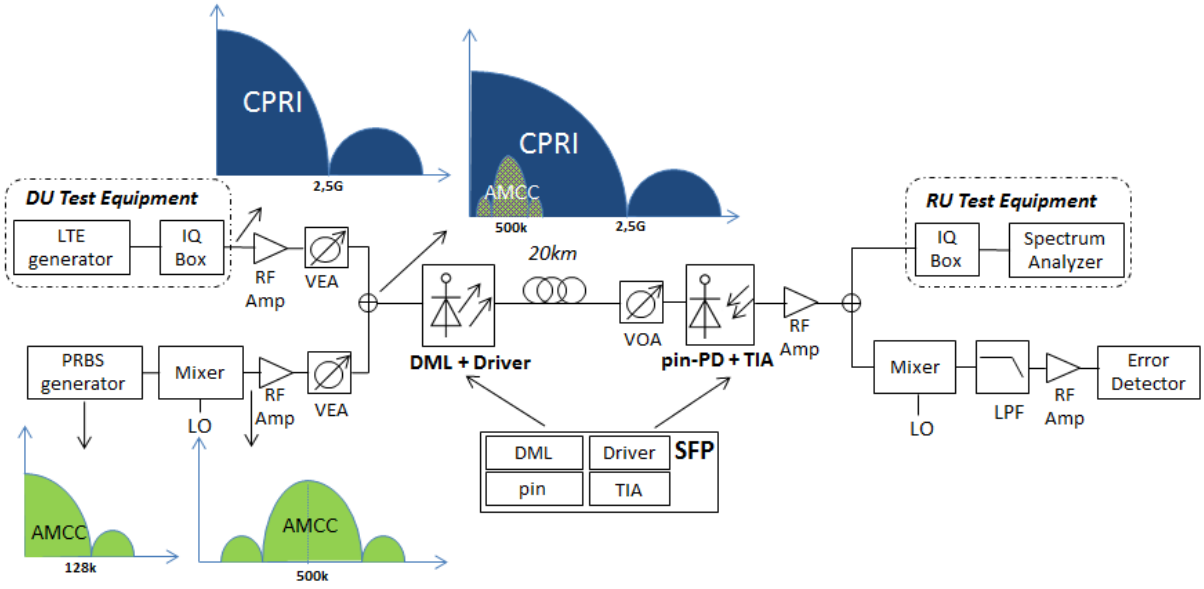

Figure II-3 : Pilot tone experimental setup

II.2.1.2.2. Experimental results and discussion

We focus our analyses on three main performance indicators: Bit Error Rate (BER), Error Vector Magnitude (EVM) and jitter. We started by investigating the BER variation of both CPRI and AMCC signals as a function of the relative modulation index, the latter being defined as the ratio of the peak to peak voltage value of the AMCC with respect to the CPRI signal as mentioned earlier. The results for a CPRI 3 (2.45 Gbit/s) and a 128 Kbit/s AMCC transposed to 500KHz are depicted in Figure II-4 for different relative modulation indices, the objective here is to find an optimal index where the BER of both signals (CPRI and AMCC) is minimal.

Figure II-4 shows that error free AMCC and CPRI transmissions ($\mathrm{BER} \leq 10^{-8}$ and $\mathrm{BER} \leq 10^{-12}$ respectively) could be obtained for modulation indices between 18% and 20%. Only 10^{-8} BER was targeted for the AMCC signal, since with such low bit-rate signals, achieving lower BER measurement would take very long time. The obtained modulation indices range is higher than the value adopted in the standard and the one found in [60]. We believe that such difference can be attributed to the low sensitivity of the equipment used for the AMCC BER measurement and to the fact that the used driver and TIA (embedded in the commercial SFP) are not designed for the amplification of low frequency signals.

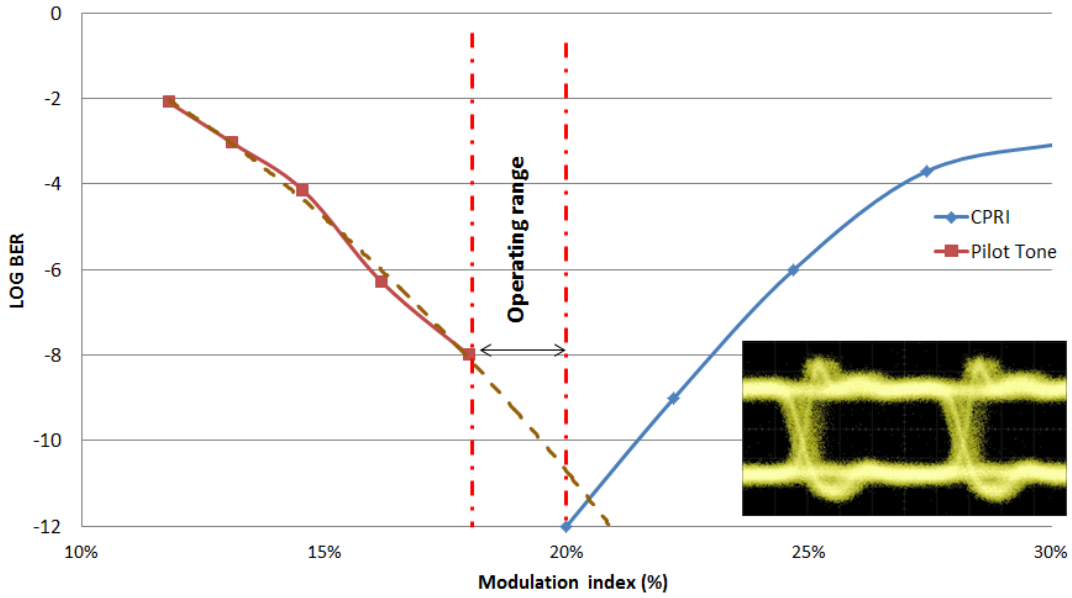

Figure II-4 : CPRI and Pilot Tone BER performance for different modulation index and optical eye diagram at 20% modulation index

In order to evaluate the impact of introducing the AMCC in a fronthaul link, we fix the relative modulation index to an optimal value of 20%. Figure II-5 displays the obtained CPRI eye diagrams at the input of the RU test equipment (after opto-electrical conversion by the SFP PIN) at 2.45 Gbit/s with and without the AMCC signal. Some noise on the zero and one levels can be noticed as well as some jitter due to the introduction of the control signal.

Figure II-6 shows the impact of the AMCC signal on the LTE EVM while varying the Received Optical Power (ROP) at the input of the PIN photodiode. Measurements are carried out for CPRI 3 and 6 (2.4576 Gbit/s and 6.1440 Gbit/s respectively) firstly without the AMCC and then with a 128 Kbit/s AMCC up-converted to 500 KHz and with a 128 Kbit/s AMCC up-converted to 1 MHz. 64 QAM modulation is used for LTE transmission since it has the most stringent EVM requirement (8 %) according to the 3GPP standard [61]. We notice a penalty of 0.85 dB in the optical budget when inserting the AMCC on CPRI 3 and 1.35 dB for CPRI 6 for a fixed EVM of 0.06%. We also observe very similar performances when the AMCC is at 500 KHz and 1 MHz. Figure II-6 also shows that an optical budget of up to 22 dB (with CPRI 3) can be obtained before achieving 3% EVM which allows for a 5% extra margin with respect to the 3GPP standard for the degradations that might be caused by the amplification in the RU.

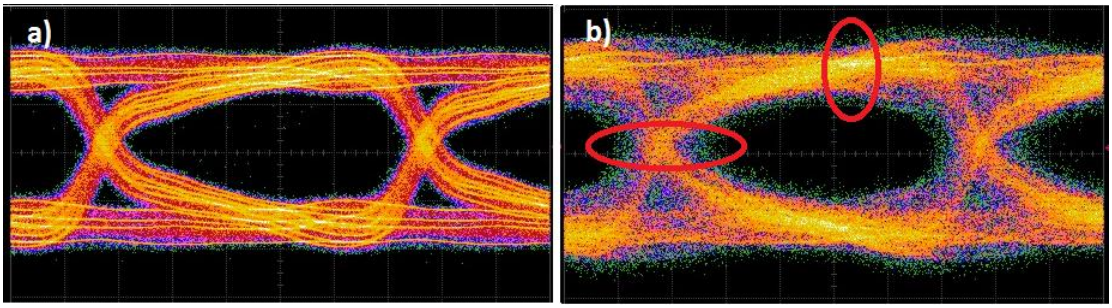

Figure II-5 : Eye diagrams of received CPRI 3 without (a) and with (b) pilot tone transmission.

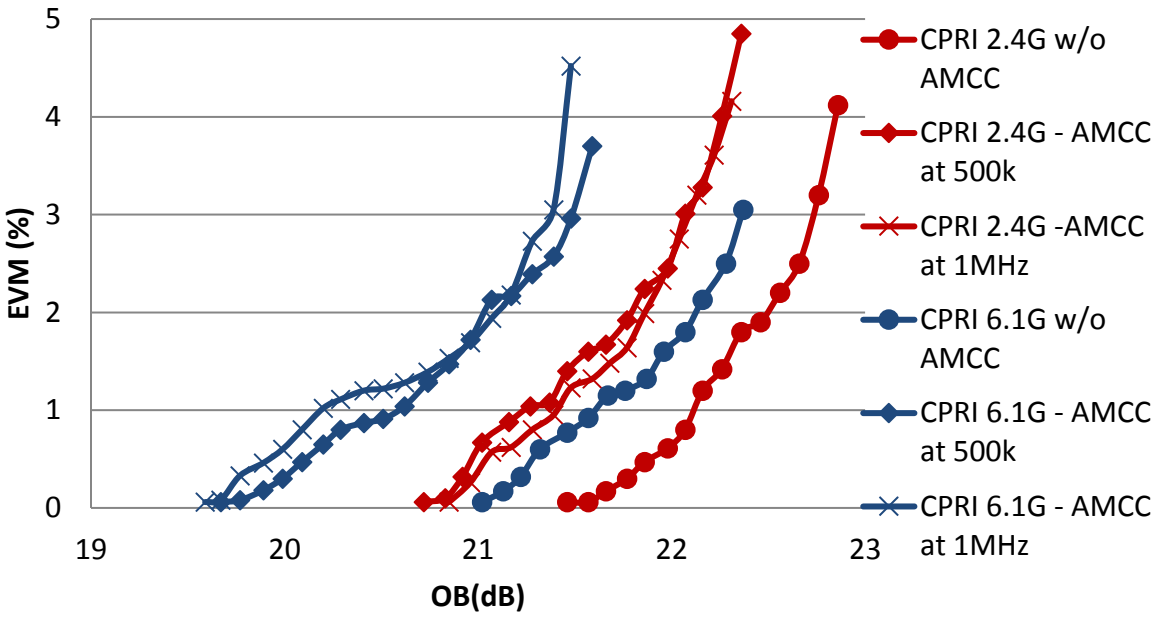

Figure II-6 : LTE EVM performance as a function of the Optical Budget (OB)

We also evaluated the AMCC performance in terms of BER for 128 Kbit/s and 64 Kbit/s bit-rates and for an up-conversion to 500 KHz and 1 MHz as depicted in Figure II-7. We notice a better performance at 128 Kbit/s which we believe is due to the filter characteristics at the receiver side. On one side, by transmitting at 64 Kbit/s and using a 250 KHz low-pass filter at the receiver, we keep more lobes of the AMCC signal spectrum, which allows having a more squared time-domain signal, thus a better transmission. However, it also implies that more energy of the CPRI signal is contained inside the filtered AMCC, which, on the other side, degrades performances. Evaluations with narrower filters need to be carried out to confirm that the characteristics of the low pass filter are the only factor responsible of the AMCC performance variation. The shape of the obtained BER curves can be explained by the presence of a limiting TIA in the SFP, which causes a sudden BER deterioration.

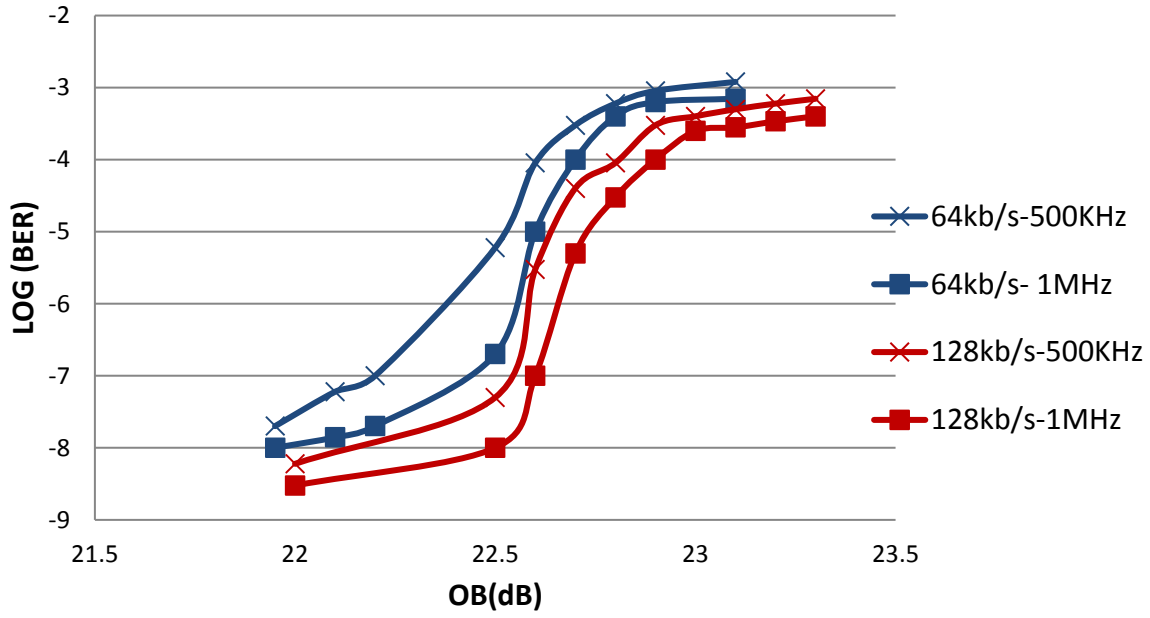

Figure II-7 : AMCC BER performance as a function of the Optical Budget (OB)

We also observe a slight performance improvement at 1 MHz certainly because the AMCC channel is better positioned with respect to our components frequency responses.

Finally, we evaluated the jitter introduced in the CPRI at 2.45 Gbit/s upon the insertion of the AMCC. The presence of a low frequency signal in the CPRI prevented us from using the accurate dual-Dirac jitter estimation approach [62]. An alternative method was then carried out by means of an analysis of the CPRI eye diagram. In order to verify the reliability of the eye diagram approach, we first performed a reference measurement without the AMCC and compared it to the dual-dirac approach.

We measured 132 mUI with the dual-Dirac model and 148 mUI with the eye diagram which validated our method. Table II.1 shows the measured jitter on the CPRI at the input of the RU test equipment with and without AMCC. A significant amount of jitter is introduced upon AMCC insertion. Nevertheless, the maximum jitter value defined by the CPRI specification is still respected. We must notice that lower jitter values could be obtained after filtering out the AMCC from the CPRI signal by means of a band-stop filter. However, the impacts of such filtering on the CPRI performances need to be evaluated.

Table II.1**:** Jitter measurement on the CPRI3 eye diagrams with and without AMCC

Jitter at Receiver w/o AMCC	Jitter at Receiver with AMCC	Maximum value (CPRI specification)
148 mUI	406 mUI	650 mUI

To sum up, we experimentally demonstrated a real time AMCC implementation using a commercial SFP for fronthaul transport over WDM-PON. Performance measurements were carried out on CPRI and AMCC signals. An optimum relative modulation index range between 18% and 20% was found allowing for error-free transmission for both CPRI and AMCC. Also, an optical budget of up to 22 dB could be demonstrated using CPRI at 2.45 Gbit/s with an additional 5% margin on the recommended EVM values. This optical budget is compliant with the optical path loss class L1 (8 to 17dB) specified in ITU G.989.2 [63], which is defined between the ONU and the wavelength multiplexor, the latter typically introducing 4 to 5 dB optical attenuation. The obtained results are very promising and show that RF pilot tone implementation can be done with a low cost (by reusing the current SFPs system) while respecting both 3GPP and CPRI specifications.

II.2.1.3. Evaluation of a PtP WDM industrial prototype

II.2.1.3.1. Description of the system under test

The WDM-PON system under test is a prototype having three upstream channels in the C-band and three downstream channels in the L-band. The multiplexing of these channels is achieved with a cyclic Arrayed Waveguide Grating (AWG) offering 40 channels with a channel spacing of 100 GHz in L-band and ~97 GHz in C-band. They are located in the Central Office (CO) and at the Remote Node (RN) as shown in Figure II-8. One colored OLT is operating up to 10 Gbit/s and the two others at 1 Gbit/s. The ONUs are colorless, they are tuned to the wavelength corresponding to the AWG port they are attached to, using a feedback-based wavelength locking process.

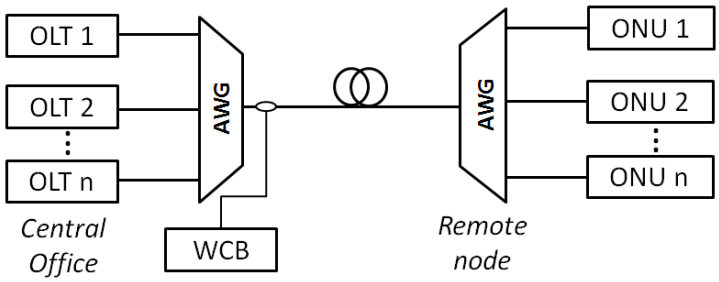

Figure II-8 : WDM-PON system architecture

In order to distinguish upstream signals and their deviation with respect to the ITU grid, a unique pilot tone in the frequency range [100 KHz – 1 MHz] is added to each ONU's upstream signal. The Wavelength Control Board (WCB) located at the OLT site measures the received power from different ONUs thanks to a Fast Fourier Transform (FFT) before and after a common centralized Fabry-Perot (FP) wavelength-locker. This wavelength-locker uses an etalon as a centralized discriminator which has a sinusoidal response over the (C-Band) spectrum with a 100 GHz free spectral range. It is operated so that ITU frequencies are located halfway up on the rising edge of its response curve. The ONU wavelength deviation can be calculated from the ratio of the signals' FFTs before and after passing through the FP etalon. By comparing this ratio with the ITU frequencies, the system can determine any deviation less than +/-25 GHz [64].

In the downstream, the feedback of the information on wavelength deviation and power levels is also implemented by using pilot tones with an additional Embedded Communication Channel (ECC) at the rate of 1 Kbit/s. This pilot tone is added to the downstream WDM spectrum via an over-modulation performed by a variable optical attenuator [64].

This prototype is based on ITU-T G.698.3 which is a standard destined to DWDM transmissions for the metro networks. In fact, it was originally developed in the context of a metro network project, thus it has slightly different specifications than the PtP WDM of the ITU G.989.2 but the principle remains the same. More details on the system implementation were published by the equipment vendor in [64] and [65]. The purpose here was to illustrate the feasibility of wavelength tunability implementation in PtP WDM and evaluate the impact of such system on the CPRI and LTE performance. This system being based on a baseband over modulation control channel (unlike the RF pilot tones studied in the previous section), this section will also allow demonstrating the impact of introducing a control channel with this method.

II.2.1.3.2. Experimental setup

Figure II-9 shows the used experimental setup to measure performances of a business service and a fronthaul link using the proposed system.

An Ethernet tester is used to emulate the transmission of a 1 Gbit/s Ethernet business service on one wavelength. The performance is evaluated in terms of frame loss.

In the adjacent channel, a mobile fronthauling service is transmitted using a signal generator for LTE generation and an IQ box for LTE to CPRI conversion.

The standardized E-TM3.3 LTE test model is used with 20 MHz carrier bandwidth. CPRI performance measurements are carried out in the downlink direction at three CPRI line rates: 2.45 Gbit/s, 4.91 Gbit/s and 9.83 Gbit/s.

At the reception after 20 km transmission over single mode optical fiber, an IQ box is used to convert the CPRI signal to LTE before analysis with an electrical Spectrum Analyzer (SA). This measurement equipment emulates the DU and RU as a first set-up before using a commercial DU and RU to confirm the measured values. The optical transmission is achieved at the DU side with colored OLTs offering 22 dB of Optical Budget (OB) for a Bit Error Rate (BER) of 10^{-12}. At the RU side, colorless ONUs (OB= 24 dB) with a pilot tone based tuning process are used. In order to evaluate the impact of this wavelength locking process and of the transmission on an adjacent channel, Error Vector Magnitude (EVM) measurements are done at the output of the RU using an SA. Jitter on the electric signal is measured at the transmitter (1) and at the receiver (2) with a Digital Storage Oscilloscope (DSO) as shown in Figure II-9 and a frequency accuracy evaluation of the LTE signal is carried out with an SA, this time at the output of a commercial RU operating at 2.645 GHz. A latency measurement is done as well using CPRI measurement equipment to assess the delay introduced by the WDM-PON system.

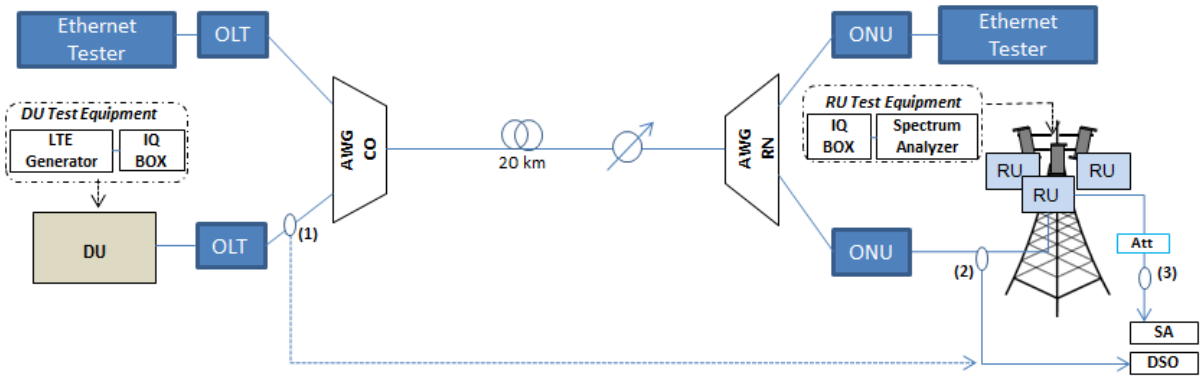

Figure II-9 : Experimental setup (PtP WDM system evaluation)

II.2.1.3.3. Experimental results

The operation in adjacent channels could affect the transmission due to crosstalk. Also, using pilot tones for the wavelength tuning generates noise as it is shown on the eye diagrams depicted in Figure II-10. To address these points, we investigated the transmission performance in terms of Ethernet frame loss, EVM and frequency accuracy of the LTE signal, and jitter on CPRI signal.

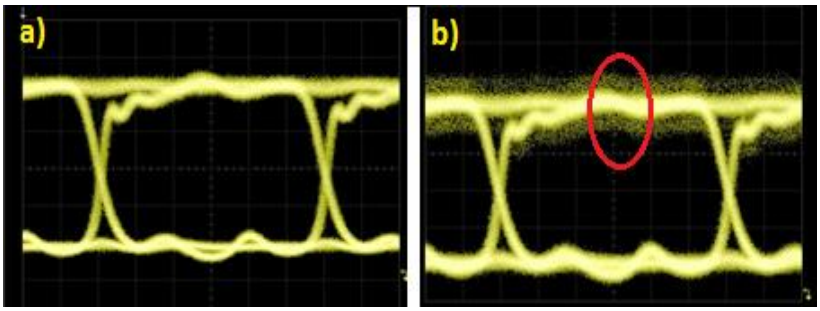

Figure II-10: 2.45 Gbit/s Eye Diagram before (a) and after (b) adding a pilot tone

A. EVM values and Ethernet frame loss

First, we started by investigating EVM values of the LTE signal and Ethernet frame loss while attenuating the Received Optical Power (ROP) in the ONUs with a Variable Optical Attenuator (VOA). For QPSK, we measured 0.07% of EVM for ROP greater than -25.5 dBm when using the test instrumentation. The Ethernet transmission in the adjacent channel was frame loss free at this ROP. We start losing Ethernet frames at ROP = -28 dBm. A degradation of the EVM value (1 pp) is noticed when we use a commercial RU due to the amplifier noise. The same EVM value is obtained when using a dark fiber fronthaul. Therefore, no EVM degradation is introduced by pilot tone use.

The same test was done for a 64QAM transmission using the test model E-TM3.1 at the three tested line rates (2.45 Gbit/s, 4.91 Gbit/s and 9.83 Gbit/s), leading to the same EVM value (0.07%).

No EVM variation is observed when we remove the Ethernet signal. Thus, there is no inter-channel crosstalk impact on EVM.

These results are compliant with 3GPP maximum EVM value of 17.5% for QPSK and 8% for 64QAM.

B. Jitter introduced by the system

Secondly, we evaluated the jitter introduced by the system on the CPRI signal. The measured values in Unit Intervals (UI) are displayed in Table II.2. We notice that there is more jitter at the receiver compared to the measured values at the transmitter, which we believe can be attributed in part to the active components used for the wavelength locking operation in the ONU. We also observe that the measured values comply with the CPRI specification for line rates 2.45 Gbit/s and 4.91 Gbit/s. However, the maximum value is slightly exceeded at 9.83 Gbit/s. It is important to note here that the design of the WDM-PON prototype was not optimized for best timing performance. Resynchronization with an appropriate Clock & Data Recovery (CDR), absent in this prototype, would substantially improve the jitter results and should provide specification compliance also at 9.83 Gbit/s.

Table II.2: Jitter measurements at different CPRI line rates

	2.45 Gbit/s	4.91 Gbit/s	9.83 Gbit/s	Maximum values according to CPRI specification
Deterministic jitter at Transmitter (1)	58.2 mUI	139.9 mUI	192.3 mUI	170 mUI
Total jitter at Transmitter (1)	71.7 mUI	139.9 mUI	192.3 mUI	350 mUI
Deterministic jitter at Receiver (2)	103.5 mUI	199.8 mUI	383.2 mUI	370 mUI
Combined Deterministic and Random jitter at Receiver (2)	135.9 mUI	271.7 mUI	536.8 mUI	550 mUI
Total jitter at Receiver (2)	136.mUI	271.5 mUI	537.8 mUI	650 mUI

C. Fronthaul BER and synchronization

Jitter is a phase variation whose frequency components are above 10 Hz [66]. Therefore, this phenomenon could introduce errors in the transmission, if the decision regarding the signal's amplitude is not made at the correct interval in time due to the introduced phase shift [66]. Moreover, the synchronization of the User Equipment (UE) with the network can also be affected. In fact, the central clock generating the LTE frequency in the RU should be synchronized to the bit clock of the received CPRI signal. Thereby, imprecisions in the transmitted clock could influence the accuracy of the generated LTE frequency and the synchronization of the UE consequently. According to 3GPP, the most stringent requirement on LTE frequency accuracy on the air interface is ±50 ppb (Parts per Billion) for wide area base stations.

In order to verify these two potential jitter impacts, we started by measuring the BER with the CPRI test equipment. We obtained a BER < 10^{-12} for the three CPRI line rates as required in the CPRI specification. Afterwards, we measured LTE frequency deviation at the output of a commercial RU for 24 hours using 2.45 Gbit/s CPRI line rate since it was the only available line rate in commercial systems at that moment. The time interval between the measurements was set to one second. The results with respect to 2.645 GHz, the nominal LTE frequency, are depicted in Figure II-11.

We measured ±1.4 ppb when using fronthaul over dark fiber while 99.99% of the measured points using the WDM-PON system had ±2 ppb frequency deviation.

The few remaining points were up to 20 ppb certainly due to electric jitter or brief fluctuations of the optical power or wavelength. Nonetheless, these values remain below the maximal value defined by the 3GPP standard (±50 ppb). Yet again, implementing CDRs for resynchronization should improve these results.

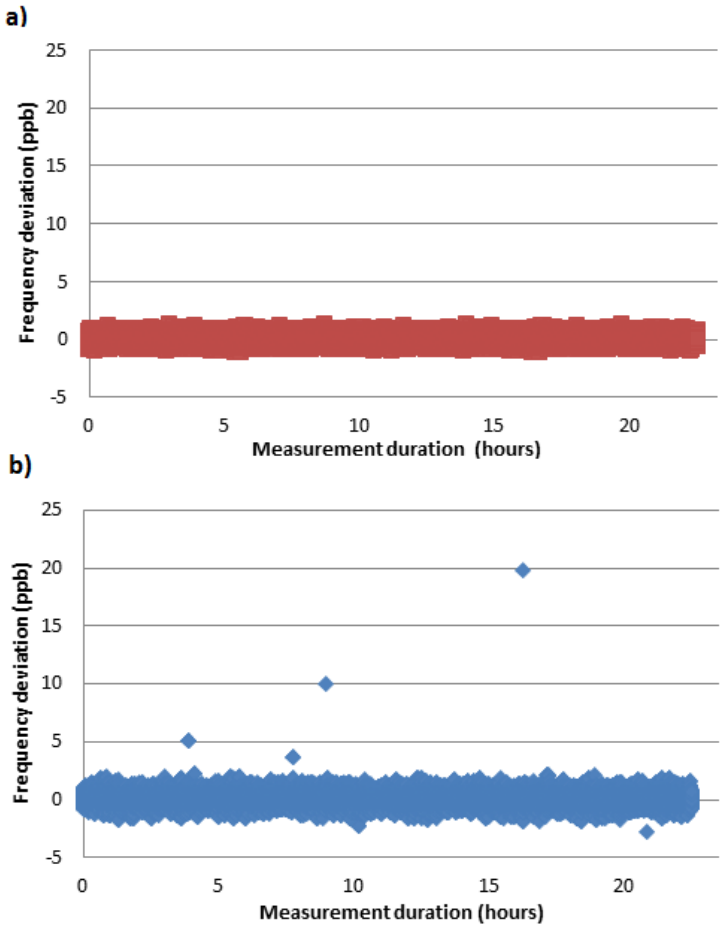

Figure II-11 : a) Frequency deviation measured at the RU output using fronthaul over dark fiber

b) Frequency deviation measured at the RU output using fronthaul over WDM-PON

D. Latency

As stated in Chapter I, latency is among the dimensioning parameters that we also need to consider. RAN vendors recommend a maximum round trip delay of 150 µs, i.e. 15 km optical fiber to allow CoMP implementation. Only 26 m are lost for the maximal fronthaul distance due to the latency introduced by the system (130 ns).

To summarize, in this subsection, it was demonstrated, by means of the evaluation of an industrial prototype, that the wavelength tunability for PtP WDM was feasible with the introduction of an over-modulation-based “AMCC-like” signal. End to end performances in terms of frame loss, EVM, jitter and frequency accuracy have been carried out in the lab and on LTE commercial fronthaul. Compliance with the 3GPP standard has been shown with the need of few adjustments on the system.

II.2.1.4. OAM via RDDMI

As stated in the introduction of this subsection, PtP WDM is expected to transport optical infrastructure monitoring data as well. A sophisticated solution to achieve this monitoring is to make advantage of the Digital Diagnostic Monitoring Interface (DDMI) provided by the SFPs. In fact, DDMI is an interface common in the SFPs following the specifications of SFF-8472

published by the Small Form Factor (SFF) committee. It allows a real-time access to the device operating parameters. It provides information about temperature, supply voltage, transmit bias current, transmitted and received powers. Therefore, the idea is to convey this data through the AMCC channel investigated in II.2.1.2. This idea can also be applied in a CWDM single-fiber transport solution which is lacking monitoring too, as stated in Chapter I. The solution is shown in Figure II-12.

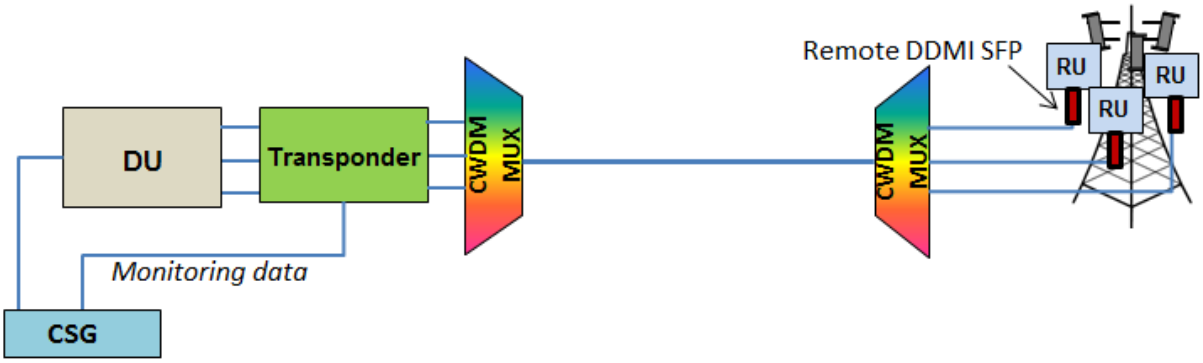

Figure II-12 : RDDMI solution for WDM monitoring

In this architecture, called semi active, there is no need for active equipment at the antenna site. RDDMI SFPs (also called smart SFPs) are used in each RU where the monitoring data provided by the DDMI are sent by means of a baseband over-modulation (according to the manufacturer). At the reception in the central office, a transponder is used to retrieve the monitoring data before sending it in the aggregation network through the Cell Site Gateway (CSG). It will be received by the fixed operator supervision center. An experimental evaluation of a prototype of this solution has been carried out and the results were compared to the measured performances of a mono-fiber SFP CSC (presented in Chapter I) from the same manufacturer with similar specs (bandwidth, optical budget). .

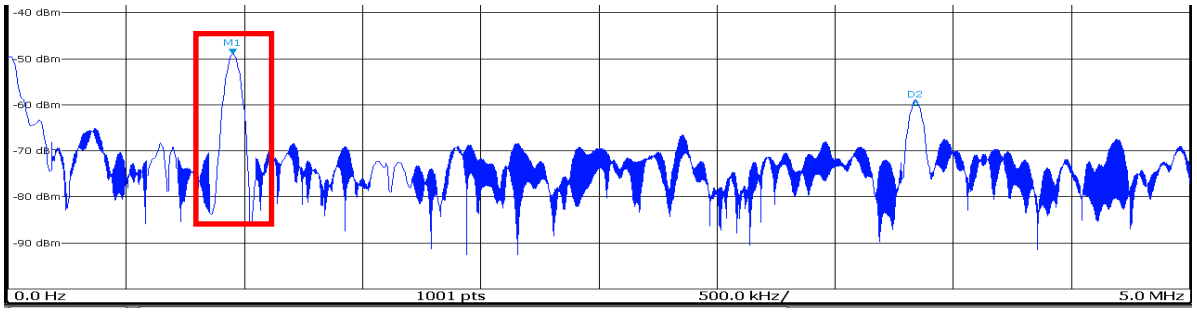

Figure II-13 : Pilot tone on RF spectrum

Figure II-13 shows a screenshot of the RF spectrum of the signal transmitted by the RDDMI SFP after retrieving the CPRI signal. The inserted Pilot tone is then at 954 KHz with a RF power level of -48 dBm.

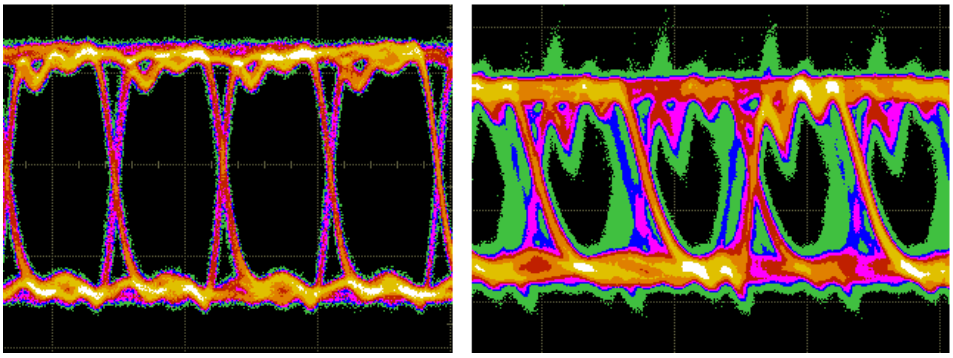

Figure II-14 : (a) Eye pattern of a CSC SFP (b) Eye pattern of a RDDMI SFP

Figure II-14 depicts the eye diagram of a CSC SFP and a RDDMI SFP. As noticed in Figure II-5 and Figure II-10, the introduction of a pilot tone brings noise to the CPRI signal which causes the closing of the eye vertically (EVM degradation) and horizontally (added jitter).

Table II.3 : EVM measurements with SFP RDDMI and SFP CSC for different received optical power levels

	EVM (%)	
P(dBm)	SFP RDDMI	SFP CSC
-3,64	0,06	0,06
-15,36	0,06	0,06
-17,49	0,3	0,24
-18,4	19	16,8

EVM measurements were done with RAN test equipment to compare the SFP's performance with and without pilot tone for different received optical power. The obtained results are shown in Table II.3. Similar EVM values were measured with and without pilot tone for optical power levels up to -15.36 dBm. The SFP RDDMI will most likely present less optical budget compared to the SFP CSC which could have been demonstrated with finer measurements (by taking smaller power variation steps). This was not done due the limited time frame allocated to this industrial evaluation.

In this subsection, it was shown that the monitoring of the fronthaul infrastructure (CWDM or PtP WDM) can be achieved thanks to the transmission of the DDMI data via a pilot tone with minor impact on the CPRI and LTE performance. This, in addition to the wavelength tunability, makes PtP WDM a complete solution of fronthaul allowing the transport of up to 40 CPRI links.

In the core network, where the use of WDM is very common, the use of solutions like Optical Transport Network (OTN) to increase the number of bands per wavelength is prevalent. An

investigation is done in the next subsection on the use of this technology in mobile access networks.

II.2.2. Time division multiplexing

OTN was standardized by the ITU-T under the recommendation G709 [67]. It specifies a digital wrapper to create Optical Data Units (ODU) by encapsulating different frames of data regardless of their native protocol. It also provides Operations, Administration, Maintenance, and Provisioning (OAM&P) functionalities and a forward error correction (FEC) mechanism. This permit wrapping frames from different protocols together into a single entity that can be reliably transmitted and efficiently managed in a multi-wavelength system. Building an OTN container goes through different levels of encapsulation as shown Figure II-15. The data of the client is mapped into Optical Payload Units. Depending on their data rate, an OPU is mapped in an Optical Data Unit (ODU) or multiple OPUs are multiplexed in an ODU. The ODUs are in the same way mapped or multiplexed in Optical Transport Units (OTU).Table II.4 shows the data rates of these units [68].

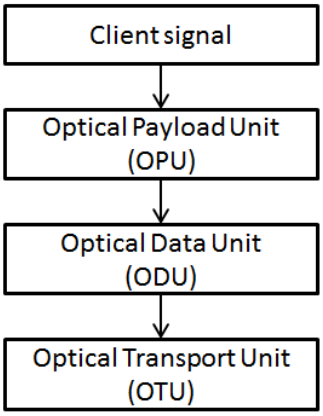

Figure II-15 : OTN encapsulation levels

CPRI mapping over OTN has been recently included in the ITU-T supplement 56 of the G-series [70]. CPRI options 1 to 3 are specified to be mapped into an OPU via the generic mapping procedure while CPRI options 4 to 8 shall be mapped into an OPU via the bit-synchronous mapping procedure [70]. OPU2r was defined as a new container for either 6 CPRI3 signals (6x2.457 Gbit/s) or 3 CPRI4 signals (3x3.072 Gbit/s) or 3 CPRI5 signals (3x4.915 Gbit/s). The OTU2r frame structure may or may not include a FEC mechanism.

Table II.4 : Data rates of the OTN containers (Gbit/s)

	Data rates (Gbit/s)		
Level of the OTN container	OTU	ODU	OPU
0	-	1.24	1.23
1	2.66	2.49	2.48
2	10.79	10.03	9.99
3	43.01	40.31	40.15

Transporting CPRI over OTN presents a challenge especially because of the jitter and also latency potentially introduced by the mapping and de-mapping of CPRI in OTN frames. Some investigation elements were brought in [69] where the authors compared the performance of OTN, passive and active WDM for the CPRI transport. In this context and in order to have a better understanding of this solution, an experimental evaluation has been carried out on an industrial prototype (cf Figure II-16).

The evaluated prototype permits the encapsulation of 3 option 3 CPRI signals (3x2.45Gbit/s) and 2 Ethernet signals at 1 Gbit/s (2x1GEth) in one wavelength at 10 Gbit/s. It provides a converged transport solution for backhaul and fronthaul. The optical transmission is done with uncolored SFPs on the client interface and with colored XFPs (larger form factor than SFP, used originally for 10Gb/s transmission before emergence of SFP+) on the line interface. This also allows removing the burden of wavelengths management for the mobile network operator.

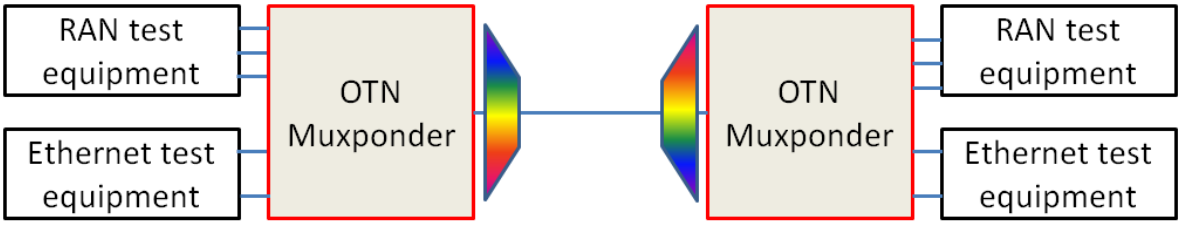

Figure II-16 : OTN experimental setup

After 2 days running traffic, no errors occurred in the Ethernet transmission and the CPRI transmission had a BER of 10^{-15} which is compliant to the CPRI specification. Using the RAN test equipment, the one-way latency measurements showed 28.87µs in the downlink and 28.9µs in the uplink. The one-way latency tolerated in the fronthaul link is 75 µs corresponding to the propagation in 15 km optical fiber. With this OTN equipment, the latency budget would be limited to 46.13 µs corresponding to the propagation in 9.2 km optical fiber. The latency imbalance between the uplink and downlink could also be an issue of the CPRI transport over OTN. Indeed, the 3GPP limited its end-to-end value to ±163 ns, only ±16 ns were specified by RAN providers for the fronthaul segment. The measurements showed 30 ns of latency imbalance with the used metrology equipment. The accuracy of the used metrology equipment being +/-10 ns, this measurement must be done with more accurate metrology equipment for confirmation.

Jitter measurement were also performed, the results are depicted in Table II.5. Much jitter was introduced by the OTN equipment exceeding the maximum value defined by the CPRI specification. This will have an impact on the RU synchronization since the central clock responsible for the frequency generation in the RU is synchronized with the clock of the CPRI signal. Simulation analyses of such jitter issue were performed by ITU-T [70] showing that to meet the 2 ppb defined by the CPRI specification, stringent desynchronizer (Phase Locked Loop – PLL) bandwidth is required, much lower than 300 Hz normally used in OTN. In order to be compliant to the specification, it is needed to redesign the OTN equipment with very stable oscillators and sharp filters. More details on this analysis are brought in the ITU supplement [70].

Table II.5 : Jitter measurement on OTN equipment

	Measured values without muxponders	Measured values with muxponders	Maximum values (CPRI specification)
Deterministic jitter	0.91 UI	0.11 UI	0.37 UI
Combined deterministic and random jitter	1 UI	0.14 UI	0.55 UI
Total jitter	1 UI	0.14 UI	0.65 UI

The use of OTN to transport CPRI will turn out to be very expensive, especially for access networks where the number of needed equipment is tremendous. On the other hand, PON systems also based on TDM, are very much appreciated in this network segment. Studies have been done on this subject [71] [72] [73]. The obtained results were promising thanks to the used of low latency dynamic bandwidth allocation (DBA) algorithms and CPRI compression (discussed in Chapter IV). However, the number of connected ONUs per PON is still unsatisfactory in these works. Nevertheless, the use of TDM over multiple wavelengths as specified in the TWDM flavor of NG-PON2 would permit connecting an interesting number of ONUs.

The use of PON systems would require the packetization of the CPRI signal in Ethernet frames which is a whole other problematic. It was actually initiated at first to leverage the current backhaul equipment and to achieve statistical multiplexing thus to optimize the transport resources. The latter can be done only on load-dependent traffic which is not the case of CPRI. Initiatives were therefore done to enable the multiplexing of backhaul and fronthaul on the same physical link which required some improvement on the Ethernet standard.

In this context, an IEEE Task Group on Time Sensitive Networking proposed standard for time-sensitive data transmission over Ethernet with very low latency and high availability. Notably, IEEE 802.1 CM defined a standard network profile for the fronthaul segment and IEEE 1904.3 defined an encapsulation of Radio over Ethernet (RoE). Recently IEEE 1914.1 defined the next generation of fronthaul interface based on new functional splits which is investigated in Chapter V.

II.2.3. Remote powering

Always in the context of integrating the fiber-based fronthaul in the network, an investigation was done with the energy team of Orange Labs on a remote powering solution. In fact, in the case of a massive deployment of micro and small cells to extend radio coverage and capacity, providing power supply to all the antenna sites in the traditional way will turn out to be very pricy. Indeed, the cost of connection to the power supplier and the subscriptions as well as the onsite batteries maintenance is going to drastically increase. The proposed solution is shown in Figure II-17; it allows providing power to the RUs from a centralized energy source which is compliant with the C-RAN concept also aiming to simplify the antenna sites.

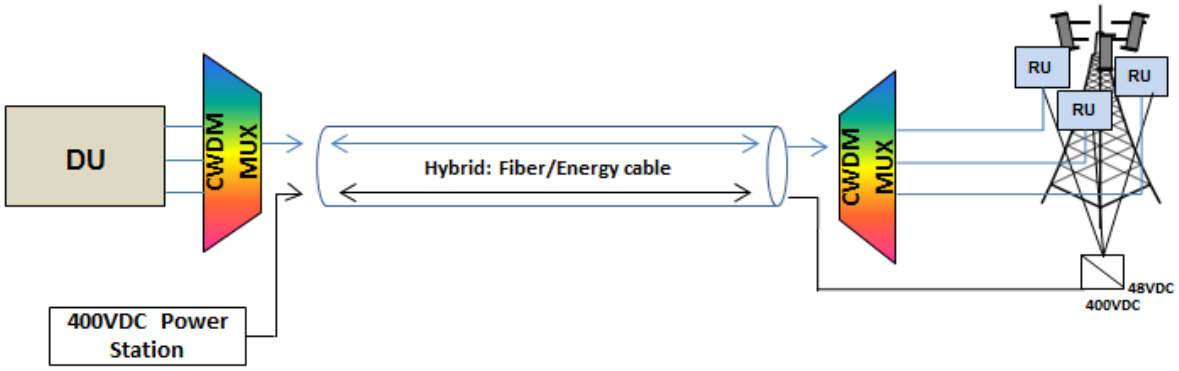

Figure II-17 : Remote powering solution

In this solution, 400 VDC power is remotely provided from the central office through a hybrid energy/optical cable or through a classic energy cable if the fiber is already deployed. A picture of a hybrid cable is depicted in Figure II-18. The copper pair section can go from 1.5 mm² to 25 mm² depending on the cable length and the power need on the antenna site. The higher the current, the thicker the cable and the higher the cable cost. For instance, a micro site comprising 3 RUs consuming 350 W each can be remotely powered with 4 km reach using 6 mm² section cables. The calculations were published by the Orange Labs energy team in [74]. In the antenna site, there is no need for rectifiers and batteries onsite, only 400 VDC to 48 VDC converters are needed. In the future, these converters can be embedded in the RAN equipment which will facilitate the deployments. The published economic study [74] on this solution showed up to 16% cost reduction with respect to the traditional local powering. This solution can be used also to power up active equipment in the fronthaul. Notably, an experimental investigation of wireless transmission of CPRI was carried out and reported in the following section where the powering of the wireless fronthaul equipment (WFE) was done with this remote powering solution.

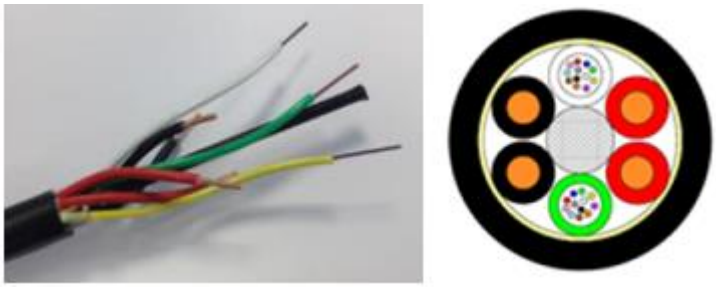

Figure II-18 : Picture of a hybrid energy/optical cable (left) Example of a cable with 2 copper pairs and 4 optical fibers (right)

II.3. Wireless fronthaul

A major problem encountered in the fronthaul deployment is the occasional complication in the fiber deployment, due to obstacles such as highways or rivers or to difficulties to access to the buildings. A wireless transmission of the CPRI signal can therefore be interesting. Giving the CPRI bit-rates (2.5 Gbit/s to 10 Gbit/s per link), however, the wireless transmission can be challenging since it will require very large bandwidths. The use of cmWaves (3 GHz to 30 GHz band) or mmWaves (30 GHz to 300 GHz band) will therefore be

mandatory since it is the only bands offering such bandwidths, unless an optimization is done on the CPRI signal before the wireless transmission. To our best knowledge, few investigations were done on the wireless fronthaul but only on the analog RoF based fronthaul [76] [77] [78]. Thus, no work has been done on the transport of CPRI over wireless.

Two approaches were experimentally investigated in this subsection. An evaluation of wireless fronthaul equipment operating in the e-band (60 – 90 GHz) was carried out; the experimental results are reported in sub-section II.3.1. Moreover, the evaluation results of the wireless fronthaul equipment with optimized spectral efficiency (operating in the sub-6 GHz spectrum) are exposed in sub-section II.3.2.

II.3.1. Solution without enhanced spectral efficiency

The evaluated solution permits a transparent transport of a CPRI 3 signal while conserving the integrity of the CPRI frame. It transmits the signal over a 500 MHz bandwidth in the E-band (71 GHz - 76 GHz / 81 GHz – 86 GHz) using a 64 QAM single carrier modulation. The latter consists in transmitting 6 bits per symbol and thus transmit the CPRI signal in 500 MHz bandwidth. Figure II-19 shows screenshots of spectrum analyzer measurements at the output of the wireless fronthaul equipment in which we see the 500 MHz bandwidth signal at both frequencies (73.3 GHz and 83.3 GHz). Filtering has been done to eliminate the secondary lobes of the signal, thus allowing compliance with the spectrum mask defined by the ETSI [79], also shown in Figure II-19.

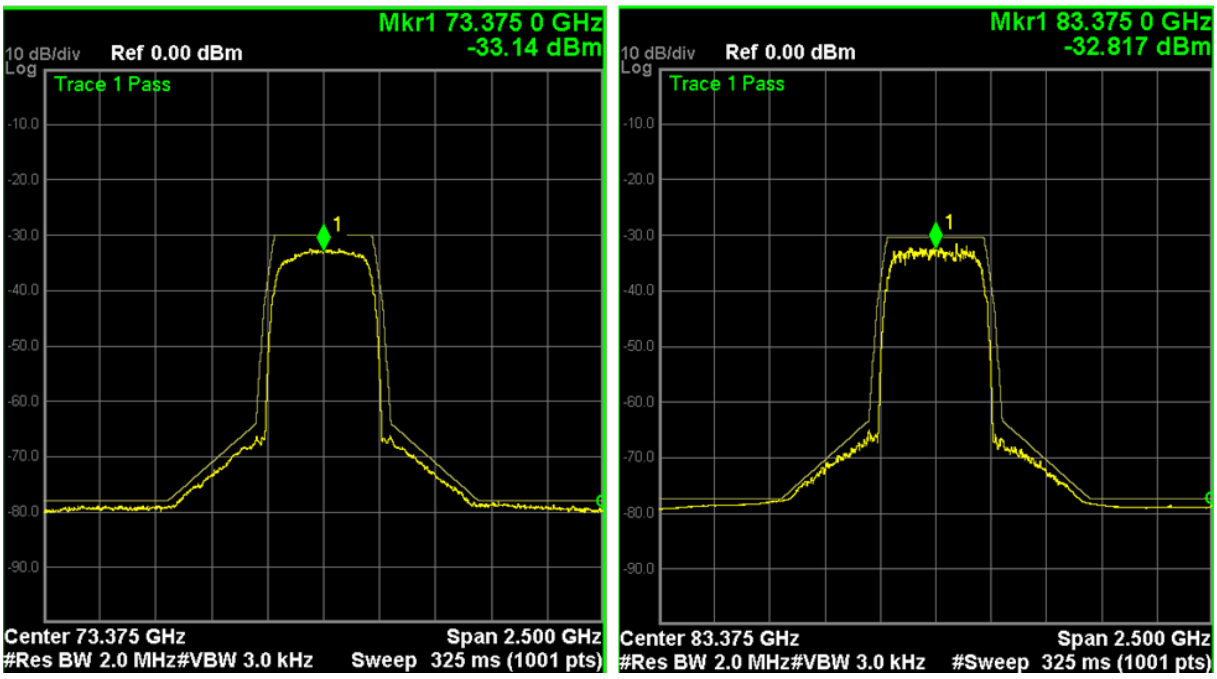

Figure II-19 : Spectrum of the wireless fronthaul signal at 73.37 GHz (left) and 83.37 GHz (right)

As shown in Figure II-20, EVM measurements were also done by connecting the transmitter and the receiver of the Wireless Fronthaul Equipment (WFE) using a waveguide adapted to operate in this frequency range. A RF variable attenuator is then used to evaluate the sensitivity of the WFE. The transmit power of the latter is +12 dBm, which is the maximum possible value with this equipment.

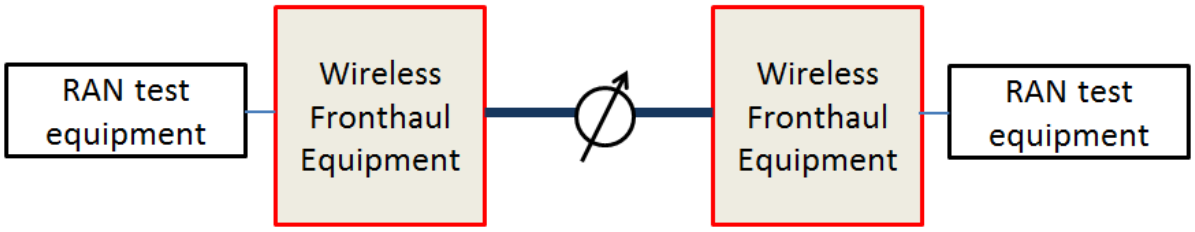

Figure II-20 : WFE evaluation experimental setup

The measurements were done with a RAN test equipment transmission LTE signal with 20 MHz bandwidth 2x2 MIMO and 64QAM modulation.

The 3GPP requirement for this configuration is 8% EVM, only 3% is taken for the lab evaluation to have 5 points margin for the possible degradation in the RU due to amplification. The obtained results are shown in Figure II-21.

Similar results were obtained for both frequencies; the reach of the transmission will however depend on the used frequency and also on the weather conditions. The E-band transmissions are known to be sensitive to rain, leafs and such.

A latency measurement was also performed with the RAN test equipment in order to determine the signal processing delay introduced by the WFE. We measured 12.5 µs without the transmission over the air. Knowing that the recommended value by RAN vendors is 75 µs, 12 km is the distance of optical fiber left for the wireline segment of the fronthaul link (instead of 15 km without WFE).

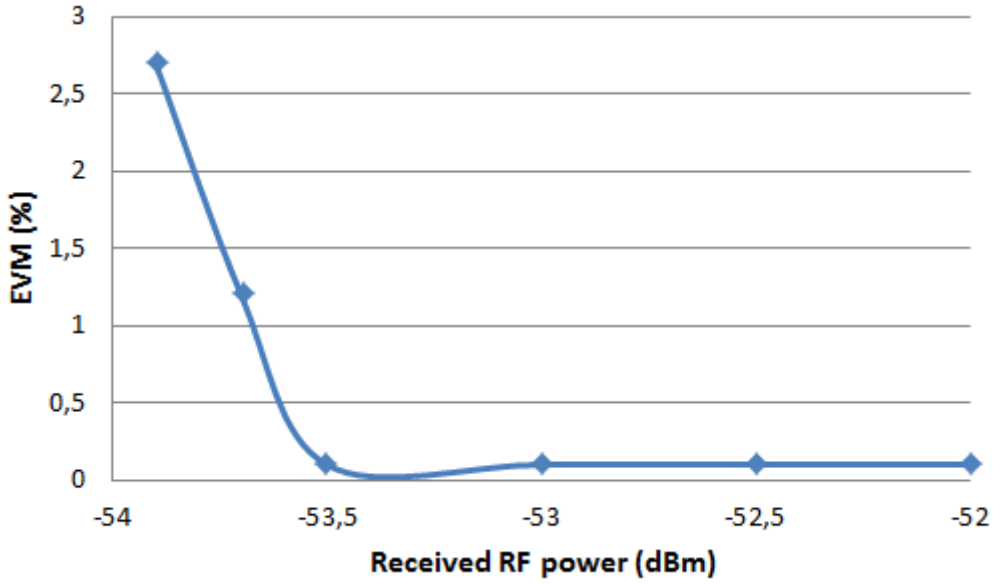

Figure II-21 : EVM (%) vs Received optical power in the WFE (classic solution)

II.3.2. Solution with enhanced spectral efficiency

As said before, the transmission of CPRI signals over wireless channels can be challenging mainly because of CPRI's poor spectral efficiency. QAM modulation used in the previous solution allowed improving the spectral efficiency of CPRI by a factor 6. This permitted a

transmission over 500 MHz bandwidth (only available in the E-band). The transmission in these frequencies is known for being fragile to weather conditions and also the components used for such systems are costly. In order to be able to transmit in lower frequencies where less bandwidth is available, further spectral efficiency optimization must be done. A first approach would be to perform a compression on CPRI before wireless transmission, this approach was not investigated for wireless but CPRI compression results are reported in Chapter IV. Another approach would be to use more advanced modulation technics (like OFDM) which are more appropriate for wireless transmissions. In this subsection, an experimental investigation is done on WFE with enhanced spectral efficiency. The principle of the solution can be summarized as follows: after separating the Control and Management (C&M) data from the IQs in the CPRI signal. The C&M data is M-QAM modulated and transmitted via a dedicated channel. The IQs are transformed close to their original form (Orthogonal Frequency Division Multiplexing, OFDM) which permits transmitting the signal in 20 MHz bandwidth. This operation would be equivalent to “going backwards to LTE”. The IQs of 2 other CPRI links are transformed to OFDM as well before aggregation using Frequency Division Multiplexing (FDM) [75]. The obtained signal is transmitted in the 5.8 GHz bands (unlicensed).

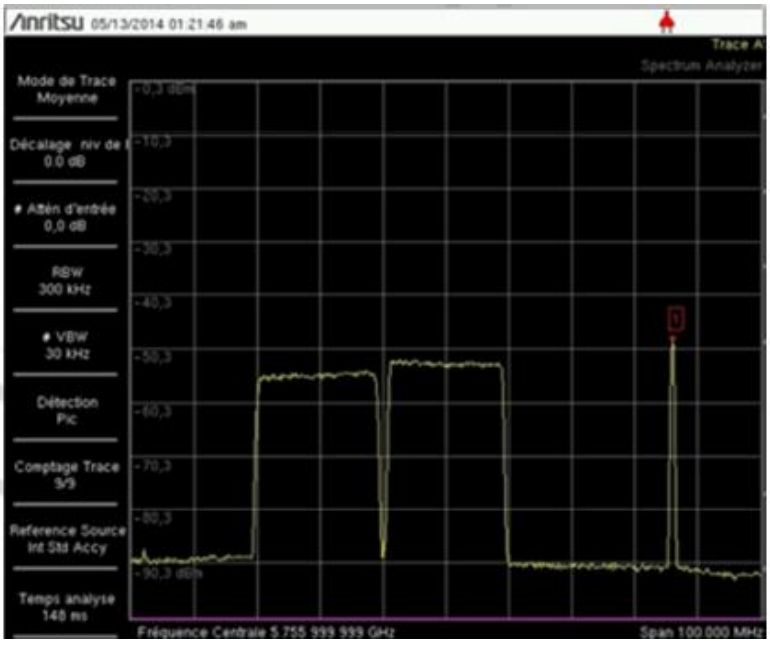

Figure II-22 : Spectrum of the wireless fronthaul signal at 5.75 GHz

An experimental evaluation (similar to the one shown in Figure II-20) was carried out on an industrial prototype. Figure II-22 shows the measured spectrum at the output of the WFE. The signal is effectively transmitted over 20 MHz bandwidth. 2 bands are measured since the generated LTE signal is in 2x2 MIMO. Also, on the right-hand side of the spectrum we can see the C&M channel.

As for the previous solution, the sensitivity of the WFE was evaluated by measuring the EVM values at the output of the RU test equipment for different levels of RF attenuation in the wireless fronthaul segment. For this measurement, the transmitter and the receiver of the WFE are connected with the appropriate waveguide. Figure II-23 shows the obtained results.

The EVM threshold is 3% as for the previous experiment. Thus, we obtain a sensitivity of 60 dBm.

The latency introduced by the system has been measured as well, the obtained value in 9 µs, which is lower than the value obtained in the previous solution (WFE without spectral efficiency optimization) despite the fact that the cards used in this solution contain more digital signal processing operations.

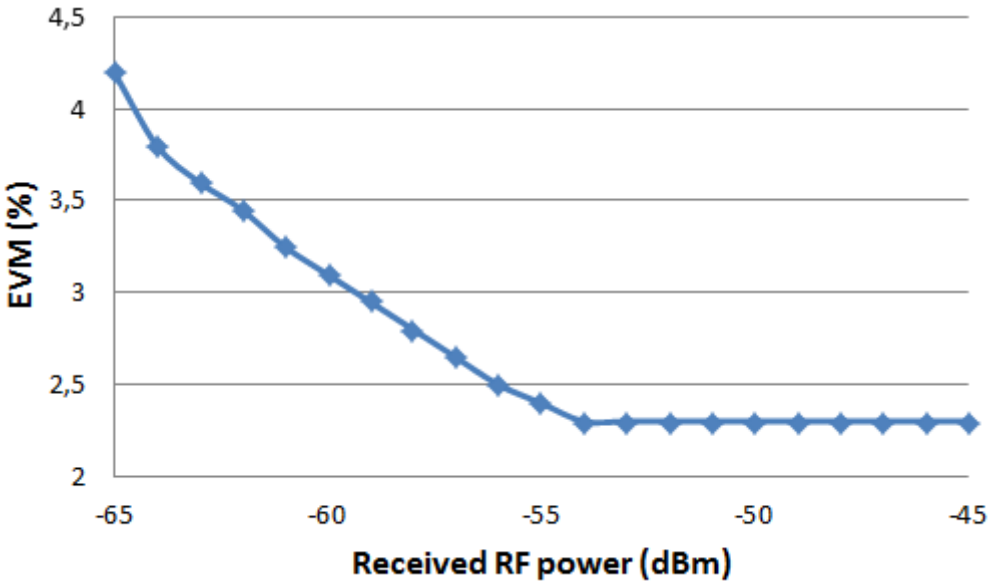

Figure II-23 : EVM (%) vs Received optical power in the WFE (enhanced spectral efficiency)

In order to further investigate the performance degradations that might be caused by this technology and also to demonstrate the solution to other Orange Labs teams, an outdoor experimentation has been carried out using this WFE and the remote powering solution explained in II.2.3.

The experimental setup is shown in Figure II-24. At the transmitter side, a LTE signal is generated by a signal generator then converted to CPRI using an IQ box. These two components emulate the DU at first before using a commercial DU to confirm the measured values. Standardized E-TM3.3 LTE test model is used with 20 MHz carrier bandwidth. We test the CPRI at 2.457 Gbit/s in the downlink direction.

CWDM multiplexors are placed after the DU transmitter and before the RU. The fronthaul link includes 5 km of fiber and a wireless Over the Air (OTA) section of 110 m, the Wireless Fronthaul Modules being set outdoor in Point-to-Point Line of Sight and remotely powered. The optical transmission is done with bidirectional single mode SFPs offering 23 dB of optical budget for a bit error rate of 10^{-12}. At the receiver side, an IQ box is used to convert the CPRI to LTE before analysis with a Signal Analyzer (SA). After a photodiode, a Digital Storage Oscilloscope (DSO) allows measuring the jitter on the electric signal at the transmitter and at the receiver.

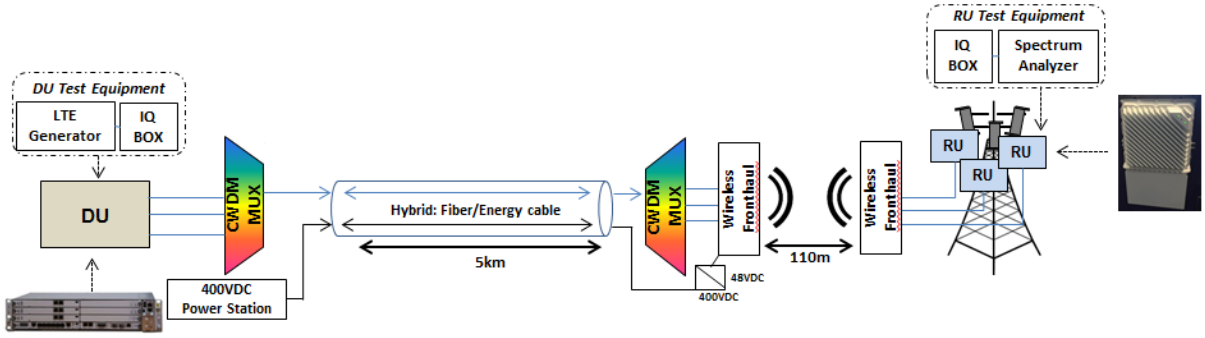

Figure II-24 : Experimental setup (wireless fronthaul with remote powering)

Finally, the SA permits to measure the frequency accuracy budget of the CPRI. Moreover, a frequency accuracy measurement of the LTE signal is performed with the SA at the output of a commercial RU operating in the 2.6 GHz band.

We investigated the transmission performance from three aspects: jitter, CPRI frequency accuracy and LTE frequency accuracy.

First, we investigated the jitter introduced by the WFE. As depicted in Table II.6, some jitter is introduced in the link when introducing the WFE in the fronthaul link. Nevertheless, the measured jitter respects the CPRI specification. Similar results were obtained when performing the measurement on commercial RAN equipment.

Table II.6 : Jitter measurements for combined optical fiber and wireless fronthaul with and without transponders

	Measured values	Maximum values according to the CPRI specification
Deterministic Jitter at Transmitter	0.11 UI	0.17 UI
Total Jitter at Transmitter	0.12 UI	0.35 UI
Deterministic Jitter at Receiver	0.11 UI	0.37 UI
Combined Deterministic and Random Jitter at Receiver	0.14 UI	0.55 UI
Total Jitter at Receiver	0.14 UI	0.65 UI

As stated before, the introduced jitter could have an impact on the RU synchronization. Indeed, the central clock responsible for frequency generation in the RU is synchronized with the clock of the CPRI signal. Therefore, inaccuracies in the transmitted clock could affect the precision of the generated LTE frequency thus the synchronization of User Equipment (UE). According to 3GPP, the most stringent requirement on LTE frequency accuracy on the air interface is ±50 ppb for wide area base station. The maximum contribution of jitter from the CPRI to the base station frequency accuracy budget is limited to ±2 ppb conforming to the CPRI specification.

We started by investigating the CPRI frequency accuracy in the fronthaul segment with and without WFE. The CPRI Frequency Deviation (FD) remains practically stable between the transmitter and the receiver in the case of optical fiber fronthaul (without WFE) while we notice a FD difference of 0.4 ppb between the transmitter and the receiver when adding a

wireless section. The measurement results are presented in Table II.7; the measured FD at the reception (±1.13 ppb) respects the maximum value defined by the CPRI specification (±2 ppb). Similar results were obtained when performing the measurement on commercial RAN equipment.

Table II.7 : Frequency deviation at the output of the transmitter (DU Tx) and at the input of the receiver (RU Rx)

Optical fiber fronthaul		Combined optical fiber and wireless fronthaul		Maximum value according to the CPRI specification
DU Tx	RU Rx	DU Tx	RU Rx	
±0.73 ppb	±0.78 ppb	±0.73 ppb	±1.13 ppb	±2 ppb

Finally, we measured LTE FD at the output of a commercial RU with respect to nominal LTE frequency. As represented in Figure II-25, we measure ±3.8 ppb FD with the proposed architecture while we obtain ±1.4 ppb when using dark fiber. The results respect the 3GPP standard that limits the maximum FD value of LTE at ±50 ppb.

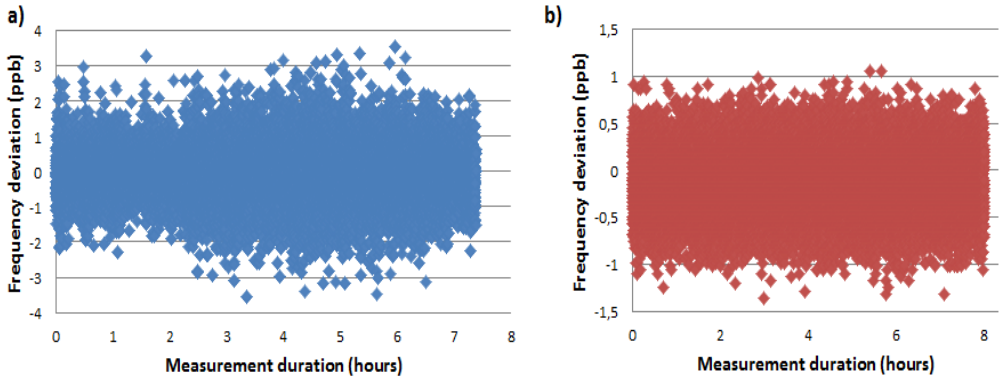

Figure II-25 : a) Frequency deviation measured on RU radio output using fiber plus wireless fronthaul
b) Frequency deviation measured on RU radio output for reference

Accordingly, the performed measurements showed that the introduction of the WFE with optimized spectral efficiency comes with some performance degradations but within the permitted range by the 3GPP standard and the CPRI specification.

II.4. Conclusion

In this chapter, an experimental investigation, mainly based on industrial prototypes evaluations, was done on fiber and wireless CPRI-based fronthaul. The introduction of pilot tones in WDM permitted to achieve wavelength tunability and monitoring with minor impact on the CPRI and LTE performance. The use of time multiplexing in addition to WDM turned out to be, after experimental study, latency consuming and costly with poor added value, especially in view of the improvements brought to WDM (AMCC, optical channels subdivision).

The use of remote powering seemed to be a promising solution to decrease the energy costs of the mobile networks while being compliant with the C-RAN architecture. It is based on the

use of hybrid energy cable/optical fiber and 400 VDC energy supply which was experimentally demonstrated.

Wireless transmission can also be used for CPRI transport when it is complicated to have access to optical fiber. It can be done over mmWaves with a simple QAM modulation on the CPRI signal or in the sub-6GHz frequency bands by performing a multi-carrier modulation on the CPRI signal. In both cases, some performance degradations are introduced but within the limits allowed by the standard (3GPP, CPRI).

This chapter demonstrated the feasibility of the CPRI-based fronthaul integration using appropriate solutions for access networks. The obtained results were valorized by the publication of four articles in national and international conferences (JNOG, OFC, ECOC, EuCNC, cf. appendix A).

Optical fiber solutions are based on transceivers allowing 20 km transmission as required in Chapter I and a bit-rate of 25 Gbit/s which is largely satisfactory for the transport of LTE interfaces but unlikely for 5G interfaces. As mentioned in Chapter I, the CPRI bit-rate scales with the MIMO order and bandwidth of the radio signal. Thus, enormous traffic will need to be transported from the central office to the antenna sites jeopardizing the cost limits of access networks. Therefore, solutions enhancing the CPRI spectral efficiency will need to be provided to enable the transport the 5G interfaces over the access networks.

Chapter III. Mixed Analog & Digital RoF

III.1. Introduction

While Digital RoF provides increased robustness to optical noise and thus better receiver sensitivities, it is known for its inherently poor spectral efficiency. Indeed, each sample of the mobile signal is digitized with a high number of bits (e.g. 15 for CPRI) in order to reduce the impacts of quantization noise on the radio signals. For instance, a 20 MHz bandwidth downlink LTE signal in 2x2 MIMO configuration can provide a maximum bit-rate of ~150 Mbit/s in the radio front but will require 2.5 Gbit/s in the fronthaul link. Also, bit-rates scale with the number of sectors, antennas (if spatial diversity or multiplexing is adopted), radio access technologies (2G, 3G,4G…) and frequency bands of a mobile site; therefore, very high bit-rates need to be transported between the central office and the antenna site.

Whereas the use of WDM can alleviate the CPRI bit-rate burden for LTE, it will surely not be enough to enable the capacities expected in 5G if the current D-RoF approach is maintained. Several solutions are identified to tackle this issue, such as the compression of the fronthaul signal thanks to intelligent quantization algorithms which will be reported in Chapter IV, the transposition of some radio protocol layers from the DU to the RU with different functional splits which will be discussed in Chapter V and the transport of mobile signals in their native modulation format or other non-binary modulation scheme through analog radio over fiber (A-RoF) which is the focus of this chapter.

A-RoF has been studied for the past decades but actual deployments have targeted a restricted number of applications such as indoor scenarios (buildings, stadiums, subway stations, etc.). Analog Distributed Antenna System (DAS) is a typical example of such application. For instance, in the downstream DAS link (Figure III-1), RF signals from the RUs are power adjusted and aggregated before directly modulating a laser (DML). After propagation, the signal is converted back to the electrical domain with a photodiode at a remote note and eventually split before being fed to one or multiple indoor antennas. While analog DAS has the merit of enabling a neutral (multi-carrier, multi-frequency) indoor distribution infrastructure, it faces, however, the same challenges as any A-RoF transmission, namely i) the conditioning of the signals needed to avoid degradations during RF aggregation; ii) the limits imposed by optical noise and its impact on the receiver sensitivity; iii) the potential nonlinear conversions on the transmission chain, which could give rise to in-band and out-of-band noise and finally iv) the RF power constraints of electrical/optical devices and the limitations they impose to the signal-to-noise ratio (SNR) of the system as we increase the bandwidth of the transmitted signal.

In this chapter, an architecture mixing A-RoF/D-RoF is proposed. It would allow leveraging preexisting DAS infrastructures by pushing back the need of a migration into a WDM solution

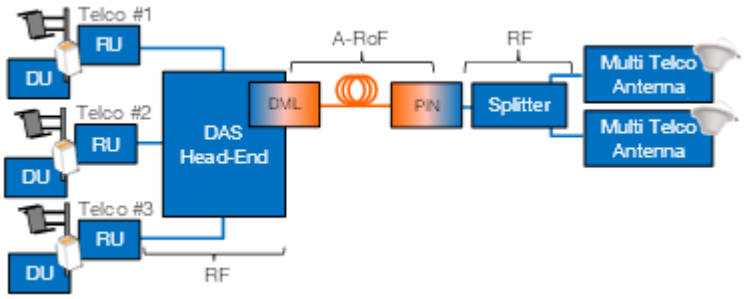

Figure III-1 : Analog DAS

thanks to a more spectrally efficient transmission while guaranteeing, at the same time, full compatibility with currently deployed RAN equipment. Offline A-RoF RAN schemes with more or less complicated optics have been reported in [80], [81] and a CPRI-compatible, real-time system capable of transporting 53 Gbit/s CPRI-equivalent data was recently shown in [82]. The proposed downlink scheme shown in Figure III-2 has twice the spectral efficiency of the scheme reported in [82]. The CPRI signals coming from different DU hotels (different mobile operators at different distances) are D-RoF to A-RoF converted at an SFP compatible Head-End. The A-RoF signal, composed of a group of bands, then directly modulates a DML. After propagation, the received A-RoF signal is directly detected at the remote unit and converted back to D-RoF. This CPRI signal can thus be transparently used with a RU of any specific operator. The proposed C-RAN compatible architecture would also enable access to transmission performance indicators at the antenna premises, and per-operator management/evolution of the radio front. Contrary to the distributed RAN architecture reported in [83] and since the DU signals that are collected at the Head-End are standard CPRI signals, the A-RoF signal is created from scratch, i.e., the system will not suffer from any degradations related to conditioning of received signals during aggregation. This feature also allows RF power to be more easily set to enable linear operation of the DML.

In this chapter, a real-time demonstration of the proposed architecture is provided with up to 9 x 10 MHz MIMO 2x2 downlink LTE signals corresponding to an equivalent fronthaul bit-rate of 11.05 Gbit/s (9 x CPRI 2) and using less than 200 MHz of an off-the-shelf DML bandwidth. In order to address the previously mentioned challenges of an A-RoF transmission, an investigation is also done on the robustness of the proposed system to optical noise. The compromise between SNR and the bandwidth of the A-RoF signal is therefore assessed. The nonlinear noise power spectrum density brought by the optical transceiver is also experimentally investigated. Moreover, a nonlinear model is used to assess by means of simulations some of the nonlinear phenomena observed experimentally. Those three points ultimately allows us thus to find an optimal balance between optical noise, RF power constraints and nonlinear conversions in order to provide a realistic estimative of the maximum number of CPRI signals that could be A-RoF transmitted with a specific off-the-shelf laser while respecting specific end-to-end error vector magnitude (EVM) constraints.

The rest of this chapter is organized as follows. In section III.2, an experimental study is performed in the linear domain where we focus on the limitations caused by the optical noise and the RF power constraints of the laser. In section III.3, an analysis of the nonlinear effects generated by the laser is carried out; experimentations are done and complemented by simulation analyses. Finally, the conclusion of the chapter is in section III.4.

III.2. Impact of Optical Noise and RF Power Constraints

The great advantage of an A-RoF transmission compared to D-RoF lies in its increased RF

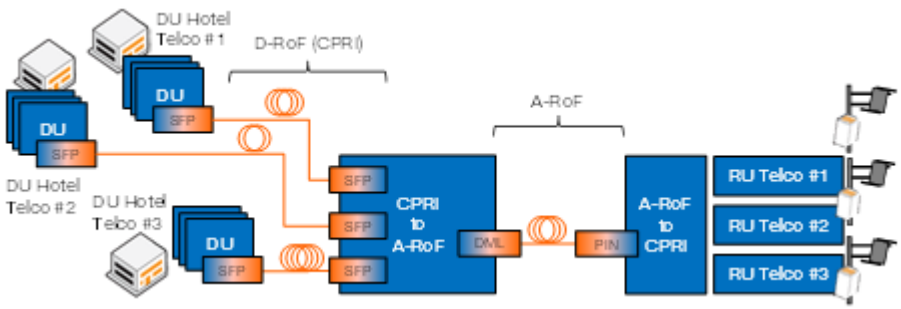

Figure III-2 : Proposed mixed A-RoF/D-RoF architecture

spectral efficiency. An a priori analysis would give us a ~60-fold increase on the number of signals that could be A-RoF transmitted taking the bandwidth of one single D-RoF signal as reference. For instance, if we consider a 10 MHz downlink LTE single-input single-output (SISO) signal, we would need an optical transmitter with at least 614.4 MHz bandwidth to accommodate CPRI 1 data. Up to 58 IF-transposed LTE signals could be transmitted in their native modulation format within the same bandwidth considering 500 KHz spacing between them. However, this value represents only a higher bound on the real spectral efficiency of an A-RoF transmission. This is because an actual A-RoF transmission is subjected to the power constraints on both electronic (ADC, amplifiers) and optical devices (emitter and receiver) of the transmission chain. In this section, an experimental study is conducted in order to define the actual number of RF bands that could be transmitted while keeping a linear functioning of the laser and the ADC. The spacing between the transmitted RF bands is fixed to 500 KHz in this section. The preliminary setting on the different setup's components concerning their optimum operating are also reported.

III.2.1. Experimental setup

Figure III-3 shows a block diagram of the performed experimental setup and a picture of the actual experimental platform is depicted in Figure III-4. A signal generator creates a source CPRI 2 (1.23 Gbit/s) sequence corresponding to a 10 MHz, downlink LTE signal with MIMO 2x2 configuration. An optical splitter allows replicating this signal (inset A in Figure III-3) before transmission it over different lengths (5, 10 and 15 km) of standard single mode optical fiber (SSMF) in the D-RoF portion of the network. We used off-the-shelf mono-fiber SFPs in the D-RoF links. Using an FPGA developed by an industrial partner, D-ROF to A-ROF conversion is carried out: CPRI data corresponding to the IQ time-domain samples are converted into two (one for each antenna) orthogonal frequency division multiplexing (OFDM) bands with 10 MHz each, which are digitally transposed to an intermediate frequency (IF) [84]. CPRI control and management (C&M) data is transported separately at 240 MHz. An additional operation and management (OEM) low bit-rate channel for the A-RoF link is transported at 100 MHz. For this experiment, we have six real-time signals (two bands per SFP) and twelve overloading signals generated with an arbitrary waveform generator (AWG) and whose parameters are shown in Table III.1. Those are conveniently pre-distorted and power adjusted with electrical amplifiers and variable electrical attenuators in order to remove the influence of the AWG frequency response and to provide the same power levels as the real-time signals respectively. The bands are separated by 500 KHz and the whole A-RoF spectrum (C&M channels included) occupies less than 200 MHz, as shown by the inset B of Figure III-3.

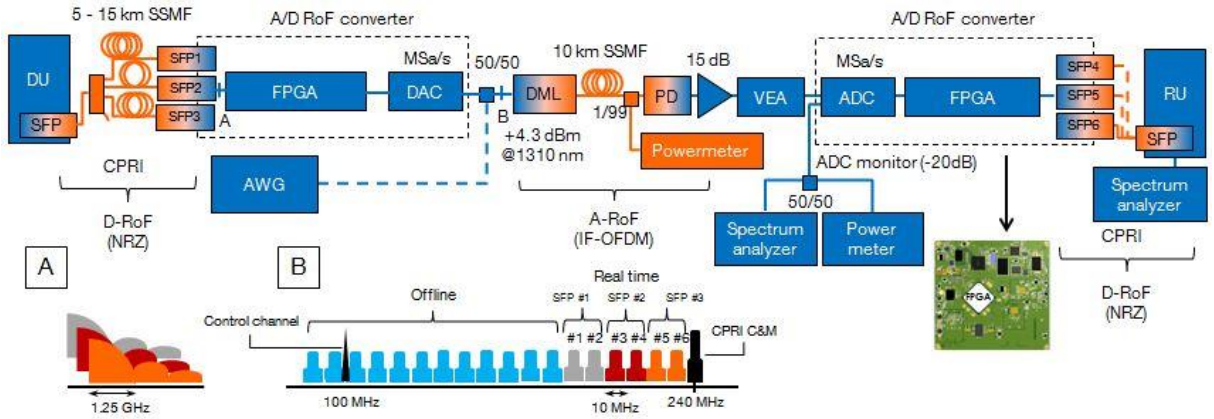

Figure III-3 : A-RoF/D-RoF experimental setup

Figure III-4 : A-RoF/D-RoF experimentation (photo)

The RF power of the A-RoF signal generated by the Head-End DAC is properly set to avoid nonlinear operation of the laser at this part of the experiment while providing the highest possible RF power to the laser. The signal directly modulates a 1310 nm DML emitting with 4 dBm mean optical power. After propagation through 10 km of SSMF, the signal is directly

Table III.1: OFDM LTE signal parameters

Parameter	DL LTE signal
Sampling freq. (MSa/s)	15.36
IFFT size	1024
Occupied subcarriers	600
Null border subcarriers	423
CP size (samples)*	80 (5.21µs) | 72 (4,68µs)
Useful symbol duration	66.67 µs
Slot size (samples)	7680 (0.5ms)
Subcarrier spacing (KHz)	15
Occupied BW (MHz)	9.015

* First | remaining 6 OFDM symbols of slot

detected by an APD photodiode. A 15 dB electrical amplifier followed by a variable electrical attenuator (VEA) is used to set the optimum RF power at the input of the ADC at the remote site. The electrical analog signal is finally converted back to CPRI before being fed to an LTE analyzer, where EVM measurements are performed.

III.2.2. Results and Discussions

At the beginning of this experimental study, a preliminary analysis of some limiting factors was carried out. The bandwidth offered by the used DML was measured with a Vector Network Analyzer allowing the S-parameters [85] measurements. The obtained bandwidth (referred to as S21) is shown in Figure III-5. The used laser has a response variation of +/- 0.8 dB between 10 MHz and 2.1 GHz. It is therefore necessary to stay in this frequency range to have a flat response in the frequency domain. Also, to use the optimum power level at the input of the laser, measurements of EVM were done for different power attenuations at the output of the DAC. The results for the ADC monitor at -40 dBm and -38 dBm are depicted in Figure III-6. For this test, it was verified that the ADC and the photodiode were not saturated. The results show that an optimum EVM is obtained for 2dB attenuation at the output of the DAC.

The optimum power level at the input of the ADC had to be defined as well. Figure III-7 shows the EVM as function of the power level measured at the input of the ADC. A minimum EVM was obtained at - 38 dBm. The ADC is saturated above this power level. In order to avoid the saturation of the photodiode as well, measurements of EVM were done for different optical budgets. The obtained results are depicted in Figure III-8. For this test, the power was adjusted at the input of the ADC to insure its optimum operation. Since the RF budget was limited, a polynomial fitting (based on the obtained results from 9 to 14 dB) was done to show the evolution of EVM for higher optical budgets. It is shown with the dotted curve on Figure III-8. These results concern the transmission of one LTE band. These parameters had to be adjusted each time more bands are added.

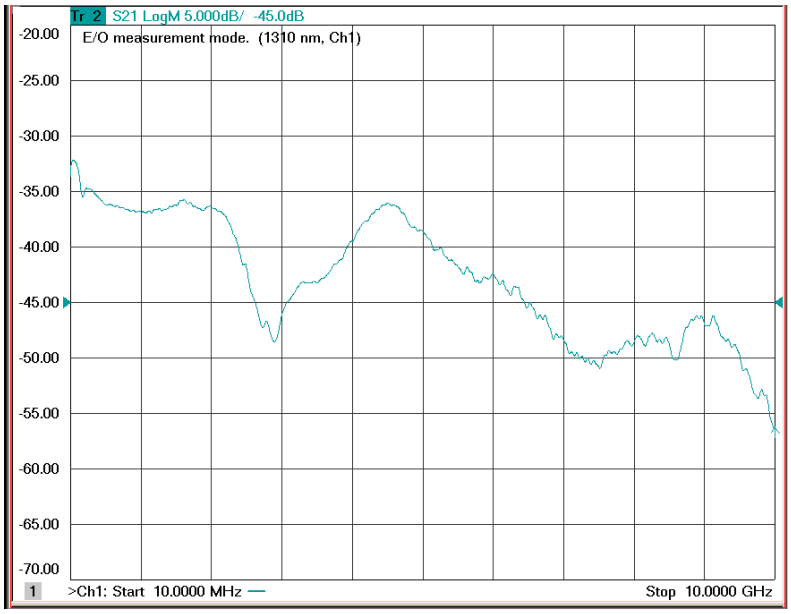

Figure III-5 : Bandwidth of the used laser

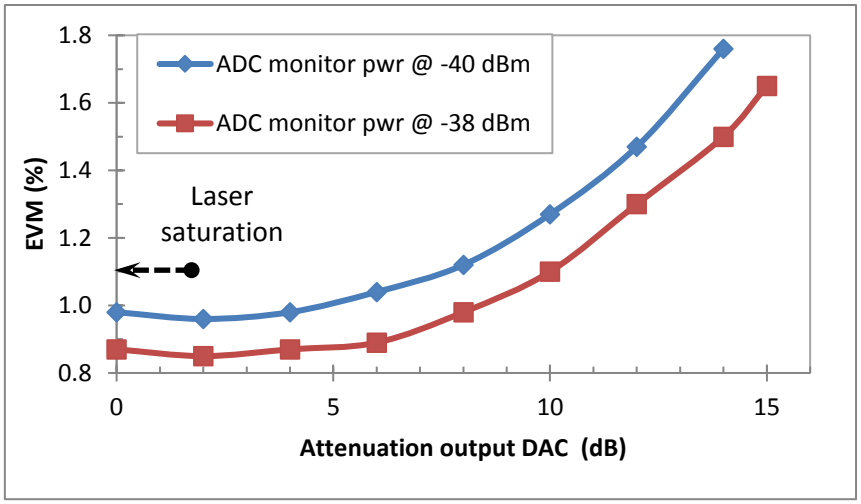

Figure III-6 : EVM (%) vs Attenuation at the DAC output (dB)

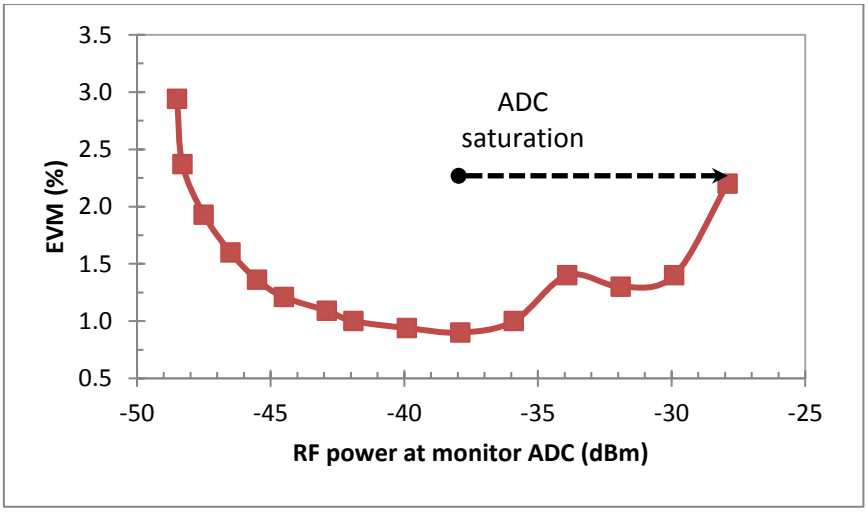

Figure III-7 : EVM (%) vs RF power at monitor ADC (dBm)

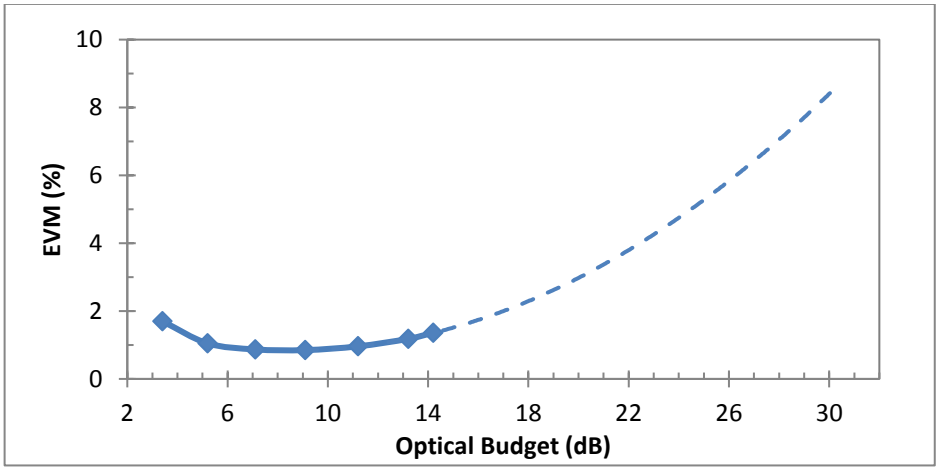

Figure III-8 : EVM (%) vs Optical Budget (dB)

It is known that the channel capacity is bounded by signal power constraints for a high number of bands (i.e., the overall signal bandwidth) according to the Shannon channel capacity theorem [86]. Since the A-RoF DAC is capable of providing a limited amount of RF power, as we increase the number of transmitted bands, i.e., the signal bandwidth, we reduce the power of each individual band and thus degrade their signal-to-noise-ratio. This can be illustrated in Figure III-9 where we can see the SNR difference between the transmission of 1 band and 6 bands. This can also be clearly seen in Figure III-10, which shows the EVM variation of the six real-time signals for different number of transmitted bands in the A-RoF link with respect to the mean optical power at the APD (for the 1 band scenario, EVM was measured alternately on each band). The difference between the optimal optical power levels at the receiver side for one and six bands also evidences the impact on the SNR as we increase the number of transmitted bands. A D-RoF measurement is also shown in Figure III-10 as an indicative basis in order to illustrate the shape of EVM evolution as function of the received optical power when commercial SFPs are used. The latter contain limiting Trans-Impedance Amplifiers (TIA) which reshapes the received NRZ signal at the reception, permitting enhanced and constant performance until the detection threshold of the TIA is reached. The purpose of this figure is not to compare A-RoF and D-RoF sensitivities since different optical components were used but the idea was to illustrate the performance shape of each concept. The received spectrum measured at the monitor port of the ADC, with 18 bands, is shown in Figure III-11. In order to avoid degradation induced by nonlinear conversions on the laser while guaranteeing optimized modulation conditions, the amplitude of the signal is carefully set each time the number of transmitted bands is changed. Also, the offline signal generation is set to a maximum of 6 bands per AWG channel in order to enable proper power leveling with the real-time bands. EVM penalties seen for a fixed optical power level at the receiver in Figure III-10 when we increase the number of bands come thus exclusively from the RF power constraint of the DML. The inset in Figure III-10 shows the received physical downlink shared channel (PDSCH) constellation for the real-time band centered at 199.7 MHz, at 11 dB optical budget.

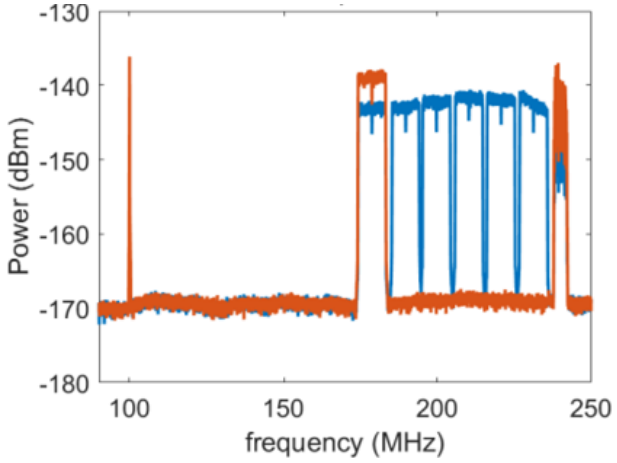

Figure III-9 : Received spectrum for 1 band (red) and 6 bands transmission (blue)

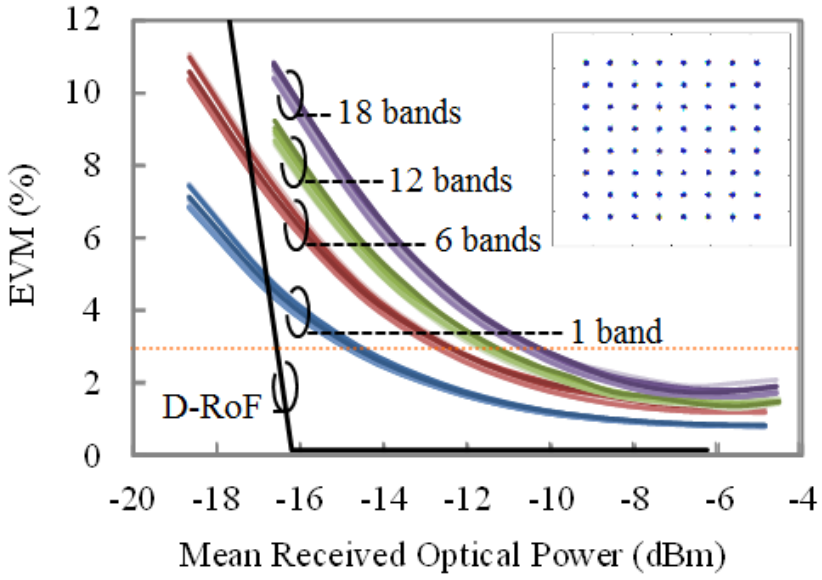

Figure III-10 : EVM (%) vs Received Optical Power (dBm)

Let us consider a target EVM of 3% in Figure III-10. This gives us a 5 pp margin to accommodate extra penalties arriving from electrical amplification of a real RU with respect to the maximum value defined by 3GPP for 64QAM [87]. While one single band can be transmitted with received optical powers as low as -14.6 dBm, extra 4.2 dB would be needed to keep the same performances with 18 bands. This would correspond to decreasing the maximum possible fiber length from ~47 km (0.4 dB/km at 1310 nm) with 1 band to ~36 km with 18 bands. Figure III-12 shows the optical budget penalty as a function of the number of bands for a fixed EVM of 3%. A complementary analysis can be made though, at fixed received optical power. At -10 dBm (14 dB optical budget), the EVM is increased from 1.1% with 1 band to 2.7% with 18 bands. The end-to-end SNR variation (obtained from the EVM) and the optical budget variation are depicted in Figure III-12.

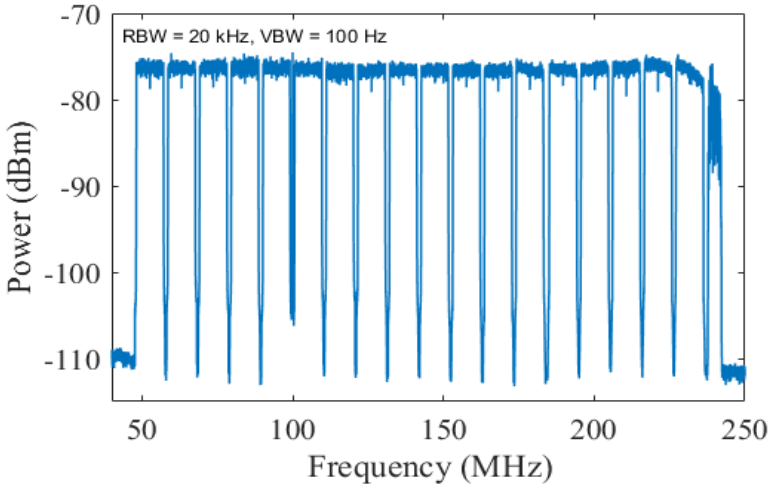

Figure III-11 : Received A-RoF spectrum

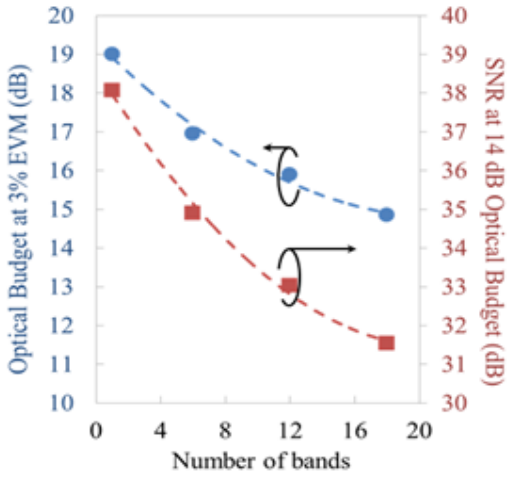

Figure III-12 : SNR and optical budget variation with the number of transmitted bands.

Figure III-13 shows an estimation of the evolution of EVM with respect to the number of transmitted bands and for three different optical budgets. A fitting has been done (following a power profile based on Shannon formula) on the results obtained in Figure III-10. We can see that 24 bands could be transmitted with 14 dB optical budget (compliant with the fiber length expected for fronthaul) while still respecting the 3% EVM constraint. This estimation concern only the degradation brought by the laser, we assume that the used DAC permit generating a sufficiently good SNR per band or that multiple DACs were used to avoid the SNR degradation.

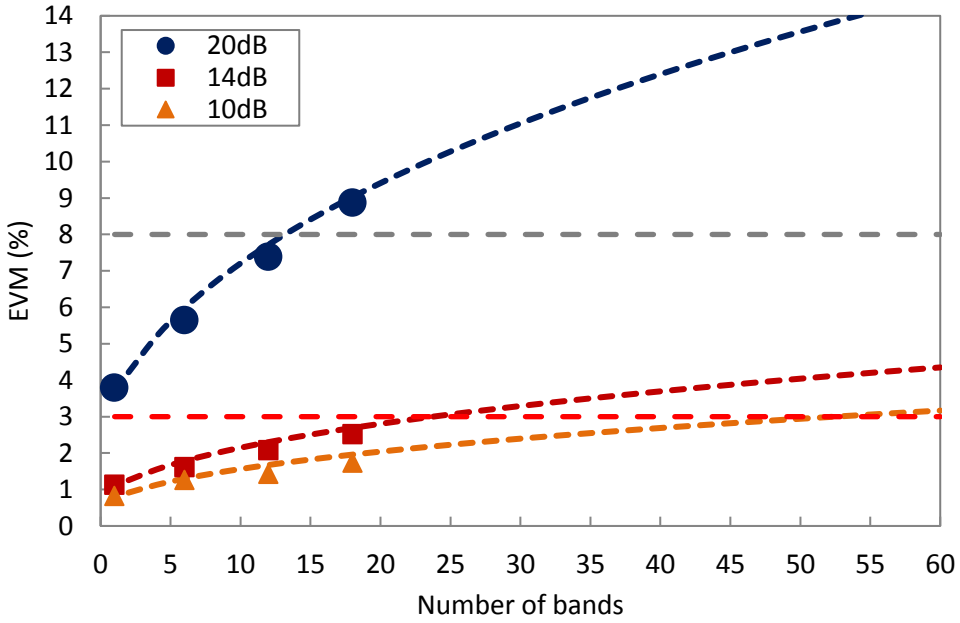

Figure III-13 : EVM evolution as function of the number of bands based on curve fitting.

III.3. Analysis of nonlinear Conversions on the Laser

After demonstrating the limitation of the A-RoF efficiency in the linear domain, this section will be devoted to the investigation of nonlinear effects caused by the increase of the RF power at the input of the laser. In fact, in order to transmit more bands than what was obtained in the previous section, more RF power would be needed to maintain the same SNR per band. Known for their high Peak-to-Average Power Ratio (PAPR), OFDM signals are clipped when they are passed through components with limited linearity range and insufficient headroom between the signal's peaks and the components operating range. This clipping causes both in-band and out-of-band distortions resulting from the generated harmonics and intermodulation products between the subcarriers and causing both a degradation of the transmission's Bit Error Rate (BER) and EVM and a spectral outgrowth leading to interference with adjacent bands. In this section, first an experimental assessment of these degradations is provided then the study is completed with some simulations due to the hardware (DAC, ADC) limitations.

III.3.1. Experimental evaluation

Using a similar experimental setup as the one shown in Figure III-3, but without the offline bands, 6 bands are transmitted, and measurements are performed for different RF power levels at the input of the laser. Since multiple components of the setup are likely to generate nonlinearities, it was decided to focus the study on the noise brought by the optical transmission (laser), thus the power level at the input of the photodiode and the DAC/ADC were optimized for each measurement.

Since the interaction between harmonics and intermodulation products generated by the nonlinear conversion on the laser can be rather complex due the extremely high number of subcarriers of the OFDM signal, the study was focused on a pragmatic analysis based on the nonlinear noise spectral density. The out-of-band noise density can be obtained from an analysis of the A-RoF signal spectrum whereas the in-band noise contributions can be estimated from the EVM degradation with respect to the ideal linear case. The goal in this section is to verify whether or not a higher robustness to nonlinear conversions on the laser can be obtained by means of a higher spacing between the A-RoF bands. This way, we can estimate how the nonlinear effects would impact the spectral efficiency of the A-RoF transmission. In this experimental investigation, three inter-band separations are evaluated: 500 KHz, 5 MHz and 10 MHz. Higher values could not be tested due to the bandwidth limitations of the used ADC. This is why we extrapolate this study to other values by means of simulations.

The obtained experimental results are depicted in Figure III-14. We can see that the EVM is largely impacted by the RF power increase in the nonlinear regime of the laser. With 6 dB power increase at the input of the laser, the EVM value goes from 2% to more than 5%. We can see also that the bands in the middle are more impacted by the power increase than the ones in the edge in the case of 500 KHz of channel spacing. For 5 MHz and 10 MHz channel spacing, the impact seems to be similar on all the bands. Furthermore, it seems that no remarkable reduction is obtained when we increase the spacing between the bands.

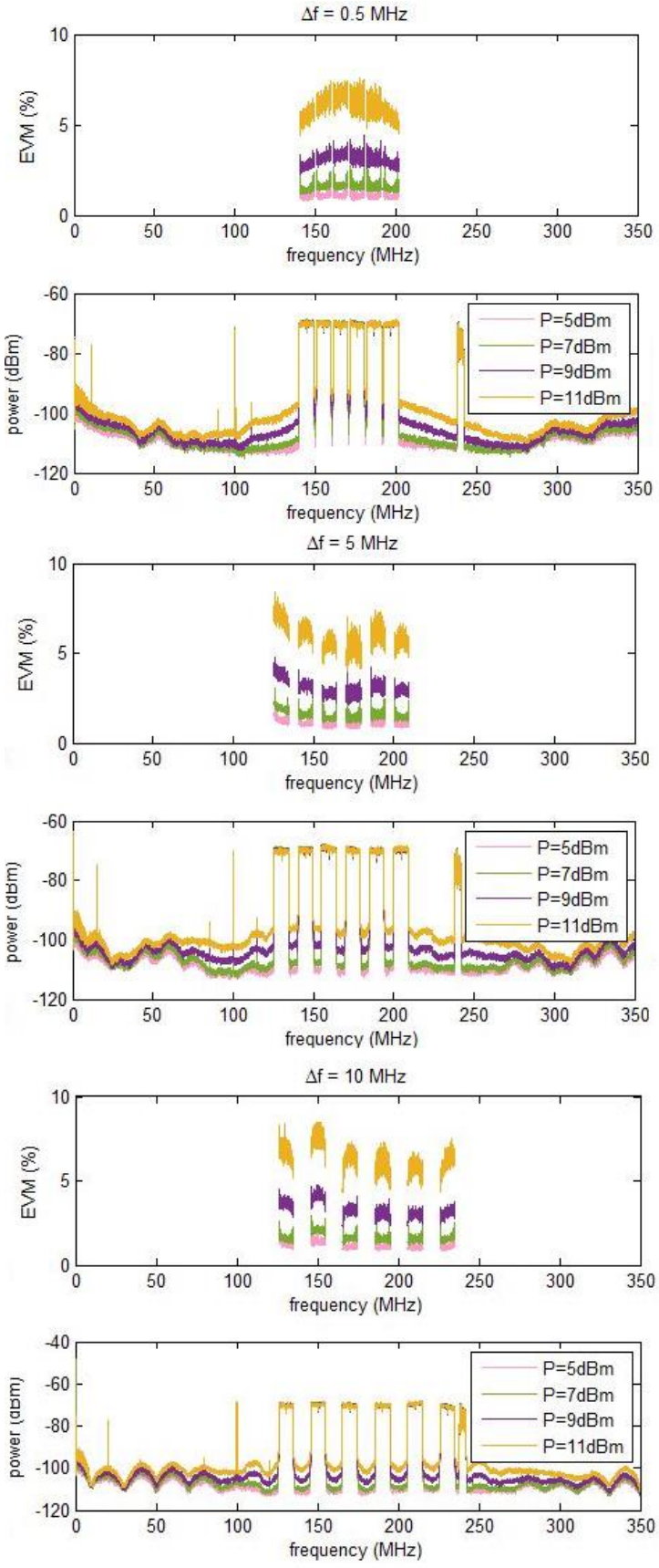

Figure III-14 : Experimental EVM and spectrum evolutions for different RF power at the laser input

The nonlinear degradation can also be perceived outside the bands as seen in the spectrum in Figure III-14. Clearly, as expected, a colored noise profile is obtained which depends on the spacing between the six bands. For 500 KHz, a block of noise is observed on the left of the first band and the right of the last one which increases when the RF power increase. With larger separations between bands, we start seeing smaller separate blocks of noise in the form of undulations caused by intermodulation products and harmonics of the signal. The performed experimental measurements didn't show a significant EVM improvement when separating the bands. Being limited by the DAC and ADC bandwidths, inter-band separations greater than 10 MHz could not be evaluated. Therefore, it was decided to use a model of the transmission system in order to complete the experimental results with simulations using Matlab and investigate if there is a minimal spacing between bands that allows reducing the effects of the nonlinear noise while limiting the impacts on the transmission spectral efficiency.

III.3.2. Modeling and simulations

III.3.2.1. Nonlinear conversion model

In order to complete the obtained experimental results; a simple model (shown in Figure III-15) was used to evaluate the nonlinear effects introduced by the laser for different levels of input power and different channel spacings. This model is based on an OFDM modulator with the PHY parameters shown in Table III.1 for the transmission. The corresponding demodulator was used for the reception. The generated OFDM signal is replicated and transposed to different intermediate frequencies.

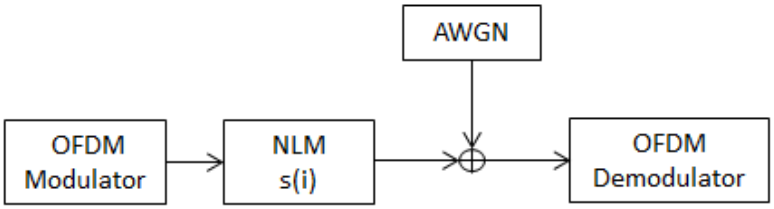

Figure III-15 : Model used for simulations

The laser used in the experimental study has a nearly linear response to input signals with low power level and becomes increasingly nonlinear as the input level increases. The Solid-State-Power-Amplifier (SSPA) model [88] which has a similar behavior was therefore used as the laser's Non-Linearity Model (NLM). Its characteristic is defined with the following equation:

$$s(i) = \frac{\mathrm{i}}{\left(1 + \left(\frac{i}{imax}\right)^{2p}\right)^{\frac{1}{2p}}} \qquad (4)$$

Where s(i) is the magnitude of the output signal, i is the magnitude of the input signal, i_{max} is the clipping magnitude and p is the parameter that adjusts the smoothness of transition from the linear to the nonlinear region. The parameters i_{max} and p were given arbitrary values (i_{max} = 0.9 and p = 3) since they have no impact on the purpose of the simulation. The obtained characteristic is depicted in Figure III-16. Despite the simplicity of this model, it is sufficient to achieve the targeted study. An Additive White Gaussian Noise (AWGN) is also added in such a way that the obtained noise level is comparable to the one obtained

experimentally. As for the experimentation, the RF power is normalized at the output of the laser in order to evaluate the optical non-linear effects only. Finally, we realized Root Mean Square (RMS) EVM measurements over 20 LTE slots (= 1 frame = 10 ms).

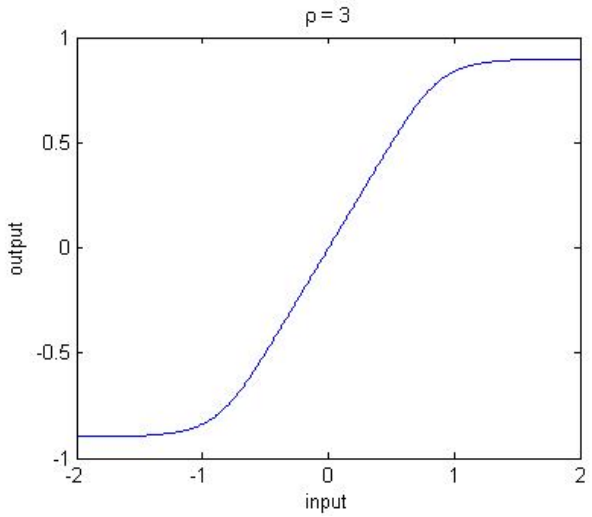

Figure III-16 : Laser characteristic modeled using SSPA model

III.3.2.2. Simulation results

The first step in the simulation was to validate the implemented model. For this matter, spectrum and EVM measurements were performed for different input levels at the laser and different channel spacings. The obtained simulation results are represented in Figure III-17. We observe similar behavior and a very good agreement with the experimental results. With higher power level at the input of the laser, EVM is more degraded and there is more spectral regrowth. Also, the noise spectral density profile is quite similar to the one obtained experimentally for all tested separations between bands. Indeed, a little flat noise is noticed when the power at the input of the laser is high and the more the power increases the more undulations as the one observed in the experimental results appears. Thus, the proposed model is fairly representative of the system under study.

In order to complete the experimental work on the impacts of nonlinear noise, EVM measurements were performed based on simulations for wider channel spacings. The obtained results are shown in Figure III-18. A slight improvement is observed when separating the bands up to 40 MHz and then the EVM value stabilizes. Less than 1pp improvement can be obtained of the EVM value by using higher inter-band spacing, which is almost negligible compared to the in-band degradation itself.

The disturbance can also be qualified by EVM degradation; Figure III-19 shows the simulation results for EVM values as function of the power input level at the laser for 500 KHz channel spacing. The simulation of EVM depending on the input RF power is shifted compared to the experimentation simply because a non-linear model with normalized amplitude was arbitrarily chosen for the simulations. Indeed, the actual RF power levels were not the focus of the study and we concentrated on the spectral profile of the nonlinear noise.

These results reveal that inner-band distortions, i.e. those coming from the own subcarriers of the OFDM signals themselves; seem to be stronger than inter-band distortions. Namely, the Subcarrier-to-Subcarrier Intermixing Interference (SSII) is the major contributor in EVM degradations.

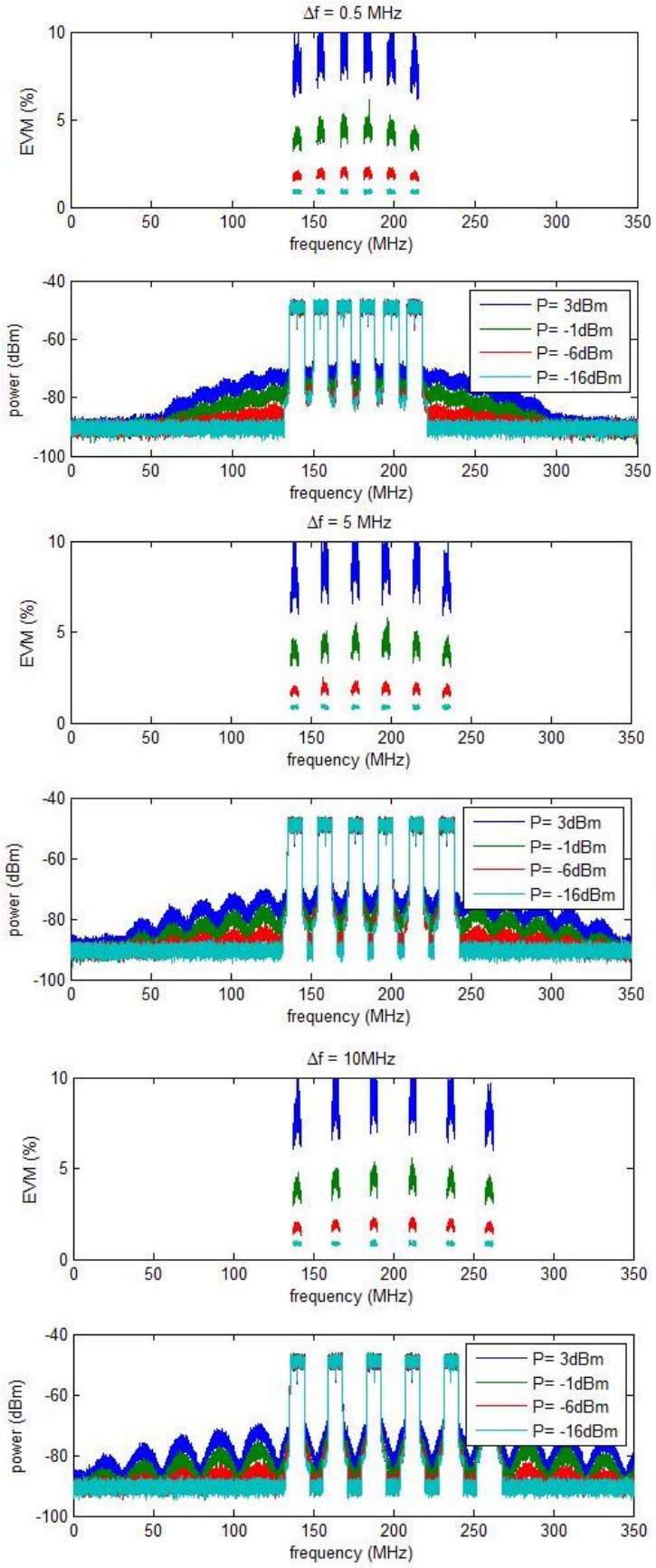

Figure III-17 : Simulation results for EVM and spectrum evolutions for different RF power at the laser input

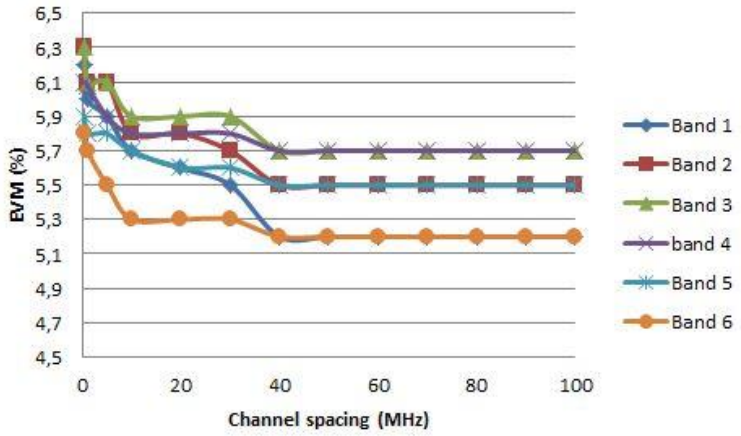

Figure III-18 : EVM (dB) vs Channel spacing (MHz)

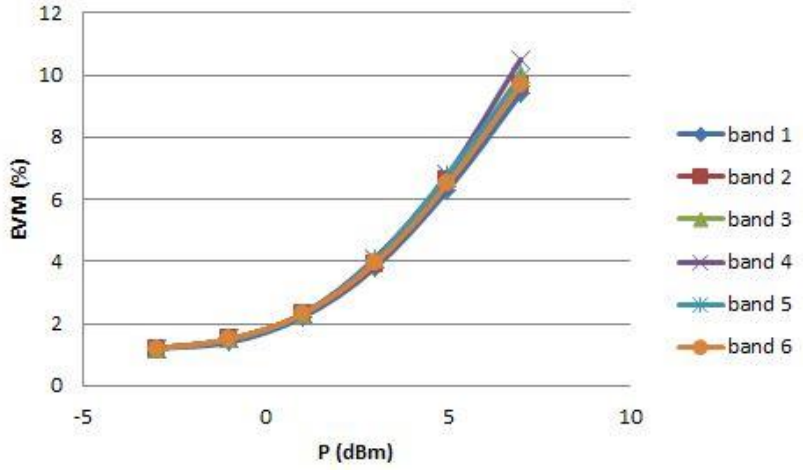

Figure III-19 : EVM (%) vs Input Power (dBm)

We can see for the experimental results as for the simulations that the EVM curve is flat in the linear case (the slight degradations at the signal borders in the experimental case are likely to come from the low-pass filter operation, which was not implemented in the simulations); the same EVM is obtained for all the subcarriers.

When nonlinearities are introduced, we can observe that the EVM curve has a concave profile; the subcarriers of the middle are more impacted by the nonlinear distortions which confirm the SSII phenomenon mentioned before. When passing through a nonlinear component, the OFDM signal composed of multiple subcarriers (600 in our case) is distorted. This is manifested by the appearance of harmonics and intermodulation products of the subcarriers which is referred to as SSII.

The latter acts as noise, which could disturb the neighboring bands, but as it turned out insignificantly. It mostly disturbs the channel itself. Methods exist for the mitigation of nonlinear distortion, the most popular ones are SSII cancellation [89] [90] [91] and Volterra equalization [92] [93].Algorithms exist to calculate the SSII [94] which permits retrieving it at the reception but these are beyond the scope of this study. To mention that the complexity of these algorithms will certainly introduce extra latency unwanted for the fronthaul link. This

effect could be most certainly changed by different subcarrier spacings but we recall that such parameter depends on the mobile propagation dispersive channel characteristics.

III.4. Conclusions

In this chapter, we proposed an architecture mixing A-RoF and D-RoF transmissions having a goal to enable the possibility to leverage the existing DAS infrastructure (multi-carrier from several mobile operators that sharing antenna site). A greater purpose of this study was to propose a solution to the highly increasing CPRI bit-rate in 5G by offering a spectrally efficient fronthaul based on analog RoF.

An experimental study was carried out in real time using an off-the-shelf optical transceiver. The strength of this study was its pragmatism; the “DAC” and “ADC” used are suited for an access network equipment, cost wise. Unlike the ones that are embedded in Lab test equipment usually used for offline transmissions to study this issue. Therefore, the performed experimentation shows the real gain of A-RoF compared to D-RoF. The obtained results show that 24 LTE bands with 10 MHz bandwidth can be transmitted within the laser linearity range while being compliant with the 3GPP standard concerning EVM, instead of 60 bands as promoted theoretically. More bands could be transmitted with higher RF power at the laser input, but this could imply nonlinear in-band and out-of-band effects. Inter-band distortions have the least impact on performance and can be slightly mitigated by using at least 40 MHz channel spacing (in the case of the used system and configuration). Inner-band distortions have a greater impact on the EVM value. Nevertheless, solutions exist to mitigate these effects. The cost and the latency that they will introduce will need to be evaluated.

The results obtained in this chapter were published in an international conference (ICTON, cf appendix A).

Chapter IV. CPRI compression

IV.1. Introduction

Based on the results obtained in chapter III, it was shown that the transport of analog signals over fiber to enhance the CPRI-based fronthaul interface was not the optimum solution. Even if it allowed to greatly improve the spectral efficiency of the transported signals, it showed difficulties of its implementation mainly because of RF power and linearity constraints. Also, the absence of a mass market of analog pluggable optoelectronic transceivers would make the field deployment of such solution difficult. Therefore, the use of solutions based on digital RoF is preferable since it benefits from the maturity of commercially available small-form factor pluggable transceivers used for optical metro/access applications. Also, since the signal is transmitted by means of ON/OFF keying, it provides extended robustness to optical noise and thus improved receiver sensitivities with no particular constraints on the RF power.

An approach to enhance the spectral efficiency of the interface in the D-ROF domain is CPRI compression which is the focus of this chapter. In fact, data compression has been a subject of study for a few decades now and targeted specially images, audio and video compression applications to optimize their storage and transmission in telecom networks.

Two types of compression exist: lossless and lossy. In few words, lossless compression is fundamentally based on the redundancy reduction without loss of information. Concerning its application on CPRI, few works have been done and were mainly based on the removal of redundancy in the spectral domain. Notably [95] [96] demonstrated bandwidth reduction by filtering non-modulated guard subcarriers. A maximum of 30% compression was obtained based on simulations. Time domain redundancy removal was also proposed by removing the Cyclic Prefix of the OFDM signal [97] which permits a compression of about 7% in normal cyclic prefix mode. Another kind of lossless compression based on entropy coding was also proposed. It consists in using more bits to represent symbols with higher entropy thus the symbols containing more information. In this case we talk about variable-length coding [98]. Huffman coding [99] is the most common entropy technique wherewith [100] achieved 75% CPRI compression for an EVM of 2.1%.

The second type of compression is lossy and basically based on quantization which is the process of mapping a large set of samples to a smaller set following a given resolution. The higher the resolution, the better the signal fidelity we obtain and the higher the bit-rate we get. Therefore, a trade-off exists between signal fidelity and bit-rate. The quantization in this case can be scalar if the input of the quantizer is unidimensional or vector if the input of the quantizer is multi-dimensional. Few works were done on this subject as well, generally based on simulations. In [101], the authors proposed a non-uniform quantization with compression rate of 66% for 2% EVM. In [102], a compression rate of 69% with approximately 2% EVM distortion was proposed using decimation, an enhanced block scaling and a uniform quantizer. Lloyd-Max scalar quantization with noise shaping was considered elsewhere where 66% compression were reported for 2% EVM [103], and vector quantization was proposed in [104] [97] (subsequently to our work) where 77% compression was achieved for 2% EVM. Another quantization technique was used in audio signal digitization. It is based on a compander which basically rest upon the use of a logarithmic function to transform the signal's PDF to a uniform distribution then quantize the signal with a uniform quantizer (most appropriate for this distribution). At the reception, the inverse of the used logarithmic function is used to recover the initial signal. Therefore, this technic allows an optimized quantization

regardless of the signal's PDF. The μ-law used in the US and Japan and the A-law used in Europe are based on this quantization technic [105]. Although it was decided not to include it in this study.

Unlike ORI which shall support a compression of at least 50% based on down-sampling and non-uniform quantization [108] [109], the CPRI specification [110] designates a uniform quantization with 15 bits resolution with no mention of compression. In this context, this chapter assesses CPRI compression with real time and offline experimentations. The focus is on scalar and vector quantization based on fixed-length coding. The purpose is the optimization of the digitization process in order to obtain a minimum CPRI bit-rate while maintaining performances compliant to the standard. In section IV.2, an investigation is done on the CPRI compression based on uniform quantization. Non-uniform quantization with smart algorithms such as Lloyd-Max is assessed in section IV.3 and a real-time evaluation of enhanced compression methods based on spectral redundancy removal and "frequency domain quantization" is discussed in section IV.4.

IV.2. Uniform quantization

Figure IV-1 shows the transfer function of a quantizer. We talk about uniform quantization when equally spaced decision thresholds are used for the entire signal. It is not the optimum quantization method when the signal's PDF is a Gaussian as it is the case of LTE downlink signals (Figure IV-2). In fact, the occurrence probability of the amplitude levels in LTE follows a Gaussian law, therefore using equal quantization accuracy in the center and the extremes of the Guassian will not permit an optimum use of the available quantization levels. Nevertheless, it is usually used in industrial solutions for the ease of its implementation.

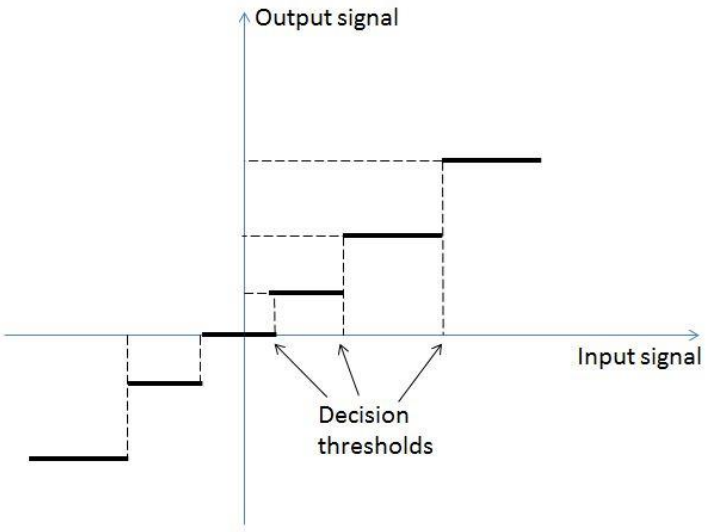

Figure IV-1 : Transfer function of a quantizer

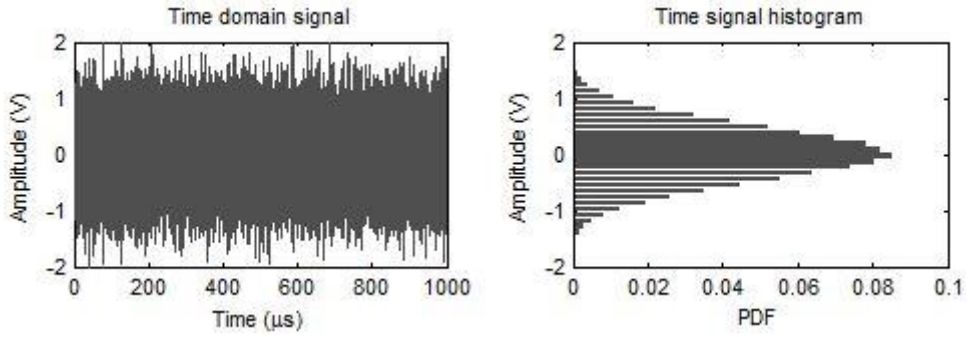

Figure IV-2 : Example of time domain LTE signal (left) and corresponding Probability Density Function (right)

The CPRI specification recommends a quantization resolution between 8 and 20 bits. For industrial implementations, a uniform quantization is employed with 15 bits resolution, 2^{15}=32768 quantization levels are used which permits an extremely precise signal recovery at the reception. This also implies that each quantized LTE sample is coded over 15 bits which generates very high CPRI bit-rates. During the quantization, noise is generated mainly because of granular and overloading distortions. We talk about granular distortion when an error occurs during the approximation of a signal sample to a quantization level, usually because of the poor accuracy of the quantizer (low quantization resolution). Overloading distortions happen when the value to be quantized exceeds the range supported by the quantizer which generates clipping in the quantized signal.

As mentioned before, a tradeoff is to be done between signal fidelity and its bit-rate during the quantization. In this section, this tradeoff is re-evaluated for the case of CPRI by mean of real time and off-line experimentations in order to define an optimum quantization resolution.

IV.2.1. Real-time experimentation and results

The performed experimental setup is depicted in Figure IV-3. At the transmitter side, a signal generator creates a 20 MHz LTE signal. Standardized test models E-TM3.3, E-TM3.2 and E-TM3 are used to investigate the performance of QPSK, 16QAM and 64QAM mappings respectively. Then, an IQ box handles the LTE to CPRI conversion (sampling + quantization + coding); the bit-rate is fixed to 2.45 Gbit/s. These two components emulate the BBU. At the receiver side, an IQ box is then used for CPRI to LTE conversion and a spectrum analyzer with embedded demodulator emulates the RRH and handles the LTE performance assessment. For the optical transmission, commercial Small Form-factor Pluggables (SFP) emitting at 1510 nm with 1 dBm mean optical power are used and the transmission is done over 20 km. The quantization resolution is varied in the IQ boxes in order to change the compression rate then the end-to-end EVM is assessed. The compression rate calculation is done using the CPRI bit-rate equation (1) defined in Chapter I assuming a bipolar quantizer. Basically, since the quantization resolution is the only parameter changing in the equation, the compression rate for n bits quantization resolution can be calculated as follows:

$$Compression\ rate(\%) = \left(1 - \frac{Used\ resolution\ (n\ bits)}{Original\ resolution\ (15\ bits)}\right) \times 100 \qquad (5)$$

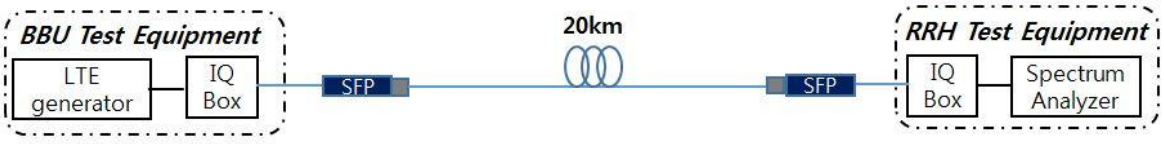

Figure IV-3 : Experimental setup for real time uniform quantization

The obtained results are shown in Figure IV-4. A target EVM of 3% is considered which gives a 5 pp margin to accommodate extra penalties arriving from electrical amplification of a real RRH with respect to the maximum value defined by 3GPP for 64QAM [112]. 3% of EVM is also the recommendation of ORI concerning compression [108].

Up to 53% of compression can be performed by simply reducing the quantization resolution with respect the targeted EVM leading to a CPRI bit-rate of 1.14 Gbit/s instead of 2.45 Gbit/s. Similar results were obtained for the three evaluated modulations (QPSK, 16QAM, 64QAM). It is also observed that 30 dB of noise was brought to the radio signal by the compression with a rate of 5.72 dB/bit which is compliant to the theory. In fact, [106] and [107] demonstrated that for a uniform quantization based on the fixed-length coding, the signal to quantization noise ratio of a quantizer using N resolution bits is defined as follows:

$$SQNR = 20log2^N = N \times 20log2 = N \times 6.02\ dB \quad (6)$$

The small difference noticed with the measured value (5.72 dB/bit vs 6.02 dB/bit) is certainly due to measurement inaccuracy.

53% compression using uniform quantization is an interesting result but not sufficient to cope with the radio evolutions expected for 5G. Higher compression rates could be obtained if the quantization levels are adapted to the PDF of the signal, which is relevant given its Gaussian shape. The IQ Box used in Figure IV-3 is limited to uniform quantization. Therefore, in order to study the non-uniform quantization, the transmission had to be done offline. It was done in the first place with uniform quantization in order to have a point of comparison with the results showed in Figure IV-4 and validate the implemented model.

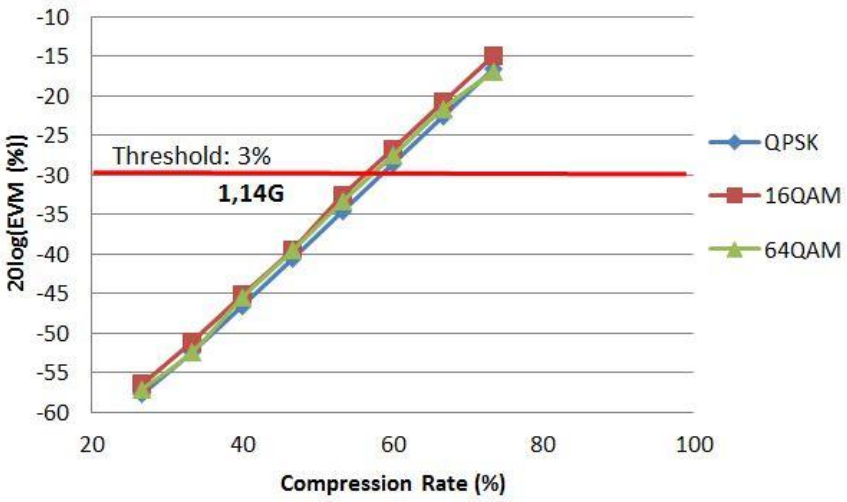

Figure IV-4 : EVM (dB) vs Compression Rate (%) for uniform quantization

IV.2.2. Offline experimentation and results

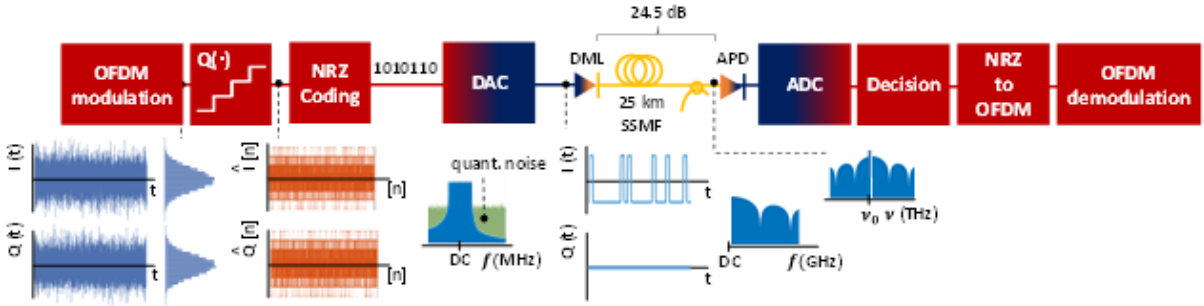

Figure IV-5 : Experimental setup for offline transmission

Figure IV-5 shows the performed offline experimentation. A 20 MHz downlink (DL) LTE signal is generated then digitized using, at a first moment, a uniform quantization approach. This consists in converting the original signal samples into one of the 2^n equally-sized possible levels using the nearest neighbor condition, with n being the number of bits used by the quantizer. Then, a coder maps the indices of each of such levels into a NRZ word. A digital-to-analog converter (DAC) operating at 2 samples/symbol generates the analog NRZ signal used to modulate a directly modulated laser (DML) of a commercial SFP module emitting at 1510 nm and with 1 dBm mean optical power. The optical signal propagates through 25 km SSMF before being directly detected by an avalanche photodiode (APD). Extra 14 dB attenuation is added with a variable optical attenuator. The received NRZ signal is digitized with an analog-to-digital converter (ADC) working at 4 samples/symbol. Decision is taken on the received NRZ data to obtain the binary sequence used on the conversion back to the original LTE orthogonal frequency division multiplexing (OFDM) modulation. This is done using look-up-tables. In order to adapt the NRZ signal to the sampling characteristics of our ADC, we perform minor changes to some LTE PHY parameters, without loss of generality. Those are shown in Table IV.1. Finally, root mean square (RMS) EVM measurements are realized over 20 LTE slots (= 1 frame = 10 ms).

Table IV.1 : OFDM LTE signal parameters

Parameter	DL LTE signal	Our signal
Sampling freq. (MSa/s)	30.72	30.00
IFFT size	2048	2000
Occupied subcarriers	1200	1200
Null border subcarriers	847	799
CP size (samples)*	160 (5.21µs) | 144 (4,68µs)	160 (5.33µs) | 140 (4.67µs)
Useful symbol duration	66.67 µs	66.67 µs
Slot size (samples)	15360 (0.5ms)	15000 (0.5ms)
Subcarrier spacing (KHz)	15	15
Occupied BW (MHz)	18.015	18.015
FH bit-rate (Gbit/s)**	1.2288	1.2000

** First | remaining 6 OFDM symbols of slot*

*** SISO, 15 bits/sample and 16/15*10/8 overhead*

A first step was to find an optimal overloading factor which sets the analog signal's amplitude at the input of the quantizer. The target is to provide the best balance between sufficient signal amplitude enabling accurate digitization and a minimum overloading distortion.

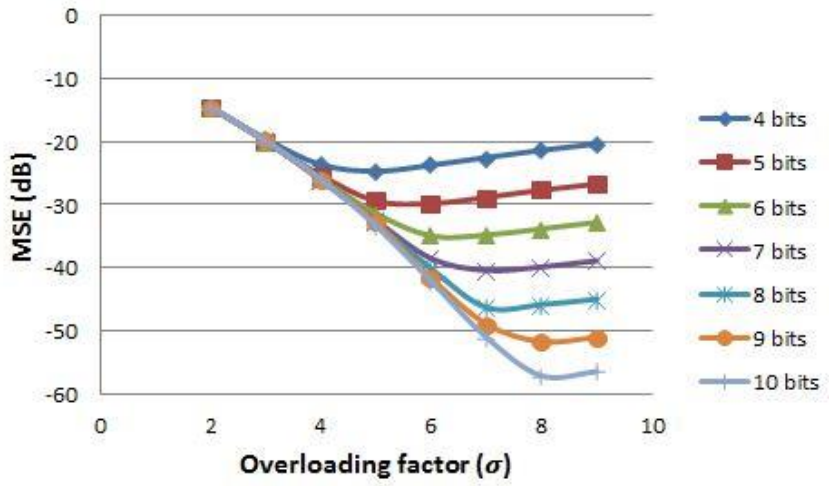

Figure IV-6 : MSE (dB) vs Overloading factor (σ) for 20MHz LTE

Figure IV-6 shows the MSE (Mean Squared Error) evolution when varying the overloading factor, the latter being expressed in terms of "σ" the standard deviation of the signal. The optimum overloading factor varies when varying the quantization resolution. Its value goes from 5σ with 4 bits resolution to 8σ with 10 bits. Therefore, adjusting the overloading factor is needed when changing the CPRI compression rate.

The obtained results are depicted in Figure IV-7 and show a perfect fit between the real-time and offline experimentations. They enabled 53% compression while being compliant with the targeted EVM value (3%), leading to a CPRI bit-rate of 1.14 Mbit/s instead of 2.45 Gbit/s.

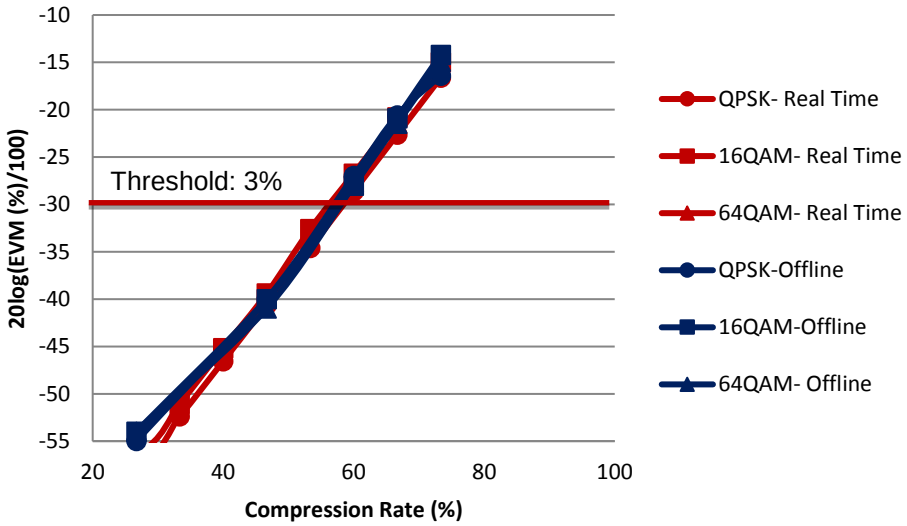

Figure IV-7 : Real time and offline compression EVM results

IV.3. Non-uniform quantization

The idea in this section is to take advantage of the Gaussian PDF of the signal and design a quantizer which adapts its quantization levels according to the probability of occurrence of the OFDM samples. More levels must be dedicated to the center of the Gaussian, and the further away from the Gaussian center the less quantization levels there are.

Such solution was proposed by Lloyd-Max algorithm (developed by Lloyd in 1957 and published by Max in 1960) [113]. It is based on a one-dimension quantization with distortion minimization measured on a Mean Squared Error (MSE) basis. The latter being defined mathematically as follows:

$$MSE = E[(x-y)^2] = \int_{t_0}^{t_k} (x-y)^2 \, p(x)dx \tag{7}$$

y being the quantized value corresponding to an input x, k the number of quantization levels and p(x) the PDF of the analog input signal. Concretely, it can be measured as follows:

$$\text{MSE}=\frac{1}{n}\sum_{i=1}^{n}(X_i - Y_i)^2 \tag{8}$$

X being the vector of samples, Y the vector of quantized samples and n the number of samples.

Lloyd-Max quantizer is based on an iterative algorithm which can be summarized fundamentally in four steps:

1. Start with an initial, arbitrary set of quantization levels y_q, q=0, 1, 2, 3…N-1

In our case, it was chosen to start with a uniform quantization.

2. Calculate decision thresholds $t_q = \frac{1}{2}(y_{q-1}-y_q)$; q=0, 1, 2, 3…N-1 which means that the decision threshold is located halfway between 2 consecutive quantization levels.
3. Calculate new quantization levels

$$y_q=\frac{\int_{t_q}^{t_{q+1}} x.p(x)dx}{p(x)dx}\text{, q=0, 1, 2, 3…N-1} \tag{9}$$

   Considering that the PDF p(x) is a piecewise constant function, this would imply that that the decision level is located at the centroid (center of mass) of the piece of the PDF defined by two consecutive quantization levels. In practice, the new quantization level takes the value of the average of all the samples corresponding to it from the previous iteration.

4. Repeat steps 2 and 3 until the MSE value is minimal. It was decided then to run the algorithm until no more than 5.10^{-4}dB MSE improvement is obtain between 2 consecutive iterations.

This algorithm was implemented and evaluated over an offline transmission using the experimental setup shown in Figure IV-5.

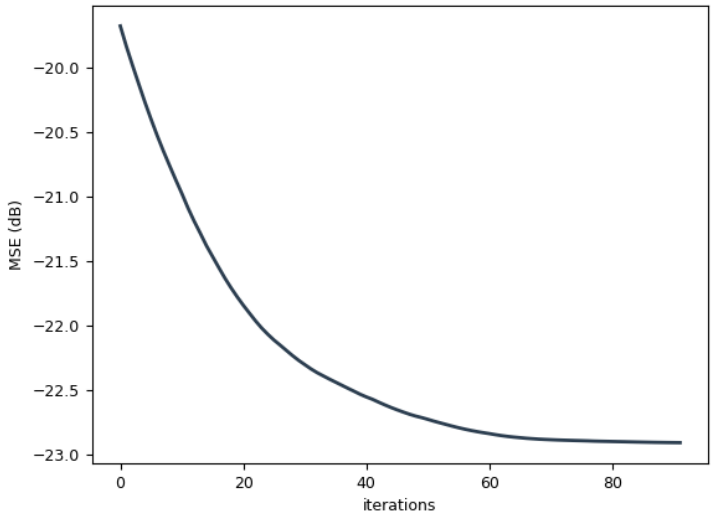

Figure IV-8 : MSE vs iterations for non-uniform scalar quantization

Figure IV-8 shows the evolution of MSE while the algorithm is running with 4 bits quantization resolution. This resolution was used to reduce the processing time (higher resolution non-uniform quantization takes very long time); the purpose being to compare the performance of uniform and non-uniform quantization. The results can be extrapolated on higher resolutions afterwards.

The Knowing that the measured MSE for a uniform quantization with an optimized overloading factor is -21.83dB, 1dB MSE improvement is noticed when the stop criterion is attained.

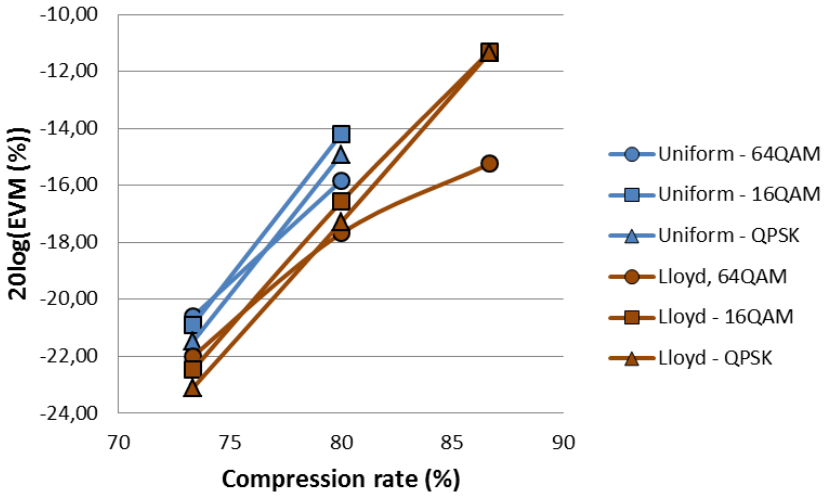

Figure IV-9 : Uniform and Lloyd quantization experimental results

Figure IV-9 shows the experimental results of uniform quantization (previously obtained offline) and non-uniform (Lloyd-Max) quantization. Based the EVM measurements, up to 2 dB quantization noise reduction is noticed when using Lloyd-Max algorithm. This optimization could permit using one less quantization bit compared to uniform quantization while maintaining the same EVM performance. In fact, an EVM threshold was defined (3%) for this study in such a way not to be exceeded when reducing the quantization resolution. The 2 dB gained with this method could therefore permit reaching the EVM threshold when reducing the number of used quantization bits. When we used 4 quantization bits (73%

compression rate), we found the 1dB improvement noticed in Figure IV-8. The higher the compression rate, the more important EVM improvement we can get with Lloyd algorithm. Therefore, a uniform quantization would be the more appropriate for a sufficiently large quantization resolution [98].

Vector quantization using the Linde-Buzo-Gray (LBG) algorithm [114] was also investigated and published in [115]. The LBG algorithm which is an n-dimensional generalization of Lloyd's algorithm allows benefiting from the statistical dependency between the samples and optimizing the space filling [111] thus providing more optimized decision threshold and better EVM results consequently. The experimental results show a maximum EVM improvement of 1dB with the 2D vector quantization (by separating the In-phase from the quadrature components) compared to scalar non-uniform quantization. Extra 2dB EVM improvement was obtained with the 4D vector quantization by separating the odd and even in the in-phase and the quadrature components. According to [116], more or less 6 dB SNR improvement is needed to be able to reduce one bit from the quantization resolution while keeping the same performance. Therefore, the transition from uniform to 4D vector quantization will permit the reduction of no more than one quantization bit in best case scenario.

More compression could surely be achieved by implementing higher dimension vector quantization. Nevertheless, it will imply high complexity for storage and computation. It could also introduce much latency in the fronthaul link which cannot be accepted.

IV.4. Complementary compression methods

Some complementary compression methods can also be used to further reduce the CPRI bit-rate. Namely, low pass filtering can be used to remove the unused LTE subcarriers and performing the quantization in the frequency domain can permit achieving better compression rates. These methods were experimentally studied using an industrial prototype.

IV.4.1. System under evaluation

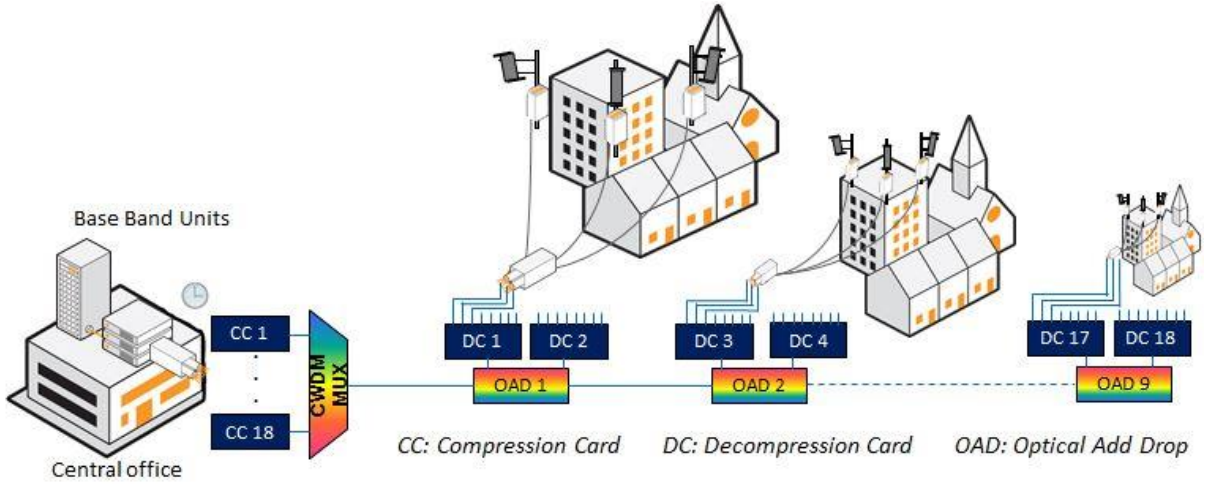

Figure IV-10 : Architecture under evaluation

The system under evaluation is composed of a compression card and a decompression cards which allow CPRI3 (2,45 Gbit/s) compression and the aggregation of 8 CPRI3 links in a 10Gbit/s frame using Time Division Multiplexing (TDM). The latter can then be used in addition to WDM to transport furthermore CPRI links. A daisy chain topology using Optical

Add Drops (OADs) can therefore be used as depicted in Figure IV-10, transporting up to 144 CPRI 3 links (360 Gbit/s).

Figure IV-11 shows the algorithm implemented in the compression card. After separating the Control and Management (C&M) data from the user data (I/Q), a compression algorithm is applied to the I/Q components. A delay compensation corresponding to the compression algorithm latency is performed in parallel on the C&M data. These two signals are then mapped into a CPRI frame with reduced bit-rate. This process is performed on several CPRI links (up to 8xCPRI3 links) before encapsulation into a 10 Gbit/s frame. At the reception, the reverse operation is applied in the decompression card to recover the signal at the initial bit-rate.

The compression process consists mainly of 4 operations as depicted in Figure IV-11: NRZ to OFDM conversion using look-up-tables, low pass filtering to remove the spectral redundancy, switching to the frequency domain by performing a Fast Fourier Transform (FFT) and a uniform quantization.

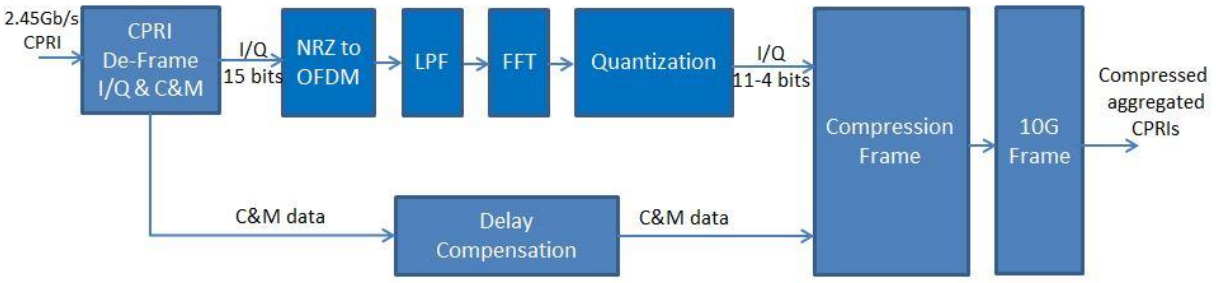

Figure IV-11 : Compression algorithm

In fact, in the LTE implementations, an inverse FFT is performed to generate the OFDM symbols. The most adequate IFFT size would be respecting the minimum required by the Nyquist sampling theorem. Although, because of implementation complexity, an IFFT size based on a power of 2 is preferable. For instance, for a 20 MHz LTE, 1200 subcarriers are used with 15 KHz width each, thus the signal's used bandwidth is 18 MHz. The smallest power of 2 which is larger than 1200 is 2048 therefore 2048 subcarriers are generated leading to a bandwidth of 30.72 MHz. Only 1200 subcarriers are useful though, the remaining subcarriers are filled with zeros. In order to get rid of this redundancy, the first step is the up sampling of the signal (by a factor 2) by an interpolation. The obtained signal is then low-pass filtered to eliminate the signal's replicas then down sampled (by factor 3) by means of decimation [96]. After this operation, the signal's bandwidth is 20.48 MHz allowing a reduction of 1/3 of the CPRI's bit-rate. Furthermore, an FFT is performed afterwards allowing the changeover to the frequency domain. Therefore, quantization will be carried out on M-QAM symbols requiring only $\log_2(M)$ quantization bits for the used data plane. For instance, 2 bits are needed for a QPSK, 4 bits for a 16QAM and 6 for a 64QAM. It is worth mentioning here that some control and synchronization signals, with different modulation formats, will also need to be transported. The obtained quantized signal is then encapsulated in a CPRI-like compression frame then in a 10 Gbit/s frame.

IV.4.2. Experimental setup and results

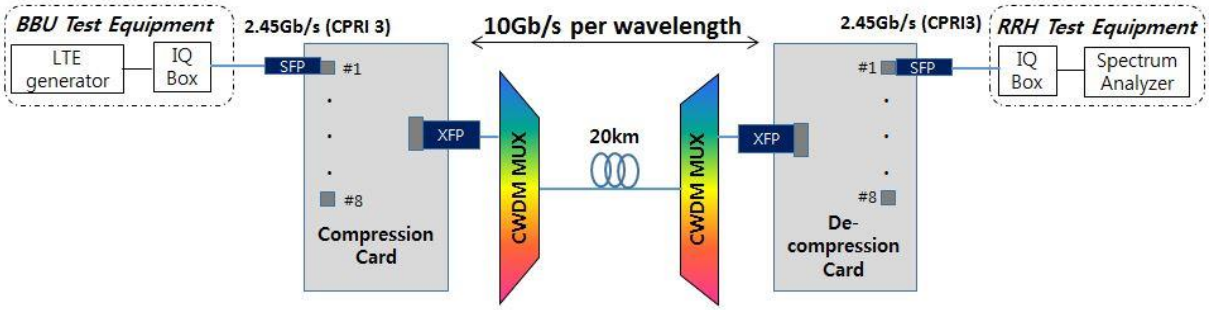

Figure IV-12 : Real time experimental setup

Figure IV-12 shows the experimental setup carried out to evaluate the performance of the system under evaluation. At the transmitter side, a signal generator creates a 20 MHz LTE signal. Standardized test models E-TM3.3, E-TM3.2 and E-TM3.1 are used to investigate the performance of QPSK, 16QAM and 64QAM mappings respectively. Then, an IQ box handles the LTE to CPRI conversion (sampling + quantization + coding); the bit-rate is fixed to 2.45 Gbit/s. These two components emulate the BBU.

The generated CPRI signal is fed to a compression card which allows the encapsulation of up to 8 CPRI 3 (2.45 Gbit/s) links into a 10G frame using TDM.

At the receiver side, a decompression card de-multiplexes different CPRI links and restores them to their original bit-rate. An IQ box is then used for CPRI to LTE conversion and a spectrum analyser with embedded demodulator handles the LTE performance assessment.

The optical transmission between the RAN test equipment and the compression/decompression cards is done with uncolored Small Form-factor Pluggable (SFP). Colored 10G Small Form-factor pluggable (XFP) are used at the output of the compression card and at the input of the decompression card which allows the use of CWDM to multiplex signals from other potential cards.

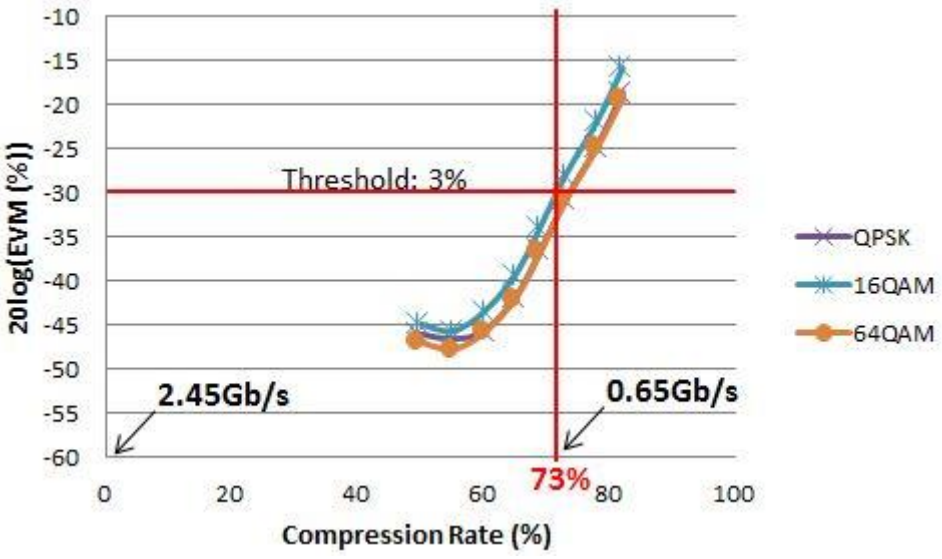

Figure IV-13 : EVM(dB) vs Compression Rate (%)

Figure IV-13 shows the obtained results in terms of EVM for different compression rates. Up to 73% of compression was achieved while respecting the target EVM of 3% leading to a CPRI bit-rate of 0.65 Gbit/s instead of 2.45 Gbit/s. Only 6 quantization bits were used in order to achieve the 73% which is less than was needed for the quantization in the time domain (7 bits as shown in Figure IV-4). 6 bits is also the resolution needed to map a 64QAM constellation, thus the performance with this resolution should have been better than 3%. This degradation is due to the fact that some control channels (Physical Downlink Control Channel, Physical Control Format Indicator Channel, and Physical Hybrid ARQ Indicator Channel) are also transported possibly with different modulation schemes and different power levels. Therefore, higher quantization resolution is needed to preserve the constellations and power levels. It is also worth mentioning that this compression is performed in an external system which bring additional noise, thus performing the compression in the RAN equipment will certainly give enhanced results.

This external processing also causes latency in the fronthaul link which was measured on the C&M CPRI channel using the appropriate CPRI test equipment. Figure IV-14 depicts the obtained 10 measurements of Round Trip Delay for each compression rate. An average RTD value of 8.5 µs was measured for practically all the tested compression rates. This value is largely below the ORI recommendation concerning the RTD (40 µs) [108]. Coordinated MultiPoint (CoMP) implementation for LTE-A tolerates a maximum RTD of 150 µs [117]. Assuming a C-band optical carrier propagating through standard single mode fibre, this would correspond to approximately 15 km. Therefore, the latency introduced by the system would reduce the maximum transmission distance by less than one kilometer (14.15 km).

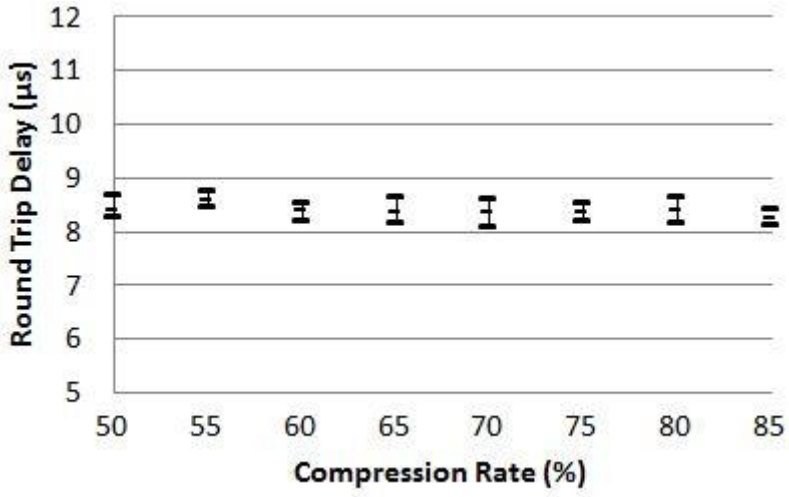

Figure IV-14 : Round Trip Delay (µs) vs Compression Rate (%)

IV.5. Conclusion

In this chapter, an assessment of CPRI compression was carried out based mainly on experimentations in real time when possible, otherwise in offline. Lossy compression based on quantization was studied. 60% compression was achieved with uniform quantization and 66.7% with non-uniform quantization using algorithms such as Lloyd-Max and LBG. With the achieved compression rate, CPRI3 (2.45 Gbit/s) links can be transported at 819 Mbit/s which permits the potential encapsulation of CPRI3 in 1Gbit/s Ethernet frames as it has been discussed by the Task Force IEEE1904.3 and possibly the use of low cost Passive Optical

Networks (G-PON / XG(S)-PON) to transport CPRI. The latency constraints for this last solution have been studied in [118].

However, these compression rates will not be sufficient to cope with the bandwidth evolutions expected for 5G, specifically with massive MIMO. But it still can be used in 5G cells which doesn't use that technology allowing therefore optimum radio coordination (CoMP, CA).

Lossless compression was also evaluated using an industrial prototype. The removal of spectral redundancy (border subcarriers) by low pass filtering allowed a compression of 33%. Moreover, the prototype had a specificity manifested in performing the quantization in the frequency domain. This allowed using 6 quantization bits with uniform quantization while 7 bits were needed for the quantization in the time domain.

This study was focused on the compression technology for the CPRI interface and conducted to the publication of two conference papers (ECOC 2016, cf appendix A). Its implementation showed however limited business application. Nevertheless, the coming eCPRI specification is expected to support natively compression, but on frequency domain signals since this interface is expected to be based on a physical layer functional split. Therefore, eCPRI compression remains a subject of study for the future 5G.

Furthermore, the results obtained in IV.4 were with external compression equipment which brings extra noise in the signal and more latency in the fronthaul link. Improved results must be obtained if this compression process is carried out in the RAN equipment. Switching to the frequency domain inside the BBU would imply moving the iFFT of the LTE modulator from the BBU to the RRH which made us rethink the current LTE functional split in Chapter V, as being discussed by the RAN community.

Chapter V. New functionnal splits

V.1. Introduction

The most recent and also most efficient solution to cope with the increasing fronthaul bit-rate is to establish a new functional split between the DU and the RU. It was indeed identified as the most promising solution for 5G [119] [120]. It would imply the emergence of an evolved fronthaul link, called “efronthaul” for evolved fronthaul, with relaxed bit-rate and latency requirements. Also with the DU virtualization being targeted in 5G, this new functional split should enable its achievement since the high layer radio functions don’t have strict real-time constraints, thus they don’t need to be implemented in dedicated hardware.

In this context, several options of functional splits which can be categorized in high layer splits and low layer splits have been proposed by the 3GPP and the eCPRI specification. An assessment of the resulting architectures as well as the technologies needed to transport these new radio interfaces is reported in this chapter. In section V.2, elements on the LTE radio protocol stack are explained in a nutshell and the different functional splits proposed by the 3GPP are described. Then, in section V.3 the considered architectures and deployment scenarios are described. Later, in section V.4, a theoretical and experimental study is carried out on a high layer functional split based on a virtualized RAN platform; also, its impact on the current access networks (Ethernet backhaul/PON) is evaluated. An analysis of low layer functional split is also reported and some adequate solutions for its transport are proposed.

V.2. New functional splits

V.2.1. LTE radio stack in a nutshell

As mentioned previously, the current CPRI-based DU contains all the LTE radio processing. Figure V-1 shows the different radio functions in the different radio network equipment. MME stands for the Mobility Management Entity; it is the equipment which manages the signaling (Non-Access Stratum - NAS) between the terminals (UE) and the core network LTE. The Packet Data Network Gateway (PGW) forms the unique gateway between the operator's IP network and the Internet. The focus in this study is on the radio functions implemented in the DU. They are grouped into 3 layers of protocol stack and according to [121] and [122] they are described as follows:

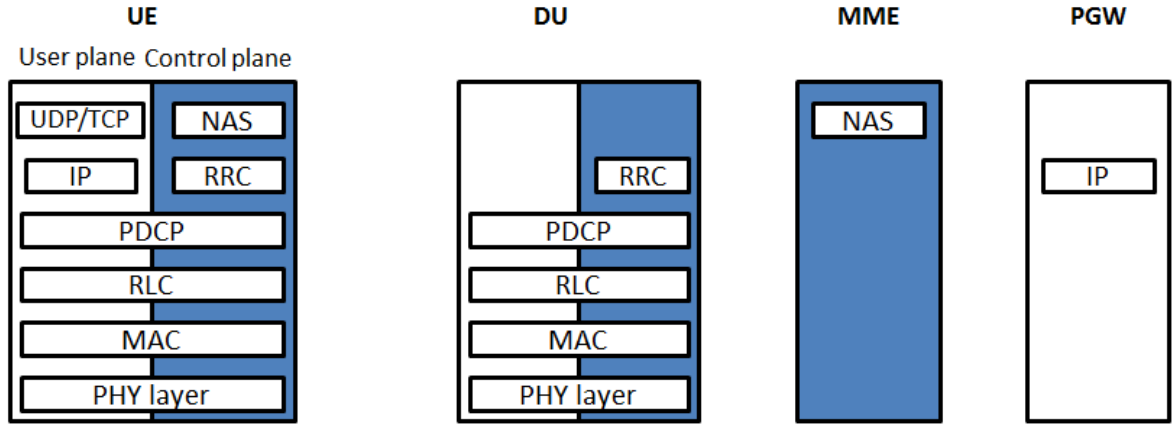

Figure V-1 : Protocol stack of the radio interface [121]

Layer 1:

The layer 1 represents the physical layer (PHY). Its role is to make sure that the data transmission over the air is robust to the disturbances of the radio channel.

The physical layer performs the following functions:

- Channel coding which adds redundancy bits to the useful data to allow the receiver to recover from errors without retransmission.
- Modulation which associates bits to symbols enhancing the bit-rate efficiency.
- Spatial processing (MIMO) which pre-codes the modulation symbols to transmit them over multiple antennas. More elements on the MIMO are brought in V.4.2.
- Multicarrier modulation which associates the signal to be transmitted over each antenna to multiple carriers, according to the OFDM principle for the downlink and SC-FDMA for the uplink.

The physical layer performs also some functions not related to the transmission but mandatory to its proper functioning and also to allow proper operation of some functions of higher layers:

- Radio measurements to estimate the transmission channel, the signal level of the serving cell and that of the cells nearby.
- Synchronization to obtain and maintain a time and frequency synchronization with the transmitter.
- Cell detection to spot the presence of a cell when turning on a UE or in the case of a handover.

More elements on the physical layer are brought in V.4.2.

Layer 2:

The layer 2 is composed of 3 sub-layers:

- PDCP (Packet Data Compression Protocol)
- RLC (Radio Link Control)
- MAC (Medium Access Control)

PDCP:

The main function of PDCP is to ensure the security to the RAN communications. It is responsible of the following functions:

- Header compression using the mechanism RoHC (Robust Header Compression)
- Ciphering of data and signalization
- Protection of the integrity of the control plan
- Detection and removal of PDCP units received twice
- In-sequence delivery by giving a sequence number to each data unit and delivering them in the right order to the next layer

RLC:

RLC is responsible of the control of the radio link between the UE and base station concerning the PDCP packets. It carries out the following functions:

- Retransmission via the ARQ (Automatic Repeat reQuest) mechanism in case an error occurs.
- Concatenation, segmentation and reassembly of the PDCP packets.
- Duplicate detection.

MAC:

The MAC protocol is responsible of:

- Multiplexing of the RLC packets in transport blocs.
- Resource allocation with a scheduling mechanism which defines the coding scheme and the modulation to be applied in the transport bloc. It depends on the condition of the transmission channel, the UE capacity and the required level of QoS (quality of service).
- Retransmission management with the HARQ (Hybrid ARQ) mechanism.

Layer 3:

The layer 3 in the radio interface is mainly composed of the RRC (Radio Resource Control) protocol. It is responsible of the configuration and control of layers 1 and 2.

This protocol has mainly the following functions:

- Broadcast of System Information in the cell for UEs seeking connection.
- Paging signaling for example to inform the UEs connected to the cell about changes in the System Information or to provide an Earthquake and Tsunami Warning System (ETWS) indication.
- Management of the RRC connections (establishment, reconfiguration…).
- Controlling the UE mobility.

For the layers 1 and 2, the LTE system uses the concept of “channels” in order to identify the type of data transported in the radio interface, the characteristics of the associated quality of service as well as the physical parameters related to the transmission. This radio interface channels are access points to the services proposed by a layer N, they allow to the layer N+1 de deliver to the layer N data that must be processed (and possibly stamped) according to the channel specifications [121].

There are 3 types of channels according to the layer they are attached to:

- The logical channels which act between RLC and MAC are defined according to the type of information they are transporting, for instance, control plane signalization or user plane data.
- The transport channels which act between the MAC and physical layer are characterized by how the data is transported on the physical resources. For example, the method of accessing the radio resources (dynamic scheduling…), FEC and MIMO transmission scheme. For instance, in a 2x2 MIMO transmission, 2 transport blocks will be generated for each Transmission Time Interval (TTI). The latter is set by the

scheduler to 1 ms. The transport block size is dependent on the MCS (Modulation and Coding Scheme) and the number of Physical Resource Blocks. The latter is the smallest unit of resources that can be allocated to a user. It is 180 KHz wide in frequency and 1 slot long in time (0.5 ms). The parameters of this channel will be used for the efronthaul bit-rate calculation in V.4.1.

- Physical channels used by the physical layer and defined by the physical characteristics of their transmission, their positioning in the frame for instance.

V.2.2. Functional split options

In this current CPRI-based RAN equipment, all the functions reported above are implemented in the DU and only RF functions are kept in the RU. New functional splits have been proposed by 3GPP in order to relax the bit-rate and latency constraints on the fronthaul link. The target is to end up with an evolved fronthaul (efronthaul) capable on transporting the 5G radio interfaces. Several groups are working on this subject; the proposed functional splits by 3GPP are shown in Figure V-2.

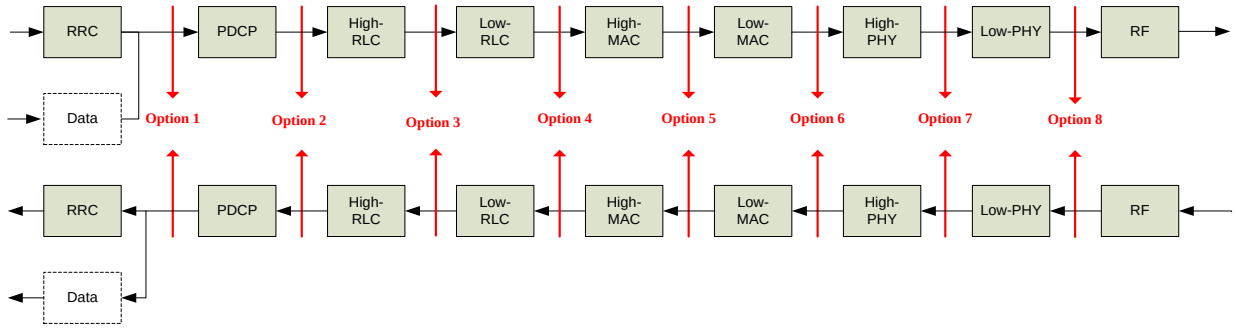

Figure V-2 : 3GPP's functional splits [123]

Option 1 (RRC-PDCP split)

In this split option, only RRC is implemented in the DU. The PDCP, RLC, MAC, physical layer and RF functions are located in the RU.

This split will permit a separation of the user plane and control plane enabling therefore user plane packets to have a direct path to their destination without transiting the centralized DU [125]. The centralization of RRC can also enable a central visibility to signal strength measurement reports and will make it easier to personalize the mobility management algorithms in order to meet the business requirements [125]. The latency requirement on this functional split is similar to the requirement on regular backhaul (S1 interface).

Option 2 (PDCP-RLC split)

Option 2 rests upon implementing the RRC and PDCP in the DU and the RLC, MAC and physical layers in the RU.

This split option will enable traffic aggregation from 5G and LTE transmission points to be centralized [123] [125]. Moreover, it will make it easier to manage traffic load between 5G and LTE transmission points [123] [125]. The fundamental driver behind this split is the Dual

Connectivity which already has been standardized for LTE. The efronthaul interface resulting from this functional split is called “F1” for 5G and “V1” for LTE according to [123]. It was also selected by the 3GPP’s working group RAN3 for normative work in Release 15 [126]. This high-level split was therefore a subject of interest in this thesis, its drivers and performances are investigated in V.4.1.

Option 3 (intra RLC split)

This option consists in splitting within the RLC functions. Two approaches have been proposed based on a Real-time/ Non-Real-time functional split.

The first approach rests upon having a High RLC composed of ARQ and re-ordering functions and a Low RLC where the segmentation and concatenation functions are implemented [123]. This approach would permit having a more robust link since the ARQ and the packet ordering is performed in the DU. Also, the ARQ centralization would permit achieving further pooling gains. Moreover, the absence of the ARQ protocol in the RU may reduce the processing and buffer requirements. However, larger buffers might be needed in the DU. Also, this split is more latency sensitive than the split with ARQ in the RU, since re-transmissions are fragile in view of transport network latency [123].

The second approach consists in having a High RLC composed on the receiving functions and a Low RLC composed on the transmitting options which makes the efronthaul link less sensitive to the transport network latency [123]. More elements on this approach are brought in the standard [123].

Option 4 (RLC-MAC split)

Option 4 consists in splitting between the RLC and MAC functions. This would permit increasing the number of features that can be scaled such as load balancing. Nevertheless, the implementation of such functional split can be very complex giving the tight coupling between the RLC function and the MAC function, especially the scheduler. Therefore, a flow control method would have to be defined to decouple the RLC and MAC in order to enable supporting this split option. [125]

Option 5 (intra MAC split)

Splitting at the level of the MAC layer can be a solution for “de-coupling” MAC and RLC. In this option most of the MAC functions are centralized and implemented in the DU. Only the HARQ protocol is moved to the RU. This functional split will enable a centralized scheduling which would enhance the capabilities for coordinated transmissions across multiple cells [125].

Option 6 (MAC-PHY split)

This split consists in centralizing the layer 2 and layer 3 of the radio signal and implementing the physical layer in the RU. In this case, the efronthaul will carry data, configuration, scheduling-related information and measurements. The generation of the radio signal is performed in the RU. Therefore, significant efronthaul bandwidth reduction is expected with this split. Although, giving that the HARQ protocol is moved to the DU, the latency requirement on the efronthaul would be similar as in the CPRI based fronthaul [125].

Option 7 (intra PHY split)

This option includes different split possibilities, each one with different bit-rate requirements. An analysis on this option is reported in V.4.2.

Option 8 (PHY-RF split)

This split is the one used in the current RAN equipment introducing a CPRI based fronthaul (c.f. Chapter I and Chapter II for more details).

The bit-rate and latency requirements for these splits according to [125] are reported in Table V.1 for an LTE 20 MHz 2x2 MIMO in the downlink and 1x2 SIMO in the uplink.

Table V.1 : Bit-rate and latency requirements for different functional splits according to [125].

RAN functional split	One-way latency (maximum value)	Downlink data rate (Mbit/s)	Uplink data rate (Mbit/s)
RRC-PDCP	30 ms	151	48
PDCP-RLC	30 ms	151	48
MAC	6 ms	151	49
MAC-PHY	2 ms	152	49
Split PHY	250 µs	1075	922
CPRI/OBSAI (low layer split)	250 µs	2457	2457

V.3. Architectures and deployment scenarios

After introducing the different functional splits proposed by the 3GPP, the focus in this thesis was on two main splits: the first one is a high layer split based on the 3GPP's option 2. The resulting efronthaul interface is referred to as F1/V1 by 3GPP. The second split is a low layer split mainly driven by the CPRI consortium. Its aim is to define an evolved CPRI interface called "eCPRI" at least 10 times more efficient (bit-rate wise) that the current CPRI interface. It will be likely based mainly on option 7, but options 6 and 8 are also possible. There are some discussions about this split within the RAN 3 working group in the 3GPP, but its standardization has been postponed for lack of the analysis maturity on this subject [127].

These two upcoming radio interfaces are depicted in Figure V-3. In the current RAN equipment, there are two parts: DU for digital unit and RU for radio unit. 3GPP recommended splitting the RAN equipment into three parts for the future networks: Central Unit (CU), Distributed Unit (DU) and Radio Unit (RU). It must be highlighted that the term DU in this thesis identifies both Digital Unit (for traditional CPRI-based RAN equipment) and Distributed Unit (for RAN equipment with virtualization). The terminology has been chosen to be compliant with the 3GPP standard documents.

Moreover, 3GPP defined several deployment scenarios with these three RAN pieces of equipment. Some of them include the use of a new 5G core network which is not in the scope of this study as it is not considered by Orange for the first phase of deployment. Thus, we propose in this chapter to describe three potential architecture scenarios including RAN and fixed network with a focus on the fixed access network. LTE and 5G are considered in

these scenarios with a backhauling (S1 interface) to the LTE's current core network. Therefore, only the option 3/3a from [123] is considered.

This assessment will consider both regular and virtual implementations of RAN equipment. For simplification, we will consider that the Digital Unit and the RU are linked with a CPRI-based fronthaul for LTE. For 5G we consider that the CU and DU are connected with the F1 interface and the DU and RU are linked with the eCPRI interface.

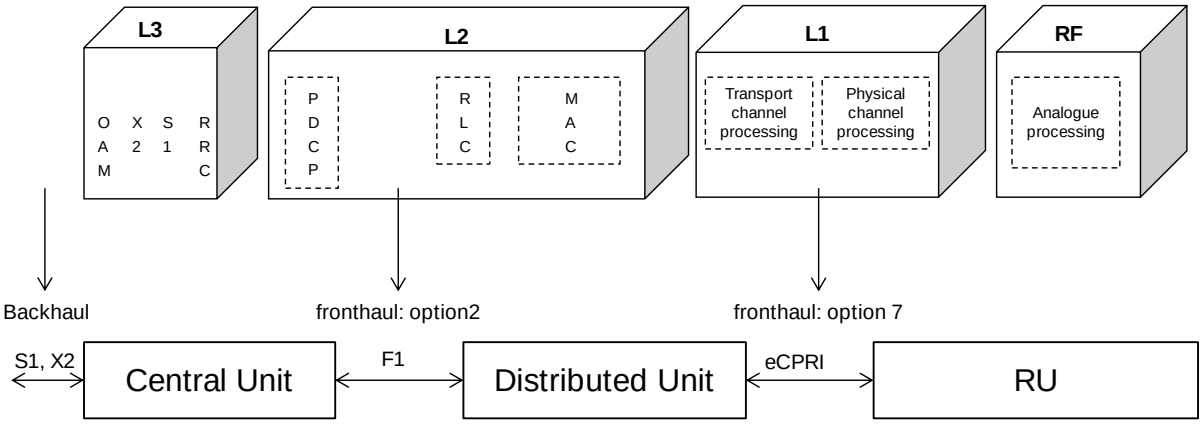

Figure V-3 : Mobile architecture with CU and DU [124].

The reason of mixing 4G and 5G technologies in this analysis is that multi-connectivity of end user to multiple cells and radio technologies is a key enabler of 5G. In fact, Dual Connectivity between 4G and 5G is an expected feature for 5G launch, especially since the spectrum to be allocated for 5G (sub-6 GHz) is limited. Therefore, using dual connectivity is essential to provide enhanced services compared to LTE. In the following, three deployment scenarios based on the 3GPP standard are described and the resulting network architecture is shown.

V.3.1. Scenario 1

The first scenario is depicted in Figure V-4, it is based on LTE and 5G RAN in regular (no virtualization) distributed mode (D-RAN), with all RAN equipment localized at the antenna site. In this case, both the low and high layer split interfaces need local links within the antenna site. An additional local interface is needed to perform the dual connectivity between LTE and 5G. It is called "Xx interface" and links the LTE DU to the 5G CU as shown in Figure V-4. This Xx interface is defined by 3GPP as the interface which allows linking the 5G base station to an LTE eNodeB connected to a core network [123], Figure V-5 shows the positioning of this interface within the protocol stack of both LTE and 5G.

In this scenario, conventional CPRI interface is used to connect the 4G DU and RU, the eCPRI interface is used to link 5G DU to RU and the F1 interface is used to connect the 5G DU and CU. The backhaul is composed of the S1 interfaces of the LTE and 5G which are aggregated / desegregated at the antenna site in access equipment called Optical Network Unit (ONU) in Figure V-4. This equipment is also called cell site gateway by the radio community. The access backhaul segment between antenna site and central office (access node) uses either Point to Point (PtP) or point to multipoint based on Passive Optical Network (PON) technology as discussed in Chapter I.

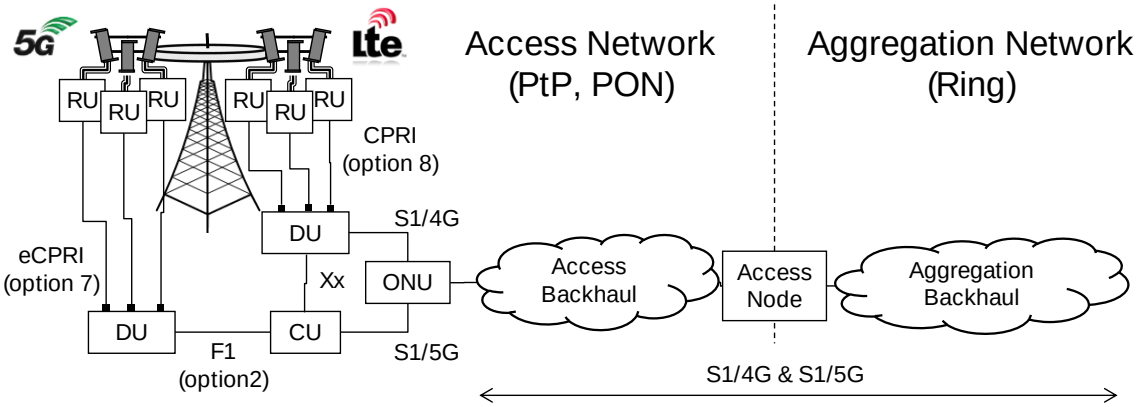

Figure V-4 : Scenario 1: Distributed architecture based on 4G and 5G RAN equipment at the antenna site only [124]

The ONUs currently deployed in Orange France networks are 1 Gbit/s Ethernet equipment. However, with the traffic evolution expected with the introduction of 5G, this equipment will need to be upgraded. In fact, it was recently decided to swap all Orange France antenna sites equipment to 10 Gbit/s capable interfaces. Concerning the backhaul aggregation network segment, it uses ring or mesh topologies with typically Internet Protocol and/or Multi-Protocol Label Switching (IP/MPLS) transport.

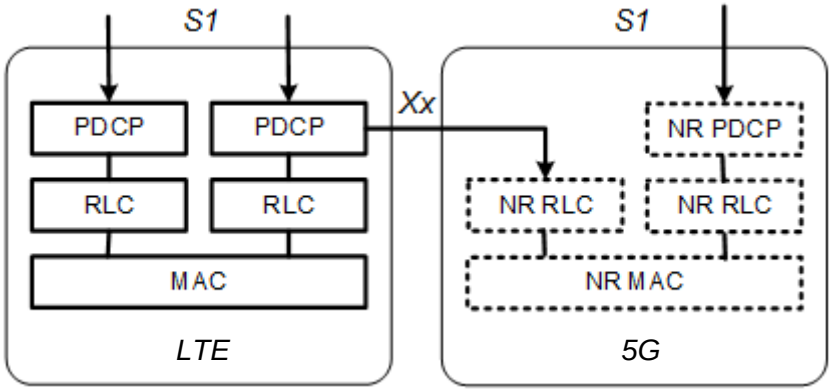

Figure V-5 : Radio Protocol architecture in option 3/3a [123]

V.3.2. Scenario 2

The second scenario, shown in Figure V-6, is based on a distributed LTE RAN (without virtualization) and a centralized 5G RAN (with virtualization). In this scenario, the 5G CU is located at the aggregation node; equivalent to a regional Point of Presence (PoP) in Orange's network. The CU functions will be most likely virtualized and will be hosted in a datacenter-like local, while the 5G DU is located in the antenna site. This scenario considers also the possibility to have 5G small-cell as shown in Figure V-6. It is considered that the 5G small-cell RAN is compact form factor equipment with DU and RU which is adequate for centralized scenario since it offers a solution with low footprint and power consumption at the antenna site.

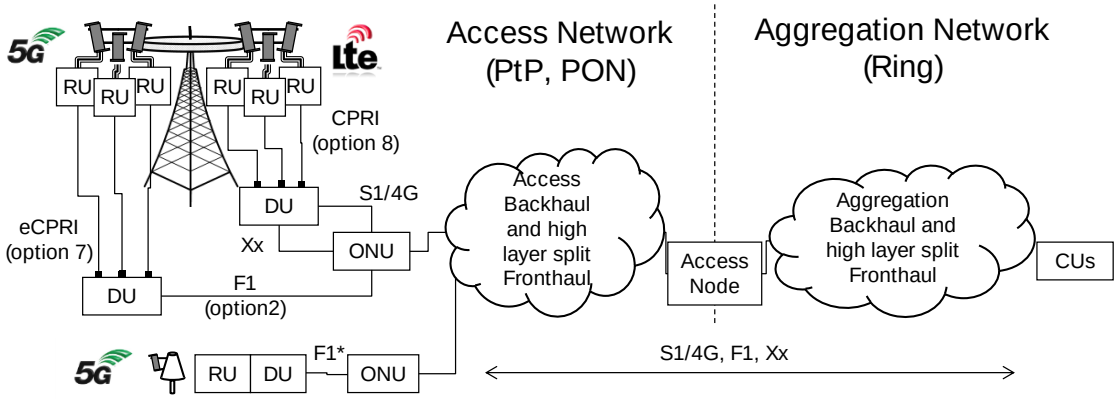

Figure V-6 : Scenario 2: Architecture mixing 5G in virtualized RAN mode and 4G in distributed RAN mode equipment [124]

In this case, the fixed transmission concerns the backhaul for LTE and high layer split fronthaul for 5G macro-cell (F1). For the 5G small-cell, an interface F1* is used on the figure since a different interface than F1 might be used. In fact, the Small Cell Forum is pushing a different fronthauling interface called Femto Application Platform Interface (FAPI) based on a MAC-PHY split [128]. Thus, it remains to be seen if such interface will be supported by the 3GPP standard or the use of F1 will be recommended for both macro and small cells, notably to facilitate the overall fronthauling.

Here, we propose to use a single ONU to collect the S1, Xx and F1 interfaces for the macro-cell. The ability of the regular current transport equipment to collect these new interfaces is studied in V.4.1. A different ONU is proposed for the small cell mainly because it will most likely have a different location compared to the antenna site ONU.

V.3.3. Scenario 3

Figure V-7 depicts the last proposed scenario. It concerns the RAN centralization of both LTE and 5G, with the virtualization mode only for 5G. The DUs are located at the central office and the CUs are located in the aggregation node.

The fixed access networks are now dedicated to low layer split (option 7 and option 8) fronthaul for macro-cell and high layer split (F1*) fronthaul for small-cell. Transport solutions for such scenario will be proposed in V.4.2. Concerning the aggregation network, it will handle the aggregation of all centralized 4G DUs backhaul and all centralized 5G high layer split fronthaul (F1 and F1*) as well as the Xx interface.

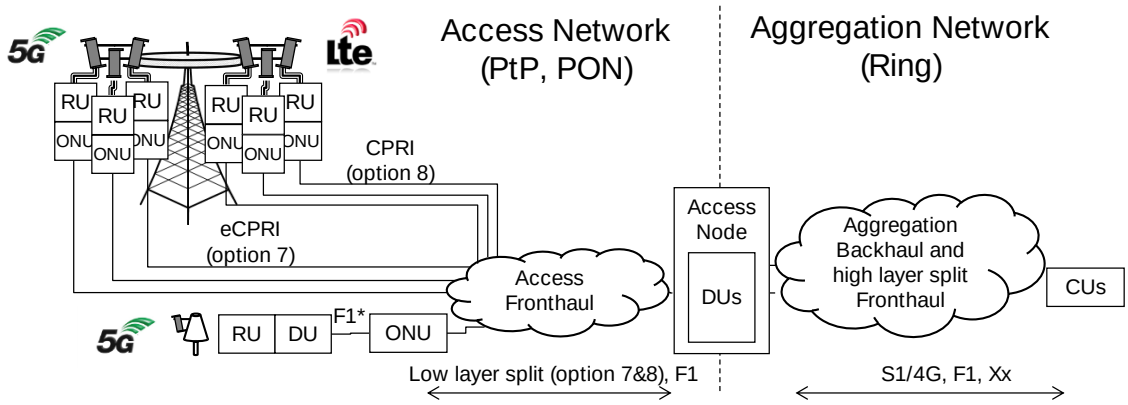

Figure V-7 : Scenario 3: Architecture mixing 5G in virtualized and centralized RAN mode and 4G in centralized RAN mode equipment [124]

V.4. Transport solution for fixed access networks

V.4.1. High layer split

As mentioned in V.2.2, the functional split option 2 based a PDCP-RLC split was identified as an interesting option by the 3GPP which defined the interfaces F1 and V1 accordingly. Therefore, this functional split represented a subject of interest for Orange who is also investigating the RAN virtualization for its future networks. In fact, RAN virtualization aims to decrease the use of specific hardware (DSP, SoC, FPGA), which are requiring more and more investments, in a market with smaller margins. However, the first Total Cost of Ownership (TCO) analysis carried out by Orange do not highlight significant gains, mainly because not all the RAN equipment can be virtualized (real-time constraint) and because main suppliers want to move revenues from hardware to software [129].

Nevertheless, some technical drivers exist to justify the RAN virtualization. Namely, as mentioned in V.3, the dual connectivity is a key feature expected for 5G. It requires the PDCP centralization which is well adapted with the virtualization [129]. Moreover, in the current LTE networks, Quality of Experience (QoE) improvements are limited by the latency from the user and applications and by the lack of communication between the RAN and applications. Therefore, Multiple Access Edge Computing (MEC) was proposed by ETSI in order to try to solve these issues by moving applications to the edge and creating open APIs (Application Programming Interface) to interact with the RAN directly [129]. The high radio layers centralization and the virtualization are seen as key enablers for these features [129].

In the radio protocol stack, some functions (Low RLC and below) have real-time constraints which cannot be handeled by the General Perpuse Processors (GPPs) currently. Chipset vendors are actively working on more powerfull GPPs but they will be unlikely ready for the 5G's first phase. Therefore, to sum-up, puting as a target enabling virtualization and dual connectivity as well as relaxing the bit-rate and latency constraints, the PDCP-RLC split appreared to be the best option.

This split option is therefore experimentally investigated in this section using an industrial prototype. The target is to define the bit-rate and latency requirements on the transport/access network needed to transport the V1 radio interface.

V.4.1.1. Experimental setup

As shown in Figure V-8, we experimentally investigated two Ethernet-based solutions for the transport of the new fronthaul interface: Point-to-Point and Point-to-Multipoint with a G-PON (Gigabit capable PON) system.

At the transmitter side, generic servers running on OpenStack host a virtual EMS (Element Management System), a virtual EPC (Evolved Packet Core) where the Mobile Edge Computing (MEC) is happening and a virtualized Centralized Unit (vCU). A 10G Top of Rack (ToR) Ethernet switch is used to connect these nodes. At the receiver side, a RU is connected to a User Equipment (UE) (here, a computer) via a mobile dongle. This industrial doesn't contain a DU, the RLC, MAC and PHY are implemented in the RU.

We use a mobile signal based on a LTE (Long Term Evolution) with 15MHz bandwidth and 2x2 MIMO (Multiple Input Multiple Output). The synchronization in this network is provided by Global Positioning System (GPS) devices connected to each RU.

For PtP efronthaul, we used common 1 Gbit/s Ethernet switches in both ends, the same as the ones currently used for collecting LTE backhaul interfaces. Packet loss and latency are then inserted with a dedicated test device in order to evaluate its impact on the mobile throughput.

For the PtMP efronthaul, an Optical Line Termination (OLT) is installed after the ToR switch and an Optical Network Unit (ONU) is associated to each RU. We allocated fixed bandwidths for the upstream to the ONUs, 200 Mbit/s for ONU 1 connected to the RU 2 and 600 Mbit/s for ONU 2 used for overloading the G-PON system. With this configuration, we evaluated the LTE throughput for different lengths of optical fiber.

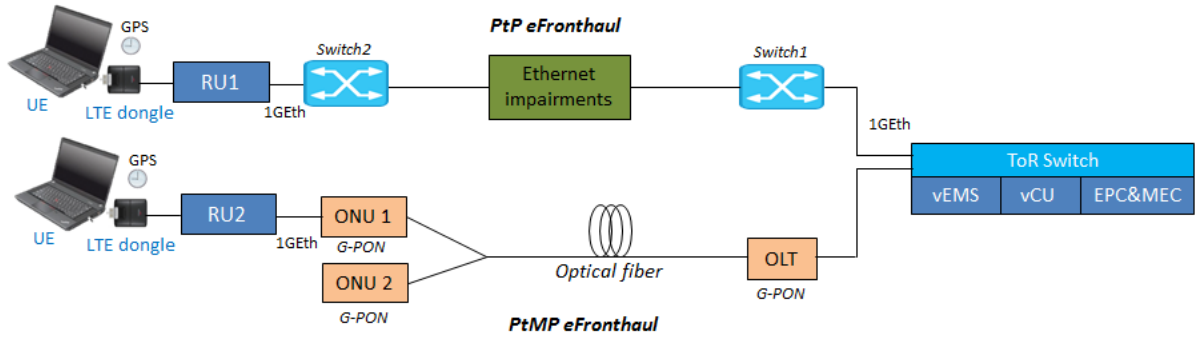

Figure V-8 : vRAN experimental setup

V.4.1.2. Experimental results and discussion

- **PtP eFronthaul**

We started our investigation with the PtP configuration. Figure V-9 depicts the impact of the used functional split on the traffic of the vRAN. For the downstream, we generated traffic with different bit-rates in the EPC and evaluated the bitrate in the backhaul, fronthaul and the UE. In the upstream, we generated traffic in the UE and measured the bit-rate in the fronthaul, backhaul and EPC. It is interesting to notice that the traffic in the fronthaul varies depending on the mobile traffic demand unlike the currently used functional split with CPRI, which works at fixed bit-rates (here, CPRI 3 corresponding to 2.5 Gbit/s in this radio configuration). In the downlink (DL), we observe an increase of 5% in the backhaul bitrate compared to the generated traffic in the EPC, which is due to the encapsulation in Ethernet frames. A 20%

increase of traffic is measured in the efronthaul compared to the backhaul. This traffic eventually stabilizes when the maximum radio throughput is reached because the vCU adapts the efronthaul bit-rate to the available radio resources. A similar behaviour is observed in the uplink (UL).

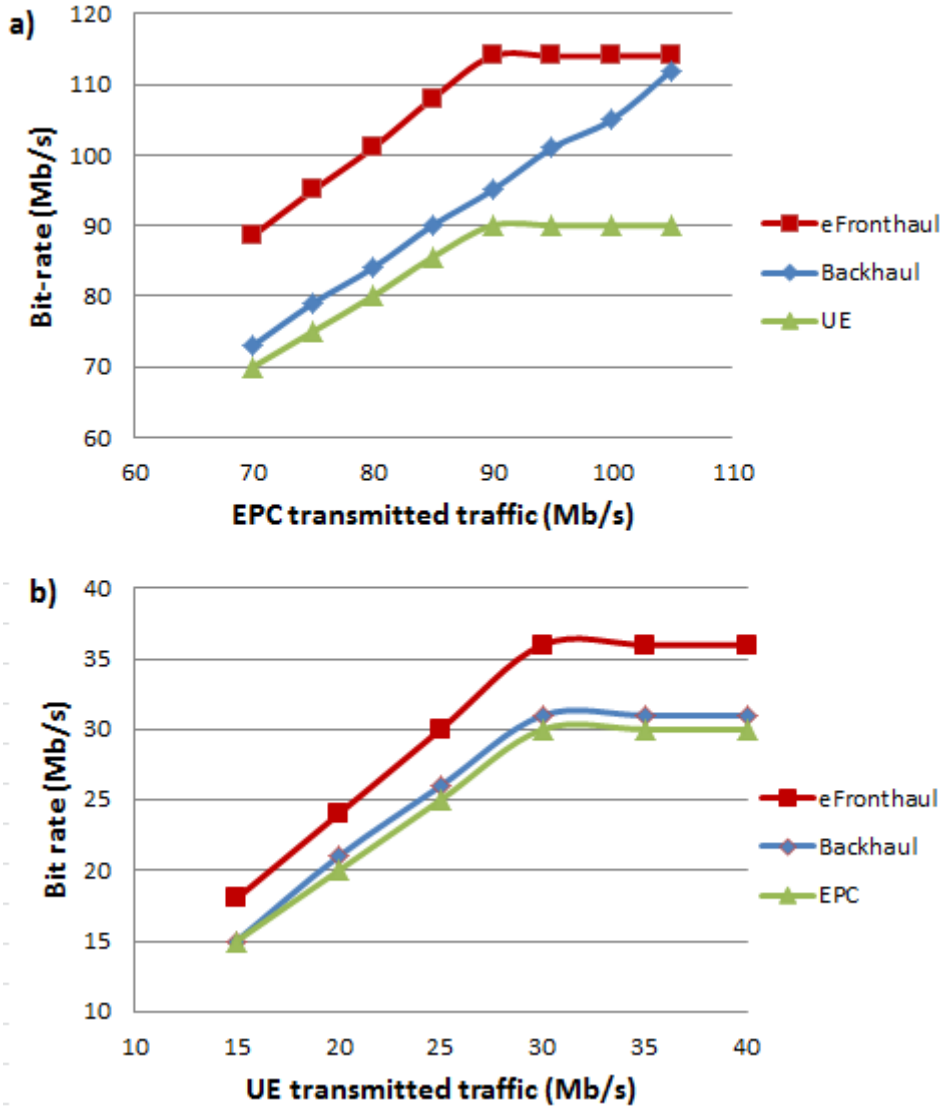

Figure V-9 : Backhaul and eFronthaul traffic in the downlink (a) and uplink (b)

Theoretically, the obtained PDCP-RLC interface bit-rate in the downlink is expressed by the following equation [125]:

$$\mathrm{F1}_{bit-rate} = \frac{IP_{TTI} \times (IP_{pkt} + Hdr_{PDCP}) \times N_{TBS} \times 8 \times 1000}{1000000} \quad (10)$$

Where IP_{TTI} is the IP packets per transport block, IP_{pkt} is the IP packet size in bytes, Hdr_{PDCP} is the PDCP header in bytes and N_{TBS} is the Transport Blocks per Transmission Time Interval (TTI). IP_{TTI} is defined with the following equation [125]:

$$IP_{TTI} = \frac{\mathrm{TBS}}{(\mathrm{IP_{pkt}} + \mathrm{Hdr_{PDCP}} + \mathrm{Hdr_{RLC}} + \mathrm{Hdr_{MAC}}) \times 8} \quad (11)$$

Where TBS is the Transport Block Size (in bits), Hdr_{RLC} is the RLC header in bytes and HDR_{MAC} is the MAC header in bytes.

The used parameters for the calculation of this equation are reported in Table V.2. 15 MHz LTE bandwidth were used in the experimentation, which corresponds to 75 resource blocks. Also, the UE was wired to the RU which permitted to have the best radio transmission conditions. Therefore, the scheduler set the higher modulation and the lower channel coding which corresponds in the Table 7.1.7.1-1 of [130] to a TBS index of 26. The Table 7.1.7.2.1-1 of the same 3GPP document gives for such number of resource blocks and such TBS index a transport block size of 55056 bits. With this value and using the two previous equations we obtain a bit-rate of 109.6 Mbit/s. Knowing that this V1 interface is encapsulated in Ethernet, 5% additional bit-rate for Ethernet framing must be added. With this, we obtain a bit-rate of 115 Mbit/s which correspondents to the value obtained experimentally (114 Mbit/s).

Table V.2 : Bit-rate calculation parameters

Parameter	Value
IP_{pkt}	1500 bytes
Hdr_{PDCP}	2 bytes
Hdr_{RLC}	5 bytes
HDR_{MAC}	2 bytes
N_{TBS}	2
TBS	55056 bits

Figure V-10 shows the impact of packet loss on the mobile LTE throughput in the downstream and upstream using TCP (Transmission Control Protocol) and UDP (User Datagram Protocol) for the mobile signal between EPC and UE. In few words, TCP continuously adapts the transmission bit-rate to the network capacity to avoid congestion while UDP transmits at a constant bit-rate. We can see that the LTE throughput is not impacted by packet loss down 1% for UDP transmission. For TCP, the impact on throughput is negligible for packet loss down to 0.1% for the downstream and 0.4% for the upstream. Therefore, the transmission is robust since only 10^{-3} packet loss for non-priority data and 10^{-5} for priority data is recommended generally for Ethernet transmissions in the backhaul. Throughput degradation is noticed between TCP DL and UDP DL at 0% packet loss, which is due to the limited buffer capacity of the used LTE dongle. Ulterior tests with another dongle done by a partner showed similar TCP and UDP throughput at 0% packet loss.

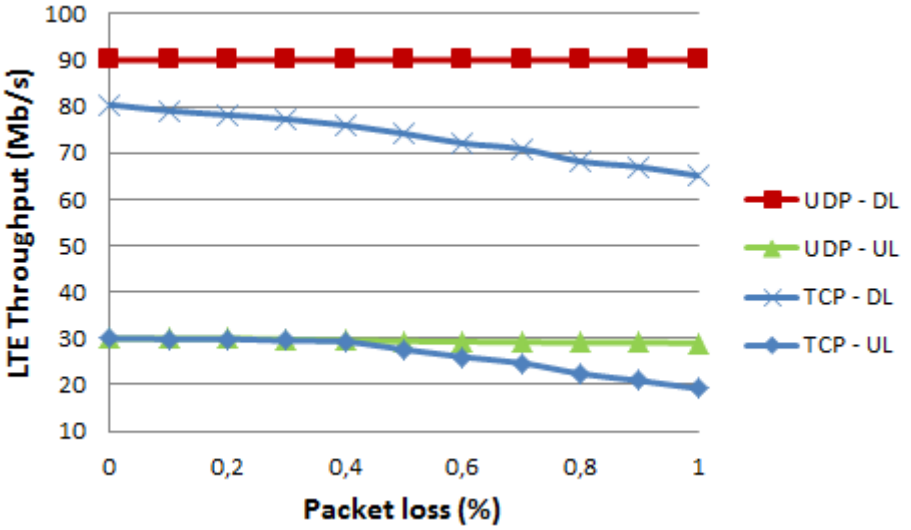

Figure V-10 : Packet loss (%) vs LTE Throughput (Mbit/s)

The one-way latency impact is represented in Figure V-11. No impact is observed for injected latencies up to 20 ms. Knowing that the latency in the current LTE network, between the master CO (regional PoP) and the cell site gateway, is between 5 and 10 ms, the re-use of the existing backhaul network to transport the V1 interface should not affect the performances in the case of LTE. However, these values must be reduced for the ultra-low latency applications expected in 5G. Therefore, new generation PoP located closer to the antenna sites as well as low latency transport equipment are needed.

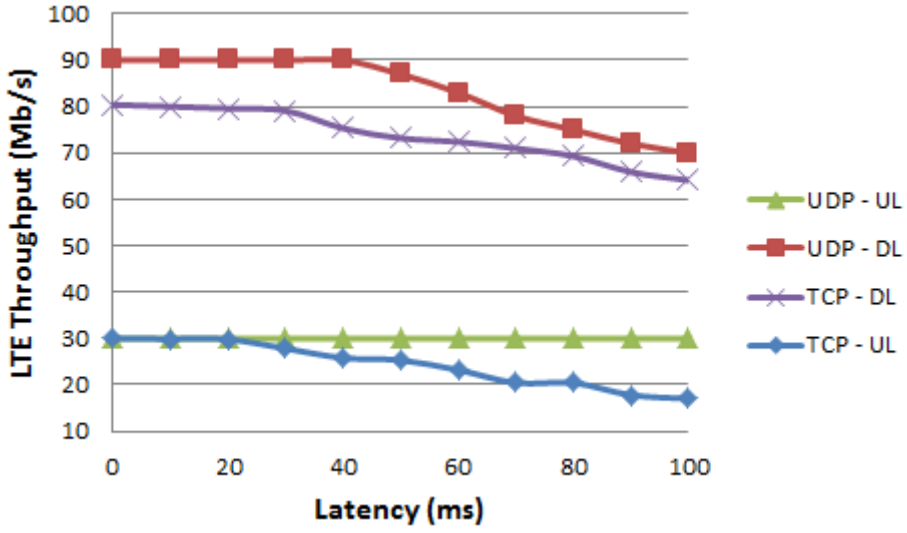

Figure V-11 : Latency (ms) vs LTE Throughput (Mbit/s)

- **PtMP eFronthaul**

PtMP architecture based on PON is also an adequate candidate to accommodate efronthaul considering the large availability of FTTH infrastructures and the low-cost of its equipment. This was also pushed by several industry actors such as NTT [131]. It was difficult to achieve this with the CPRI-based fronthaul because of bandwidth and latency issues. Since these metrics were relaxed with this new functional split, G-PON can be used for the access part of the architecture shown in Figure V-6 and Figure V-7.

As discussed in Chapter I, the upstream transmission in PON is done according to some bandwidth allocation mechanisms to enable a better use of the PON resources by permitting to take advantage of the unused bandwidth by other customers and also to attribute different service profiles to the traffic which allows a better Quality of Service. In fact, The GPON standard introduces the concept of traffic container (T-CONT) for the upstream direction which is a logical queue at the ONU associated with specific QoS requirements.

Five T-CONT types have been defined to provide different levels of QoS:

- T-CONT1 which is a fixed bandwidth type mainly used for services sensitive to delay and high priority like voice over IP.
- T-CONT2 and T-CONT3 are guaranteed bandwidth types mainly used for video services and data services of higher priorities.
- T-CONT4 is a best-effort type used for data services such as Internet and services of low priority which do not require high bandwidth.
- T-CONT5 is a mixed type, involving all bandwidth types and bearing all services.

The Dynamic Bandwidth Allocation (DBA) algorithm based on status reporting method introduces around 1 ms latency [143], which is too much for the access considering 5G requirements. One approach to reduce the DBA latency is to use a fixed bandwidth allocation (FBA) scheme (T-CONT1) as described in the experimental setup. Table V.3 shows the results for efronthaul over G-PON. No impact is noticed when overloading the system with a second ONU (named ONU 2 in Figure V-8) using an Ethernet tester. In fact, for the downstream, we obtained performances similar to PtP for 0 km and 10 km. A little impact is noticed in 25 km since the used G-PON product is designed to operate between 0 and 20 km. For TCP transmission in the uplink, we notice throughput degradation compared to PtP. This could be due to the packet latency unbalance (40 µs in the downstream and 140 µs in the upstream) and/or the packet jitter (0.9 µs in the upstream and 48 µs in the upstream) introduced by the G-PON system, which affects the queuing policies used by the vRAN equipment. Further investigations need to be carried out in order to identify the reason behind this performance degradation. Some adjustments, possibly based on coordination between the CU and the OLT as suggested in [143], might be needed to transport this new efronthaul interface with no impact on the LTE throughput and the quality of the delivered services.

Table V.3 : Mobile throughput downlink and uplink for efronthaul over G-PON

	LTE throughput (Mbit/s)			
Fiber length (km)	UDP DL	UDP UL	TCP DL	TCP UL
0	90	30	82.9	20.8
10	90	30	82.5	20.3
25	88	30	81.6	19.7

For a 20 MHz LTE cell with 2x2 MIMO, the V1 interface will have a bit-rate of 187.5 Mbit/s in the downlink and 62.5 Mbit/s in the uplink. Giving that G-PON offers 2.5 Gbit/s in the

downlink and 1.25 Gbit/s in the uplink, only 13 antennas can be served on a G-PON tree in FBA mode. Knowing that G-PON was designed to serve up to 64 residential clients, its use to transport the F1 interface in FBA mode would not be cost effective. The use of DBA will allow collecting more antennas, especially with low latency DBA algorithms being under investigation in different research centres [132] [133]. However, the impact of the use of DBA on the radio performance must be investigated.

Moreover, the F1 interface for 5G will have a much higher bit-rate compared to LTE. In the annex A of the eCPRI interface [134], 5G radio data-rate calculation were done based on a 100 MHz bandwidth and 64 antennas (8 MIMO layers) which gives 3 Gbit/s end-used data rate in the downlink. Using the 20% additional data for the PDCP-RLC split and the additional 5% for Ethernet encapsulation, we obtain 3.75 Gbit/s data-rate for the F1 interface per antenna. Such traffic cannot be handled by G-PON. More evolved PON systems (reported in Chapter I) could be used. Table V.4 shows the number of antennas potentially collected with different PON systems on FBA mode. We notice that with FBA mode, the use of XGS-PON and NG-PON2 can be interesting but only for the case of LTE.

Table V.4 : Number of antennas potentially collected with PON on FBA mode

	Number of antennas potentially collected	
PON system	LTE	5G
G-PON	13	0
XGS-PON	53	2
NG-PON2	213	10

Besides the bit-rate constraint, the network topology on the field is an essential factor to study when evaluating technology feasibility. Figure V-12 depicts the geographical location of Orange's antenna sites (2G/3G/4G) and the FTTH shared access points of the city of Limoges in France. A shared access point is the place where the connection between the optical fibers of the different FTTH subscribers and the optical fibers of the operators takes place, a shared access point links generally 300 clients. We can see that the antenna sites have a very different density compared to residential clients which makes sense since FTTH infrastructures were deployed to physically link 100% of the clients located in a given area while mobile deployments are based on a radio coverage strategy. Therefore, using dedicated PON trees for collecting the F1 interfaces in a network based on macro and micro cells might not be appropriate. However, in the case of massive deployment of small cells, a scenario with mixt trees for FTTH and mobile (antennas) clients might be conceivable. In this case, a thorough investigation needs to be carried out to define a DBA algorithm enabling to serve both types of clients while respecting their respective QoS requirements.

Consequently, PtP Ethernet is the way to go for the 5G phase 1 deployment. This solution is all the more interesting with the emergence of Flex Ethernet [135] whose standard release (agreement 2) is expected by 2017 Q4. FlexETH is based on a physical isolation. Via TDM technology, a physical port can be splitted into multiple sub channels, with independent time slots and MAC which allows ensuring a guaranteed forwarding latency and avoid congestion as recommended for URLCC services (described in Chapter I). Such solutions need to be experimentally evaluated to ensure its effectiveness compared to regular switch equipment.

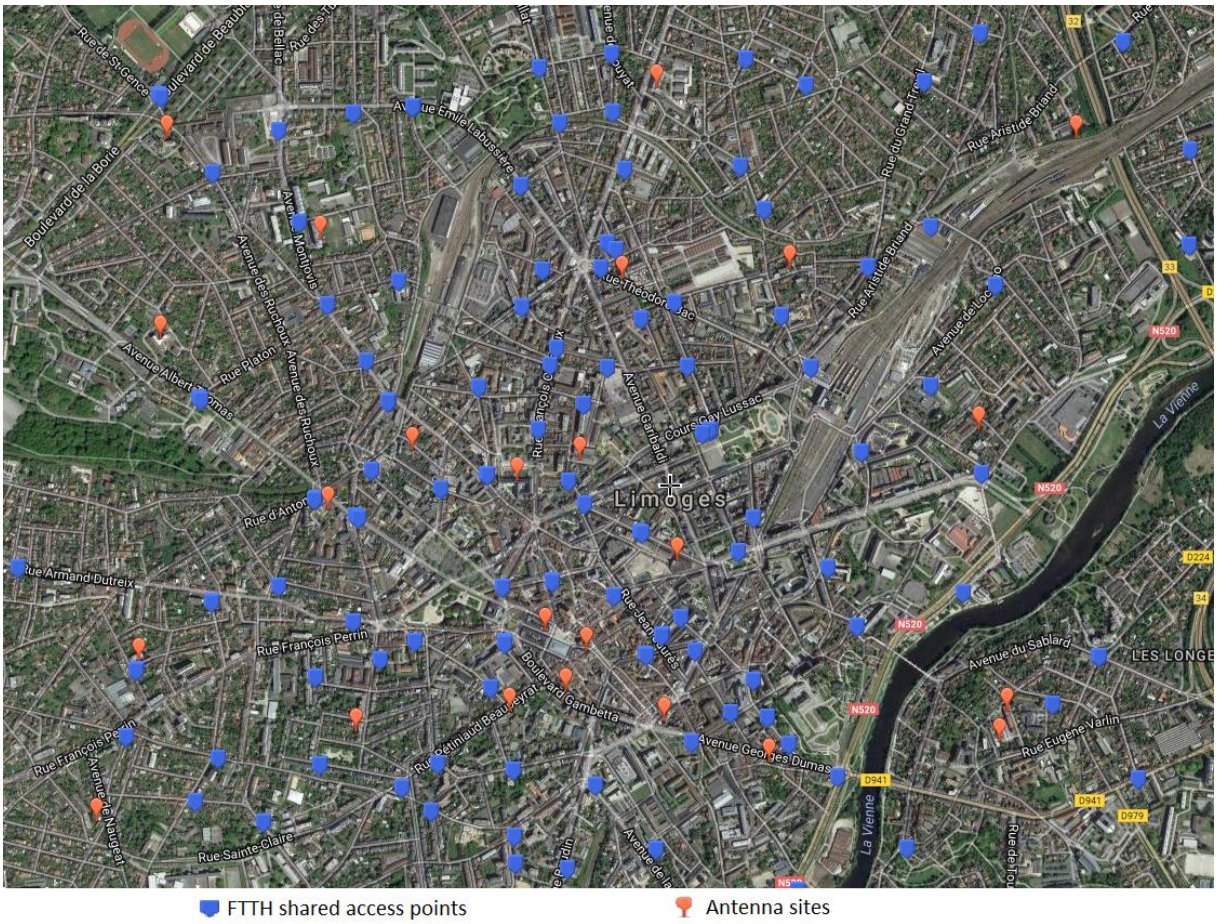

Figure V-12 : Geographical location of antenna sites and FTTH shared access points of the city of Limoges in France

V.4.2. Low layer split

As shown in Figure V-7, there is a deployment option where a low layer split is transported between the access node and the antenna site unlike the solution evaluated in V.4.1 where the V1 interface is used from the aggregation node to the antenna site. The advantage of having a low layer split in the access segment is that the centralization of the physical layer processing (entirely or partially) in the access node enables allows performing more or less inter-cells radio coordination.

A first level of radio coordination was introduced in the LTE release 8 with the Inter-Cell Interference Coordination (ICIC) for distributed RAN architecture. In the latter, the UE communicates to the base station the occurrence of some interference on certain subcarriers, so it requests to the neighboring base stations through the X2 interface to avoid serving the cell-edge UEs on theses subcarriers. Such procedure was time consuming (several seconds) and not very efficient. More efficient radio coordination features called Coordinated MultiPoint (CoMP) were introduced in the release 11 of the 3GPP. Three main types of CoMP were introduced: Dynamic Point Selection (DPS) [138], Coordinated Scheduling/Coordinated Beamforming (CS/CB) [139] [140] and Joint Transmission (JT) [136] [137]. In DPS, the UE can select the RU which presents the best SINR. This operation is done dynamically for every LTE sub-frame (1 ms). With CS/CB, the decision of scheduling is

coordinated between multiple transmission points in order to minimize interference but the transmission to a UE is done from one point. In JT, the signal destined to a UE is transmitted from different antenna geographically distributed. The principle is similar to MIMO systems but in a larger scale. Thus, joint transmission permits interference avoidance and enhancing the radio throughput consequently.

The appropriate operation of these features requires a tight coordination between some physical layer functions of neighboring base stations hence the need of centralization. The current (CPRI-based) functional split where the entire radio physical layer is centralized enabled performing all the CoMP features but its use for 5G turned out to be very challenging as explained in Chapter II. The stake for this new low functional split is to maintain the possibility to perform a decent amount of radio coordination while having a fronthaul link with variable bit-rate (dependent on the load) no more than 25 Gbit/s.

Figure V-1 shows the different splits proposed by the eCPRI specification and the 3GPP standard. Besides the element reported in V.2.1, it is worth bringing some elements on the physical layer functions depicted in Figure V-13. In fact, in the downlink, the transport channel forwards a line of code-words to physical layer module which proceeds as follows. After the channel coding, the scrambling mixes each code-word with a pseudo-random sequence dependent on the cell in question to reduce interference with neighboring cells [122]. Then the modulation mapper creates symbols of two, four, six or eight bits mapped onto in phase and quadrature component. The MIMO processing starts afterwards with the layer mapping which maps the QAM symbols onto different independent layers. Depending on the used MIMO technic, either the transmit diversity or the special multiplexing; the same data is mapped in the different layers or different data is mapped per layer respectively. Then, the pre-coder maps the layers onto the antenna ports using a precoding matrix [122]. The resource elements mapper maps afterwards the resulting data onto the radio resource grid where each data symbol in addition to the control channels are mapped into a resource element, defined by one subcarrier and one-time slot. An iFFT is latterly done to obtain a time-domain signal and the Cyclic Prefix (CP) is added.

The option 7-2 (3GPP) from the Figure V-13 appear to be an interesting low layer split option. In fact, the pre-coder is responsible of multiplying the bit-rate by the number of antennas in the case of transmit diversity. Moreover, the resource element mapper fills multiple resource blocks with control data. Therefore, moving these two elements to the radio unit would significantly decrease the 5G fronthaul bit-rate compared to conventional CPRI. The impact of such split on the radio coordination is yet to be evaluated. The eCPRI specification reported the bit-rate estimations shown in Table V.5. The split option 7-2 being between I_D and II_D we can assume that its bit-rate would be less than 25 Gbit/s. In this case, the appropriate transport solutions of this interface would be PtP fiber or PtP WDM PON as shown in Figure V-14. As reported in Chapter II, the use of PtP WDM PON will permit a low latency transparent transport (no extra framing or encapsulation) for up to 25 Gbit/s per channel making it appropriate to transport the new eCPRI interface. However, the impact of introducing the AMCC on the eCPRI, which is a frequency domain signal encapsulated in Ethernet, is yet to be evaluated in order to verify it is similar than with CPRI. Slightly different AMCC specifications might be needed.

Several investigations are ongoing on some Time Sensitive Networking (TSN) transport equipment which was adopted in the iCirrus Europeen project [141]. Nevertheless, the performance (latency, packet jitter) and the cost of such equipment need to be investigated.

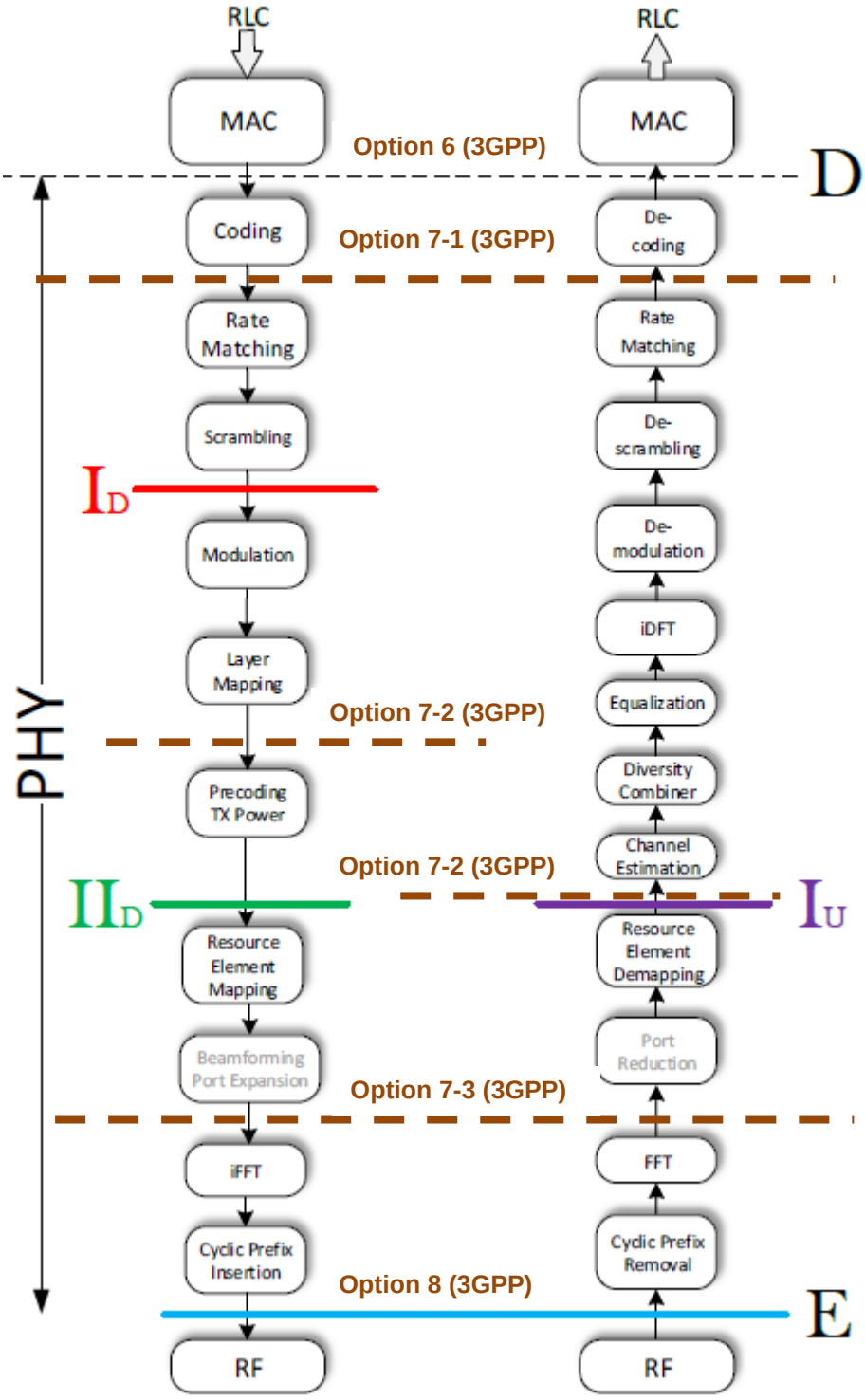

Figure V-13 : Low layer functional splits according to the eCPRI specification [134] and 3GPP [123]

Table V.5 : PHY layer splits bit-rate estimations according to eCPRI specification [134]

	Split D		Split ID		Split IID		Split E
	User Data [Gbit/s]	Control [Gbit/s]	User Data [Gbit/s]	Control [Gbit/s]	User Data [Gbit/s]	Control [Gbit/s]	User Data [Gbit/s]
DL	3	<< 1	< 4	< 10	~ 20	< 10	236
UL	1.5	<< 1			~ 20	< 10	236

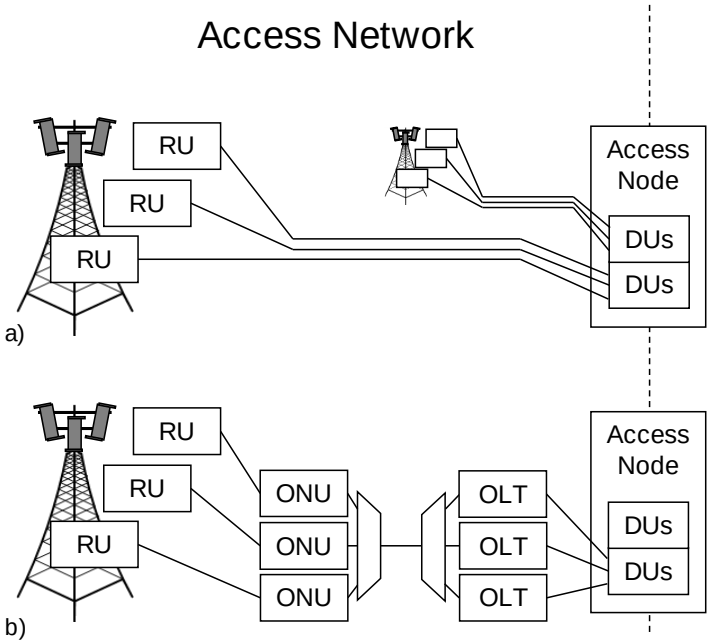

Figure V-14 : Optical access solutions for low layer split fronthaul based on a) PtP fiber, and b) PtP WDM PON [124]

V.5. Conclusion

This chapter reported an investigation on the RAN new high and low layer functional splits. A real-time experimentation of a virtualized RAN platform based on the PDCP-RLC functional split was carried out. The bit-rate of this new efronthaul interface was measured and theoretically calculated. The results show 20% increase of traffic compared to regular backhaul and about 13 times less traffic than CPRI-based fronthaul. Also, the transport of this new interface over a PtP Ethernet network and G-PON were evaluated. The robustness of this interface towards network impairments (latency and packet loss) shows potentially that current metropolitan and access network infrastructures can be used for the transport of this efronthaul with the need to do some joint adjustments in the RAN and transport equipment (OLT). The obtained results for the access network segment with GPON were based on a FBA mode. Investigations need to be performed in the DBA mode in order to allow an optimized use of the transport resources. Furthermore, the scenario where both residential and mobile clients are served by the same PON tree turned out to be the most

interesting option in case PON is considered for transporting the F1/V1. In this case, the bandwidth allocation algorithms used in PON will need to be re-evaluated.

Concerning the low layer split, several split options within the radio physical layer were proposed by the 3GPP and eCPRI specification. The main targets are to permit bit-rate independency towards the used MIMO order, to have a load-dependent traffic and to enable Ethernet encapsulation. A PHY split can permit having fronthaul bit-rate less than 25 Gbit/s for 5G which makes PtP WDM PON an appropriate candidate for its transport. However, the impact of introducing the AMCC signal on the eCPRI should be verified.

This chapter gave an overview on the emerging RAN functional splits and proposed solutions to transport the resulting radio interfaces. The obtained results were published in a journal and two conference papers (cf. appendix A).

General conclusion and perspectives

Radio mobile communications have known a tremendous success over the years with the launch of a new technology generation every decade since the 80s. Mobile communications therefore became an indispensable element of the daily lives of billions of people all over the world. They are also expected to be even more widespread with the future 5G by delivering more content, connecting much more devices and offering diverse services targeting not only private individuals but industry, transportation and heath sector actors as well.

Current mobile networks cannot be provisionned for different traffic and latency requirements. The flexibility brought by network virtualization enables delivering tailored services whenever needed. Therefore, Cloud RAN was identified as a promising solution for 5G. This RAN architecture comes with a new network segment called “fronthaul”, originnaly intended to transport digitized radio signals over fiber according to e.g. CPRI. However, this thesis showed the need for some enhancements leading to an evolved fronthaul capable of supporting 5G.

Fronthaul is emerging as a very promising and strategic solution for Orange in France and several countries in Europe and Africa since, besides flexibility, it solves a large number of operational difficulties related to the engineering of radio sites, reduces the costs of deployment and maintenance as well as it faciliates the evolution towards new radio technologies. Nevertheless, several difficulties are yet to be overcome before a massive deployment. This PhD thesis is therefore an attempt to help giving Orange a vision on the possible transport solutions for this new 5G network segment, mainly based on experimentations. The target is to be cost effective, sustainable towards the radio technologie evolutions while respecting the radio performance requirements. In this context, here is a summary of the main results obtained during this thesis:

CPRI-based fronthaul transport:

An experimental investigation was conducted on fiber and wireless solutions for the CPRI-based fronthaul transport.

For WDM, the introduction of a control channel (via RF pilot tone or baseband over modulation) on the CPRI signal enables achieve wavelength tunability and monitoring with minor impact on the CPRI and LTE performance. The use of time multiplexing with OTN in addition to WDM was also experimented and showed significant latency introduction. It is important to highlight that such OTN solutions are very costly for an access networks deployment.

An experimental demonstration of a remote powering solution is also reported. It is based on the use of hybrid energy cable/optical fiber and 400 VDC remote energy supply. Also, it is compliant with the C-RAN architecture. 16% energy cost reduction is expected with this solution compared to the traditional local powering one.

For the scenario in which it is complicated to deploy optical fiber, fronthaul links can be achieved though the wireless transmission of the CPRI interface. It can be done over mmWaves with a simple QAM modulation on the CPRI signal or in the sub-6GHz frequency bands by performing a multi-carrier modulation. Both approaches were experimentally

investigated; some performance degradations were measured but within the limits allowed by the standards (3GPP, CPRI).

Mixed Analog & Digital RoF:

An architecture mixing A-RoF and D-RoF was proposed in Chapter III. It aims mainly to allow leveraging the existing DAS infrastructure. A study was also carried out to evaluate the possibility to have a spectrally efficient fronthaul based on analog RoF. Theoretically, the latter must be 60 times more spectrally efficient compared to D-RoF. The realism of this value is investigated in this study.

In fact, a real-time experimentation was performed using an off-the-shelf optical transceiver. Using low cost components based D-RoF/A-RoF converters, a transmission of 24 x 10 MHz bandwidth LTE bands was achieved within the laser linearity range while being compliant with the 3GPP standard concerning EVM.

More bands can be transmitted with higher RF power at the laser input, but this could imply nonlinear in-band and out-of-band effects on the LTE signal. Inter-band distortions have the least impact on performance and can be slightly mitigated by using at least 40 MHz channel spacing (in the case of the used system and configuration). Inner-band distortions have a greater impact on the EVM value. Nevertheless, algorithms exist to mitigate these effects.

Therefore, as a perspective to this work, the implementation cost and the latency introduced by these algorithms can be evaluated before considering an actual implementation.

CPRI compression:

A study on the CPRI compression was carried out based mainly on experimentations. 60% compression was achieved with uniform quantization (2.4 times more efficient) and 66.7% with non-uniform quantization using algorithms such as Lloyd-Max and LBG (3 times more efficient) while respecting the performance requirements of the 3GPP standard. The obtained compression rates are very interesting but will not be sufficient to cope with the bit-rate evolutions expected with the introduction of massive MIMO and mmWaves where high bandwidths are offered. However, compression can still be used in the 5G cells where these radio features are not used.

Compression with an industrial prototype was also carried out. The removal of spectral redundancy (border subcarriers) allowed a compression of 33%. Furthermore, the quantization is carried out in the frequency domain in this implementation, which permitted using 6 quantization bits with uniform quantization while 7 bits were needed for the quantization in the time domain.

This study was focused on compression technology for the CPRI interface, which implementation showed limited business applications. Nevertheless, the recently released eCPRI specification mentions the use of IQ compression, a priori mainly in the frequency domain this time. Therefore, as continuity to this work, investigations need to be carried out on the compression of frequency domain IQ samples.

New functionnal splits:

An investigation on the RAN new high and low layer functional splits was reported in the last chapter.

A real-time experimentation of a virtualized RAN platform based on the PDCP-RLC functional split was performed. The resulting traffic as well as the transport of this new fronthaul interface over a PtP Ethernet network and G-PON were evaluated. The results show 20% increase of traffic compared to regular backhaul and about 13 times less traffic than CPRI-based fronthaul. The robustness of this new interface towards network impairments (latency and packet loss) shows potentially that current metropolitan and access network infrastructures can be used for the transport of this Ethernet-based eFronthaul with the need to do some joint adjustments in the RAN and transport equipment (OLT). The obtained results for the access network segment with GPON were based on a FBA configuration. For the perspectives, evaluations need to be performed in the DBA mode in order to enable an optimized use of the resources. Furthermore, the scenario where both residential and mobile clients are served by the same PON tree turned out to be the most interesting option in case PON is considered for xhauling. In this event, the bandwidth allocation algorithms used in PON will need to be re-evaluated.

Concerning the low layer split, several split options within the radio physical layer were proposed. The main targets are to permit bit-rate independency towards the used MIMO order, to have a load-dependent traffic and to enable Ethernet encapsulation. According to this, the new eCPRI specification was just released recently. This new interface is based either on 10 Gbit/s or 25 Gbit/s Ethernet with potentially the possibility to achieve statistical multiplexing. In the scenario where low radio layers are centralized in the CO, the transport of the eCPRI signal shall be achieved with WDM as established for the CPRI transport in Chapter II. However, the impact of introducing the AMCC signal on the eCPRI should be verified. A new protocols for time sentisitive networking are under investigation, their aim is to lower down the transport device latency and to elimitate congestion. The performance as well as the cost of such devices will need to be evaluated.

Bibliographic references

[1] Cisco Visual Networking Index: Global Mobile Data Traffic Forecast Update, 2016–2021 White Paper, https://www.cisco.com/c/en/us/solutions/collateral/service-provider/visual-networking-index-vni/mobile-white-paper-c11-520862.pdf

[2] Y. bourguen, E. Hardouin, F. Wolff. “LTE et les réseaux 4G” EYROLLES, 2015

[3] Small Cell Forum (www.smallcellforum.org, visited in July 2017)

[4] ITU-R M.1035 “FRAMEWORK FOR THE RADIO INTERFACE(S) AND RADIO SUB-SYSTEM FUNCTIONALITY FOR INTERNATIONAL MOBILE TELECOMMUNICATIONS-2000”, 1994

[5] Orange internal deliverable "Radio mobile architectures" 2014

[6] S. T. X. L. Philippe Godlewski, "Réseaux GSM", Hermès Science Publications, 2000.

[7] S. T. Zied Choukair, "Ingénierie des services télécoms UMTS et WiFi", Paris: Hermès Science/ Lavoisier, 2005.

[8] Christopher Cox “An introduction to LTE” WILEY, 2014

[9] R. El Hattachi, J. Erfanian, “NGMN 5G White Paper”, Feb 2015 https://www.ngmn.org/uploads/media/NGMN_5G_White_Paper_V1_0.pdf

[10] ITU-R M.2083-0 “IMT Vision-Framework and overall objectives of the future development of IMT for 2020 and beyond“, 09/2015

[11] Arnaud Vamparys, internal presentation, Orange, 2016

[12] D. Zhang; Y. Liu; Z. Ding; Z. Zhou; A. Nallanathan; T. Sato. “Performance Analysis of Non-Regenerative Massive-MIMO-NOMA Relay Systems for 5G“, IEEE Transactions on Communications 2017

[13] F. Al-Ogaili; R. Shubair. “Millimeter-wave mobile communications for 5G: Challenges and opportunities”, IEEE International Symposium on Antennas and Propagation 2016

[14] E. Kitindi; S. Fu; Y. Jia; A. Kabir; Y. Wang. "Wireless Network Virtualization with SDN and C-RAN for 5G Networks: Requirements, Opportunities, and Challenges”, IEEE Access 2017

[15] “Cisco. The Hierarchical Network Design Model”, may 2014 http://www.cisco.com/web/learning/netacad/demos/CCNP1v30/ch1/1_1_1/index.html. [Online, visited in July 2017].

[16] Huawei OSN 8800 datasheet (www.huawei.com) / Ciena 6500 datasheet (www.ciena.com).

[17] M. Song; E. Pincemin; V. Vgenopoulou; I. Roudas; E. Amhoud; Y. Jaouën. “Transmission performances of 400 Gbit/s coherent 16-QAM multi-band OFDM adopting nonlinear mitigation techniques”. Tyrrhenian International Workshop on In Digital Communications (TIWDC), Sept 2015.

[18] International Telecommunication Union. “Optical Transport Network (OTN) definition”. http://www.itu.int/ITU-T/2001-2004/com15/otn/definitions.html. [Online, visited in July 2017].

[19] W. J. Goralski, "ADSL et XDSL Nouvelles technologies d'accès à Internet", Osman Eyrolles Multimedia, 2000.

[20] Core Ethernet Mobile 2 wholesale offer: http://wholesalefrance.orange.fr/fr/Nos-reseaux/Reseau-Fibre-Optique/Offre-Fibre-Optique/Core-Ethernet-Mobile-2-CEM-2 . [Online, visited in September 2017]

[21] Fibre to the Home Council Europe. FTTH Handbook. http://www.ftthcouncil.eu/documents/Publications/FTTH-Handbook_2014-V6.0.pdf , February 2014. [Online; visited in September 2017]

[22] ITU-T G.984 Gigabit-capable passive optical networks (GPON): https://www.itu.int/rec/T-REC-G.984.2-200602-I!Amd1/fr [Online; visited in September 2017]

[23] Payoux Franck, “Analysis of Dyanmic Bandwidth Allocation Function for GPON : Industriel Implementation”, Technical report, Internal Orange Labs document, 2007

[24] O. Haran, A. Sheffer, “The Importance of Dynamic Bandwidth Allocation in GPON Networks”, White Paper, PMC-Sierra, 2008

[25] Gael Simon “Introduction des technologies de multiplexage en longueur d’onde dense dans les futures générations de réseaux d’accès optique ” PhD thesis 2016

[26] ITU-T G.987 “10-Gigabit-capable passive optical network (XG-PON) systems: Definitions, abbreviations and acronyms” 06/2012

[27] ITU-T G.9807.1”10-Gigabit-capable symmetric passive optical network (XGS-PON)" 06/2016

[28] Metro Ethernet Forum 12.1, “Metro Ethernet Network Architecture Framework Part 2: Ethernet Services Layer”, technical Specification, 2005, https://www.mef.net/Assets/Technical_Specifications/PDF/MEF_12.pdf

[29] Nokia, “Mobile Network Transmission”, White paper, 2000, http://tech-insider.org/mobile/research/acrobat/000414.pdf

[30] Metro Ethernet Forum, Implementation agreement MEF 22.1, “Mobile Backhaul Phase 2”, January 2012, https://mef.net/PDF_Documents/technical-specifications/MEF_22.1.pdf

[31] Next Generation Mobile Networks Alliance, “NGMN Optimized Backhaul Requirements”, August 2008, https://www.ngmn.org/uploads/media/NGMN_Optimised_Backhaul_Requirements.pdf

[32] Next Generation Mobile Networks Alliance, “Small Cell Backhaul Requirements, version 1.0”, Jun 2012, https://www.ngmn.org/uploads/media/NGMN_Whitepaper_Small_Cell_Backhaul_Requirements.pdf

[33] “Analysis of transport network architectures for structural convergence” D3.3 COMBO (COnvergence of fixed and Mobile BrOadband access/aggregation networks) European project deliverable 06/2015, http://cordis.europa.eu/docs/projects/cnect/2/317762/080/deliverables/001-COMBOD33WP330June2015EABv10Ares20153369841pdf.pdf

[34] Metro Ethernet Forum 22.1.1, “Mobile Backhaul Phase 2, Amendment 1”, July 2014

[35] “Common Public Radio Interface (CPRI),” Interface Specification, available at www.cpri.info

[36] D2.1 iCIRRUS (Intelligent Converged network consolidating Radio and optical access aRound USer equipment) European project deliverable 07/2015, http://www.icirrus-5gnet.eu/wp-content/uploads/2016/02/D2.1-Intelligent-C-RAN-architecture.pdf

[37] “Open Base Station Architecture Initiative (OBSAI)” specification, available at www.obsai.com

[38] ETSI, “Open Radio equipment Interface (ORI) (Release 4),” October 2014, http://www.etsi.org/deliver/etsi_gs/ORI/001_099/001/04.01.01_60/gs_ORI001v040101p.pdf

[39] P. Chanclou, L. Anet Neto, K. Grzybowski, Z. Tayq, F. Saliou, N. Genay “Mobile Fronthaul Architecture and Technologies: a RAN Equipment Assessment” JOCN 2017

[40] China Mobile Research Institute, “C-RAN The Road Towards Green RAN”, White Paper v.2.6, Sep.2013

[41] A. Pizzinat, P. Chanclou, F. Saliou, T. Diallo, “Things you should know about fronthaul”, Journal of Lightwave Technology, 1st March 2015, vol. 33, Issue: 5, 1077-1083, 2015

[42] Marco Vigilante et al., “To EVM or Two EVMs?” IEEE SOLID-STATE CIRCUITS MAGAZINE 2017

[43] ITU-T Recommendation G.694.2, “Spectral grids for WDM applications: CWDM wavelength grid”

[44] ITU-T Recommendation G.694.1, “Spectral grids for WDM applications: DWDM frequency grid”

[45] 3GPP TS 36.104: E-UTRA BS radio transmission and reception, section 6.5.1, Rel. 9, V9.8.0, June 2011

[46] R. Heron, T. Pfeiffer “5G wireless fronthaul requirements in a PON context”, FSAN 09/2017

[47] NetManias Tech-Blog, “Fronthaul Size: Calculation of maximum distance between RRH and BBU”, Apr 2014, available online: http://www.netmanias.com/en/?m=view&id=blog&no=6276 [visited in August 2017]

[48] ITU-T Recommendation G.8262/Y.1362, “Timing characteristics of synchronous Ethernet equipment slave clock (EEC)

[49] J. Eidson, "IEEE-1588 Standard for a Precision Clock Synchronization Protocol for Networked Measurement and Control Systems, a Tutorial" National Institute of Standards and Technology (NIST), 10 October 2005

[50] P. Chanclou, S. Randazzo, “Evaluating the different fronthaul options and the technical requirements for the different scenarios, RAN & Backhaul Networks, Session: What Are The Fronthaul Strategies”, Transport Networks for Mobile Operators, RAN & Backhaul Networks, May 2015, Berlin, Germany

[51] Next Generation Mobile Networks Alliance, “Fronthaul Requirements For C-RAN, Version 1.0”, Mar 2015, https://www.ngmn.org/uploads/media/NGMN_RANEV_D1_C-RAN_Fronthaul_Requirements_v1.0.pdf

[52] K. Murphy, “Centralized RAN and Fronthaul”, White Paper, Ericsson, 2015

[53] Next Generation Mobile Networks Alliance, “Suggestions on Potential Solutions to C-RAN”, version 4.0, 03 January 2013, http://www.ngmn-ic.info/uploads/media/NGMN_CRAN_Suggestions_on_Potential_Solutions_to_CRAN.pdf

[54] ETSI TS 136 214: LTE; Physical layer; Measurements, jan 2017, http://www.etsi.org/deliver/etsi_ts/136200_136299/136214/13.04.00_60/ts_136214v130400p.pdf

[55] ITU-T Recommendation G.694.2, “ Spectral grids for WDM applications: CWDM wavelength grid”

[56] J. Shin, S. Hong, J. Yeong Lim, S.Cho, H. Yeal Rhy, G. Yong Yi “CWDM Networks with Dual Sub-channel Interface for Mobile Fronthaul and Backhaul Deployment” ICACT, 2014

[57] Y. Koo Kwon et al. “Optical transceiver for CWDM networks with multi subchannel interface” OFC, 2014

[58] Jian Dong et.al. “Cascaded Phase Modulation for AMCC Superimposition Toward MFH Employing CPRI” IEEE Photonics Journal 2017

[59] ITU-T Recommendation G.989.2 and G.989.3, “40-gigabit-capable passive optical networks (NG-PON2): Physical media dependent (PMD)”

[60] K. Honda; T. Kobayashi, T. Shimada, J. Terada, A. Otaka, “WDM Passive Optical Network Managed with Embedded Pilot Tone for Mobile Fronthaul” Proc ECOC 2015

[61] 3GPP TS 36.141: E-UTRA BS conformance testing, Rel. 10, V10.1.0, 2011.

[62] “Jitter Analysis: The dual- Dirac Model, RJ/DJ, and Q-Scale”, Agilent Technologies (2004)

[63] ITU-T Recommendation G.989.2 Amendment 1 Annex C

[64] Jiannan Zhu et al. “First Demonstration of a WDM-PON System Using Full C-band Tunable SFP+ Transceiver Modules” Journal of Optical Communications and Networking, January 2015

[65] S. Pachnicke et al. “Tunable WDM-PON System With Centralized Wavelength Control” Journal of Lightwave Technology 2016

[66] M. Duck and R. Read “Data Communications and Computer Networks: For Computer Scientists and Engineers” second edition 2003 pp. 42-46

[67] ITU-T G.709/Y.1331 Recommendation: Interfaces for the optical transport network

[68] T. P. Walker, Optical Transport Network (OTN) Tutorial, Geneva: ITU, 2005.

[69] Y. Ma, X. Huo, J. Li, X. Jingwen. “Optical solutions for fronthaul application” ICOCN 2015

[70] ITU-T G.Sup 56 Supplement: “OTN Transport of CPRI signals Converged Mobile Fronthaul”

[71] D. Hisano, T. Kobayashi, H. Ou, T. Shimada, H. Uzawa, J. Terada, A. Otaka "TDM-PON for Accommodating TDD-Based Fronthaul and Secondary Services” Journal of Lightwave Technology 2017

[72] D. Hisano, T. Kobayashi, H. Ou, T. Shimada, H. Uzawa, J. Terada, A. Otaka “Experimental Demonstration of Accommodation of TDD-based Mobile Fronthaul and Secondary Services in a TDM-PON” ECOC 2016

[73] T. Kobaychi “Bandwidth allocation scheme based on simple statistical traffic analysis for TDM-PON based mobile fronthaul” OFC 2016

[74] O. Foucault, D. Marquet, S. Le Masson. “400VDC Remote Powering as an alternative for power needs in new fixed and radio access networks” INTELEC 2016

[75] E-Blink: “High capacity wireless communications systems and methods”, US 013/0294541

[76] P. Dat, A. Kanno, N. Yamamoto, T. Kawanishi. “190-Gbit/s CPRI-Equivalent Rate Fiber-Wireless Mobile Fronthaul for Simultaneous Transmission of LTE-A and F-OFDM Signals“ ECOC 2016

[77] Gee-Kung Chang, Lin Cheng “Fiber-wireless fronthaul: The last frontier“ OECC 2016

[78] S. Park, K. Lee, C. Song, I. Lee. "Joint Design of Fronthaul and Access Links for C-RAN With Wireless Fronthauling “ IEEE Signal Processing Letters 2016

[79] ETSI EN 302217-2-2 v2.1.1 (2013-07)

[80] J. Zhang, M. Xu, J. Wang, F. Lu, L. Cheng, H. Cho, K. Ying, J. Yu, G. k. Chang, "Full-Duplex Quasi-Gapless Carrier-Aggregation Using FBMC in Centralized Radio-Over-Fiber Heterogeneous Networks," in Journal of Lightwave Technology, vol.PP, no.99, pp.1-1

[81] X. Liu, F. Effenberger, N. Chand, L. Zhou, H. Lin., "Demonstration of bandwidth-efficient mobile fronthaul enabling seamless aggregation of 36 E-UTRA-like wireless signals in a single 1.1-GHz wavelength channel," OFC 2015.

[82] H. Zeng, X. Liu, S. Megeed, N. Chand, F. Effenberger., "Demonstration of a Real-Time FPGA-Based CPRI-Compatible Efficient Mobile Fronthaul Transceiver Supporting 53 Gbit/s CPRI-Equivalent Data Rate Using 2.5-GHz-Class Optics, " ECOC 2016.

[83] B. G. Kim, K. Tanaka, T. Kobayashi, A. Bekkali, K. Nishimura, H. Kim, M. Suzuki, Y. C. Chung., "Transmission Experiment of LTE Signals by IF-over-Fiber Using Commercial Base Station and Deployed Optical Fibers," ECOC 2016.

[84] E-Blink: “High capacity wireless communications systems and methods”, US 2013/0294541

[85] David M. Pozar, Microwave Engineering, Third Edition, John Wiley & Sons Inc

[86] H. Li, “Channel Capacity and Channel Estimation of OFDM Ultra-Wide-Band Systems”, ICCSEE 2012

[87] 3GPP TS 36.141: E-UTRA BS conformance testing, Rel. 10, V10.1.0, 2011

[88] Hanzo, L., Munster, M., Choi, B. J., and Keller, T., OFDM and MC-CDMA for Broadcasting Multi-User Communications, WLANs and Broadcasting, 1st ed. West Essex, England: John Wiley and Sons Ltd., IEEE Press, 2003.

[89] C. C. Wei, “Analysis and iterative equalization of transient and adiabatic chirp effects in DML-based OFDM transmission systems,” Opt. Exp.,vol. 20, no. 23, pp. 25774–25789, Nov. 2012.

[90] D.-Z. Hsu, C.-C. Wei, H.-Y. Chen, Y.-C. Lu, C.-Y. Song, C.-C. Yang, and J. Chen, “SSII cancellation in an EAM-based OFDM-IMDD transmission system employing a novel dynamic chirp model,” Opt. Exp., vol. 21, no. 1, pp. 533–543, Jan. 2013.

[91] H.-Y. Chen, C.-C. Wei, I.-C. Lu, Y.-C. Chen, H.-H. Chu, and J. Chen,“EAM-based high-speed 100-km OFDM transmission featuring tolerant modulator operation enabled using SSII cancellation,” Opt. Exp., vol. 22,no. 12, pp. 14637–14645, Jun. 2014.

[92] W. Yan, B. Liu, L. Li, Z. Tao, T. Takahara, and J. C. Rasmussen, “Nonlinear distortion and DSP-based compensation in metro and access networks using discrete multi-tone,” presented at the Eur. Conf. Exhib. Opt. Commun, Amsterdam, The Netherlands, Sep. 2012, Paper Mo.1.B.2.

[93] Y. Bao, Z. Li, J. Li, X. Feng, B. Guan, and G. Li, “Nonlinearity mitigation for high-speed optical OFDM transmitters using digit al pre-distortion,” Opt. Exp., vol. 21, no. 6, pp. 7354–7361, Mar. 2013.

[94] C. Wei, H. Cheng, H. Chen, Y. Chen, “Analysis of Nonlinear Distortion and SSII Cancellation in EAM-Based IMDD OFDM Transmission” JLT 2015.

[95] J. Lorca, L. Cucala “Lossless Compression Technique for the Fronthaul of LTE/LTE Advanced Cloud-RAN Architectures” WoWMoM 2013

[96] B. Guo, W. Cao, A. Tao, D. Samardzija “LTE/LTE-A Signal Compression on the CPRI Interface” Bell Labs Technical Journal 18(2), 117–133 (2013)

[97] H. Si, B. Loong Ng, M. Rahman, J. Zhang “A Vector Quantization Based Compression Algorithm for CPRI Link” GLOBECOM 2015

[98] H. Schwarz, “Source Coding and Compression” December 7, 2013

[99] D. A. Huffman, “A method for the construction of minimum redundancy codes,” Proceedings of the Institute of Radio Engineers, vol. 40, no. 9, pp. 1098–1101, Sep. 1952.

[100] L. Ramalho, M. Fonseca, A. Klautau, C. Lu, M. Berg, E. Trojer, S. Höst “An LPC-Based Fronthaul Compression Scheme” IEEE Communications Letters 2017

[101] D. Samardzija, J. Pastalan, M. MacDonald, S.Walker, and R. Valenzuela,“Compressed transport of baseband signals in radio access networks,”IEEE Transactions on Wireless Communications, vol. 11, no. 9, pp.3216–3225, Sep. 2012.

[102] Y. Ren, Y. Wang, G. Xu, and Q. Huang, “A compression method for LTE-A signals transported in radio access networks,” in 2014 International Conference on Telecommunications (ICT 2014), May 2014, pp. 293–297.

[103] K. F. Nieman and B. L. Evans, “Time-domain compression of complex-baseband LTE signals for cloud radio access networks,” in 2013 IEEE Global Conference on Signal and Information Processing (GlobalSIP2013), Dec. 2013, pp. 1198–1201.

[104] H. Si, B. Loong Ng, M. Rahman, J. Zhang “A Novel and Efficient Vector Quantization Based CPRI Compression Algorithm ” TVT 2017

[105] C. W. Brokish “A-Law and mu-Law Companding Implementation Using the TMS320C54x” Application Note: SPRA163A

[106] W. R. Bennett "Spectra of quantized signals" Bell Syst. Tech.J., vol. 27, pp. 446{472, July 1948.

[107] B. M. Oliver, J. Pierce, and C. E. Shannon, "The philosophy of PCM" Proc. IRE, vol. 36, pp. 1324-1331, Nov. 1948.

[108] ETSI GS ORI 001 V4.1.1 (2014-10)

[109] ETSI GS ORI 002-1 V4.1.1 (2014-10)

[110] CPRI Interface Specification, v. 7.0, October 9th, 2015

[111] S. Hart "Circle Packing and its Applications", The University of Melbourne, 2008

[112] 3GPP TS 36.141: E-UTRA BS conformance testing, Rel. 10, V10.1.0, 2011.

[113] J. Max, “Quantizing for minimum distortion," IEEE Transactions Information Theory 1960.

[114] Linde, Y., Buzo, A., Gray, R. "An Algorithm for Vector Quantizer Design". IEEE Transactions on Communications 1980

[115] L. Anet Neto, P. Chanclou, Z. Tayq " Experimental Investigation of Compression with Fixed-length Code Quantization for convergent Access-Mobile Networks" ECOC2016

[116] R. M. Gray, D. L. Neuhoff "Quantization" IEEE Transactions Information Theory 1998

[117] K. Murphy, "Centralized RAN and Fronthaul", White Paper, Ericsson, 2015

[118] N. Shibata, T. Tashiro, S. Kuwano, N. Yuki, Y. Fukada, J. Terada, A. Otaka "Performance evaluation of mobile front-haul employing ethernet- based TDM-PON with IQ data compression" JOCN 2015

[119] E. Pateromichelakis, J. Gebert, T. Mach, J. Belschner, W. Guo, N. P. Kuruvatti, V. Venkatasubramanian, C. Kilinc “Service-Tailored User-Plane Design Framework and Architecture Considerations in 5G Radio Access Networks” IEEE Access 2017

[120] N. Gomes, V. Jungnickel, P. Chanclou, J. Elbers, P. Turnbull “A flexible, ethernet fronthaul for 5th generation mobile and beyond” OFC 2016

[121] Y. bourguen, E. Hardouin, F. Wolff. “LTE et les réseaux 4G” EYROLLES 2015

[122] Christopher Cox, “An introduction to LTE” WILEY 2014

[123] 3GPP TR38.801 “Radio Access Architecture and Interfaces”, v2.0.0

[124] P. Chanclou, L. Anet Neto, K. Grzybowski, Z. Tayq, F. Saliou, N. Genay “Mobile Fronthaul Architecture and Technologies: a RAN Equipment Assessment” JOCN 2017

[125] Small Cell Forum “Small cell virtualization functional splits and use cases” Document 159.07.02 (01/2016)

[126] 3GPP TSG-WG3 Meeting #95-bis Spokane, USA, 3-7 Apr 2017.

[127] 3GPP TSG-RAN#75 Dubrovnik, Croatia, Mar. 6 - 9, 2017

[128] Small Cell Forum “nFAPI and FAPI specifications” Document 082.09.05 (05/2017)

[129] Arnauld de Lannoy, Orange Labs internal delivreable, 01/2017

[130] 3GPP TS 36.213 version 8.3.0 Release 8

[131] D. Hisano, T. Kobayashi, H. Ou, T. Shimada, H. Uzawa, J. Terada, A. Otaka. “TDM-PON for Accommodating TDD-Based Fronthaul and Secondary Services” JLT 2017

[132] T. Tashiro, S. Kuwano, J. Terada, T. Kawamura, N. Tanaka, S. Shigematsu, N. Yoshimoto. “A Novel DBA Scheme for TDM-PON based Mobile Fronthaul” OFC 2014

[133] S. Hatta, N. Tanaka, T. Sakamoto. “Feasibility demonstration of Low Latency DBA method with high bandwidth efficiency for TDM-PON” OFC2017

[134] eCPRI Specification V1.0 (2017-08-22)

[135] Optical Internetworking Forum “Flex Ethernet Implementation Agreement” March 2016

[136] R. Irmer, H. Droste, P. Marsch, M. Grieger, G. Fettweis, S. Brueck, H. P. Mayer, L. Thiele, and V. Jungnickel. Coordinated multipoint: Concepts, performance, and field trial results. IEEE Communications Magazine, 49(2):102–111, February 2011.

[137] Daewon Lee, Hanbyul Seo, B. Clerckx, E. Hardouin, D. Mazzarese, S. Nagata, and K. Sayana. Coordinated multipoint transmission and reception in LTE-advanced: deployment scenarios and operational challenges. IEEE Communications Magazine, 50(2):148–155, February 2012.

[138] M. Feng, X. She, L. Chen, and Y. Kishiyama. Enhanced dynamic cell selection with muting scheme for dl comp in lte-a. In 2010 IEEE 71st Vehicular Technology Conference, pages 1–5, May 2010.

[139] J. w Cho, J. Mo, and S. Chong. Joint network-wide opportunistic scheduling and power control in multi-cell networks. IEEE Transactions on Wireless Communications,8(3):1520–1531, March 2009.

[140] C. U. Saraydar, N. B. Mandayam, and D. J. Goodman. Pricing and power control in a multicell wireless data network. IEEE Journal on Selected Areas in Communications, 19(10):1883–1892, October 2001.

[141] Nathan J. Gomes “Flexible Ethernet Fronthaul” 5G Architecture Workshop, Brussels, 6 April 2016

[142] J. Terada, T. Shimada, T. Shimizu, A. Otaka, “Optical Network Technologies for Wireless Communication Network”, ECOC 2016

[143] J-I Kani, J. Terada, K-I Suzuki, A. Otaka, “Solutions for future mobile fronthaul and access-network convergence”, JLT (2016)

Appendix

Appendix A: List of publications

Peer-reviewed international journals:

- **Z. Tayq**, L. Anet Neto, J. Gomes, M. Lacouche, J. Plumecoq, L. Bellot, C. Aupetit-Berthelemot, P. Chanclou, "Investigation of Real-Time Bandwidth-Efficient Fronthaul using Mixed Analog & Digital RoF" **JOCN** (under review)
- P. Chanclou, L. Anet Neto, K. Grzybowski, **Z. Tayq**, F. Saliou, N. Genay "Mobile Fronthaul Architecture and Technologies: a RAN Equipment Assessment" **JOCN**

Peer-reviewed international conferences:

- **Z. Tayq**, P. Chanclou, T. Diallo, K. Grzybowski, F. Saliou, S. Gosselin, O. Foucault, Aupetit-Berthemelot, L. Bellot, T. Boukour, J. Plumecoq, " Performance demonstration of fiber and wireless fronthaul combination with remote powering" **OFC 2016**
- **Z. Tayq**, B. Le Guyader, P. Chanclou, S. Gosselin, T. Diallo, D.P.Venmani, C. Aupetit-Berthelemot, S. Pachnicke, M. Eiselt, A. Autenrieth, J. Elbers, " Fronthaul Performance Demonstration in a WDM-PON-Based Convergent Network" **EuCNC 2016**
- **Z. Tayq**, L. Anet Neto, P. Chanclou, C. Aupetit-Berthemelot, "Experimental Real Time AMCC Implementation for Fronthaul in PtP WDM-PON" **ECOC 2016**
- **Z. Tayq**, A. Quere, L. Anet Neto, P. Chanclou, F. Saliou, K. Grzybowski, C. Aupetit-Berthemelot, Sun Keun Yoo, Sung Eun Hong, " Performance Demonstration of Real Time Compressed CPRI Transport" **ECOC 2016**
- **Z. Tayq**, L. Anet Neto, B. Le Guyader, A. De Lannoy, M. Chouaref, C. Aupetit-Berthemelot, M. Nelamangala Anjanappa, S. Nguyen, K. Chowdhury, P. Chanclou "Real Time Demonstration of the Transport of Ethernet Fronthaul based on vRAN in Optical Access Networks" **OFC 2017**
- **Z. Tayq,** L. Anet Neto, F. Saliou, C. Aupetit-Berthemelot, J. Gomes, T. Haustein, M. Lacouche, J. Plumecoq, L. Bellot, P. Chanclou, "Real Time Demonstration of Fronthaul Transport over a Mix of Analog & Digital RoF" **ICTON 2017**
- L. Anet Neto, P. Chanclou, **Z. Tayq**, B. C. Zabada, F. Saliou, G. Simon, "Experimental Investigation of Compression with Fixed-length Code Quantization for Convergent Access-Mobile Networks" **ECOC 2016**
- P. Chanclou, L. Anet Neto, K. Grzybowski, **Z. Tayq,** F. Saliou, N. Genay, "Mobile fronthaul architecture and technologies: A RAN equipment assessment" **OFC 2017**

Peer-reviewed national conference:

- **Z. Tayq**, P. Chanclou, F. Saliou, T. Diallo, C. Aupetit-Berthemelot, "Impact de la montée en débit sur le CWDM bidirectionnel dans une architecture C-RAN" **JNOG 2015**

Collaborative projects deliverables:

I contributed in the following deliverables:

- Deliverable, **ICT-COMBO**. D3.3 "Analysis of transport network architectures for structural convergence" 2015
- Deliverable, **iCIRRUS.** D2.1 "Intelligent C-RAN Architecture" 2015

Workshops:

- **Z. Tayq**, P. Chanclou, L. Anet Neto, "Fronthaul Field Trials and Future Trends" **EuCNC** 2016, Workshop W04b (invited)

Appendix B: Error Vector Magnitude

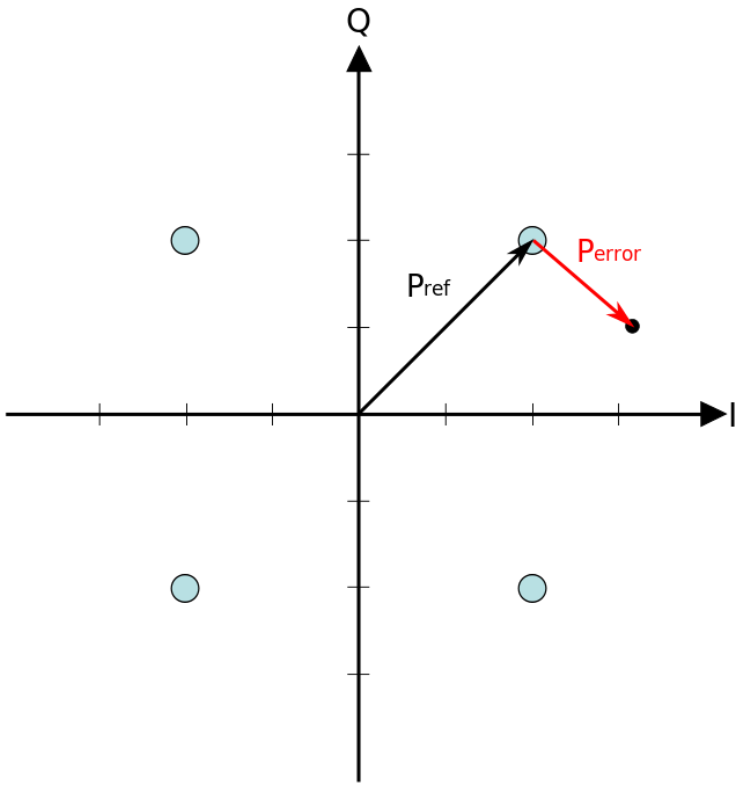

Error Vector Magnitude or EVM is a metric frequently used to evaluate the performance of a radio transmission, it represents the vector between the ideal constellation and the points of the received constellation as shown in the figure beyond. It is defined in dB with the following equation:

$$EVM\ (dB) = 10\log(\frac{P_{error}}{P_{ref}})$$

And in % with the following equation:

$$EVM\ (\%) = \sqrt{\frac{P_{error}}{P_{ref}} \times 100\%}$$

Where P_{error} is the root mean square amplitude of the error vector and P_{ref} is the reference constellation average power.

Appendix C: Jitter (Dual-Dirac Model)

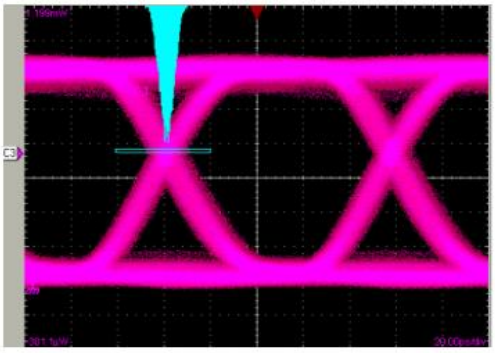

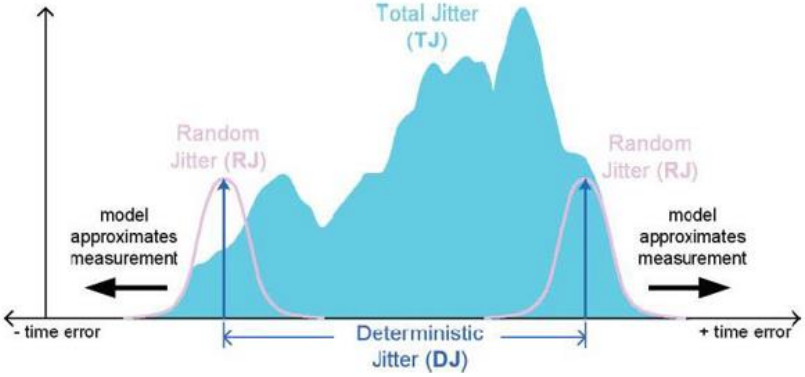

Physical jitter is a phenomenon often occurring in high bit-rate communications, it represents fast phase variations following a certain distribution as shown in the figure beyond. The quick assessment of such phenomenon represents a metrology challenge. The Dual Dirac model answers to that by enabling a quick estimation of the total jitter including the random jitter and deterministic jitter. This model assumes that the random jitter follows a gaussian distribution and can be fully described in terms of a single relevant parameter, for instance, σ the width of the Gaussian. On the other hand, deterministic jitter is assumed to follow a finite bounded distribution, formed by 2 Dirac functions. The time delay between these two Dirac functions allows to estimate the value of the deterministic jitter. More details about this model as well as the related mathematical analysis are brought in [62].

Glossary

3GPP	3rd Generation Partnership Project
ADSL	Asymmetric DSL
AMCC	Auxiliary Management and Control Channel
API	Application Programming Interface
A-RoF	analog radio over fiber
AWG	Arrayed Waveguide Grating
AWG	arbitrary waveform generator
AWGN	Additive White Gaussian Noise
BBU	Base Band Unit
BER	Bit Error Ration
BPON	Broadband PON
BSC	Base Station Controller
BTS	Base Transceiver Stations
C&M	Control and Management
CA	Carrier Aggregation
CDR	Clock & Data Recovery
CO	Central Office
CoMP	Coordinated MultiPoint
CP	Cyclic Prefix
CPRI	Common Public Radio Interface
C-RAN	Cloud RAN
CSC	Cooled Single Channel
CSG	Cell Site Gateway
CU	Centralized Unit

CWDM	Coarse WDM
DAC	Digital to Analog Converter
DAS	Distributed Antenna System
DBA	Dynamic bandwidth Allocation
DML	Directly Modulated Laser
DMT	Discrete Multi-Tone
DPS	Dynamic Point Selection
D-RoF	Digital- radio over fiber
DSL	Digital Subscriber Line
DSLAM	Digital Subscriber Line Access Multiplexer
DSO	Digital Storage Oscilloscope
DU	Digital Unit
DWDM	Dense WDM
ECC	Embedded Communication Channel
EDGE	Enhanced Data rates for GSM Evolution
eMBB	Enhanced Mobile Broadband
EPC	Evolved Packet Core
ETSI	European Telecommunication Standards Institute
ETWS	Earthquake and Tsunami Warning System
EVM	error vector magnitude
FAPI	Femto Application Platform Interface
FBA	Fixed Bandwidth Allocation
FD	Frequency Deviation

FDMA	Frequency Division Multiple Access
FEC	forward error correction
FFT	Fast Fourier Transform
FP	Fabry-Perot
FTTx	Fiber To The x
GNSS	Global Navigation Satellite System
GPP	general purpose processor
GPRS	General Packet Radio Service
GSM	Global System for Mobile communications
HARQ	Hybrid Automatic Retransmit reQuest
HSPA	High Speed Packet Access
ICIC	Inter-cell Interference Coordination
IF	intermediate frequency
ISG	Industry Specification Group
ITU	International Telecommunication Union
JT	Joint Transmission
KPI	Key Performance Indicator
LBG	Linde-Buzo-Gray
LO	Local Oscillator
LTE	Long Term Evolution
LTE-A	LTE advanced

MAC	Medium Access Control
MCS	Modulation and Coding Scheme
MEC	Multiple Access Edge Computing
MEF	Metro Ethernet Forum
MIMO	Multiple Input Multiple Output
mMTC	massive Machine Type Communications
MSC	Mobile service Switching Center
MSE	Mean Squared Error
NAS	Non-Access Stratum
NGMN	Next Generation Mobile Networks
NG-PON2	second Next Generation of Passive Optical Networks
OAD	Optical Add Drops
OAM	Operation Administration and Maintenance
OB	Optical Budget
OBSAI	Open Base Station Architecture Initiative
ODU	Optical Data Units
OFDM	Orthogonal Frequency Division Multiplexing
OLT	Optical Line Termination
ONU	Optical Network Unit
ORI	Open Radio equipment Interface
OTA	Over the Air
OTN	Optical Transport network
OUT	Optical Transport Unit

PAPR	Peak-to-Average Power Ratio
PDCP	Packet Data Compression Protocol
PDH	Plesiochronous Digital Hierarchy
PDSCH	physical downlink shared channel
PGW	Packet Data Network Gateway
pin-PD	pin-photodiode
PON	Passive Optical Network
PoP	Point of Presence
PRBS	Pseudo Random Binary Sequence
PSTN	Public Switched Telephone Network
PT	pilot tone
QoE	Quality of Experience
QoS	Quality of Service
QPSK	Quadrature Phase Shift Keying
RAN	radio access network
RAT	Radio Access Technologie
RDDMI	Remote Digital Diagnostics Monitoring Interface
RIO	Reflection Immune Operation
RLC	Radio Link Control
RMS	Root Mean Square
RN	Remote Node
RNC	Radio Network Controller
RoE	Radio over Ethernet

RoHC	Robust Header Compression
ROP	Received Optical Power
RRC	Radio Resource Control
RRH	Remote Radio Head
RTT	Round Trip Time
RU	Radio Unit
SA	Spectrum Analyzer
SDH	Synchronous Digital Hierarchy
SFF	Small Form Factor
SFP	Small Form Factor Pluggable
SISO	Single Input Single Output
SLA	Service Level Agreements
SMS	Short Message Service
SNR	signal-to-noise ratio
SOA	Semiconductor Optical Amplifier
SSII	Subcarrier-to-Subcarrier Intermixing Interference
SSMF	standard single mode optical fiber
SSPA	Solid- State-Power-Amplifier
SWSF	Single Wavelengh Single Fiber
TCO	Total Cost of Ownership
T-CONT	traffic container
TCP	Transmission Control Protocol
TDM	Time Division Multiplexing
TDMA	Time Division Multiple Access

TIA	Trans- Impedance Amplifier
ToR	Top of Rack
TRX	Transmitter and Receiver Modules
TSN	Time Sensitive Networking
TTI	Transmission Time Interval
TWDM	Time and Wavelength Division Multiplexing
UDP	User Datagram Protocol
UE	User Equipment
UI	Unit Interval
UMTS	Universal Mobile Telecommunication System
URLCC	Ultra-Reliable and Low Latency Communication
VDSL	Very-high-bit-rate DSL
VEA	Variable Electric Attenuator
VOA	Variable Optical Attenuator
vRAN	Virtualized RAN
WCB	Wavelength Control Board
W-CDMA	Wideband Code Division Multiple Access
WDM	Wavelength Division Multiplexing
WDM	Wavelength Division Multiplexing
WFE	wireless fronthaul equipment

List of figures

List of tables

Contents

Intégration et supervision des liens Fronthaul dans les réseaux 5G

Le Cloud RAN a été préconisé pour la 5G. Cependant, sa mise en place rencontre des difficultés notamment sur l'intégration du fronthaul, ce dernier généralement basé sur l'interface CPRI représente le segment situé entre la Digital Unit et la Radio Unit. Vu les contraintes de débit, de latence et de gigue sur cette interface, le multiplexage en longueur est la solution adéquate pour son transport. En revanche, les technologies radio recommandées pour la 5G augmenteront considérablement les débits CPRI, ce qui rend l'utilisation du WDM bas coût très difficile. Cette thèse traite quatre sujets principaux :

- L'introduction d'un canal de contrôle dans le CPRI permettrait la supervision de l'infrastructure WDM et l'accordabilité en longueurs d'onde des transceivers. L'impact de l'intégration de ce canal de contrôle dans le fronthaul est étudié dans le chapitre II.
- La radio analogique sur fibre peut améliorer de manière significative l'efficacité spectrale du fronthaul, permettant potentiellement le transport des interfaces 5G. Une étude approfondie sur le gain réel apporté par cette solution est rapportée dans le chapitre III.
- La compression du CPRI basée sur la quantification uniforme et non uniforme est également une solution pour améliorer l'efficacité spectrale du CPRI. Le chapitre IV démontre expérimentalement les taux de compression réalisables.
- Enfin, les nouveaux splits fonctionnels sont considérés comme une solution prometteuse pour la 5G. Deux nouvelles interfaces ont été identifiées pour les splits couche haute et couche basse. Une étude théorique et expérimentale de ces nouvelles interfaces est présentée dans le chapitre V.

Mots-clés : Cloud RAN, 5G, fronthaul, WDM, CPRI, A-ROF, compression, splits fonctionnels

Fronthaul integration and monitoring in 5G networks

Cloud Radio Access Network (RAN) was identified as a key enabler for 5G. Its deployment is however meeting multiple challenges notably in the fronthaul integration, the latter being the segment located between the Digital Unit and the Radio Unit generally based on CPRI. Giving its bit-rate, latency and jitter constrains, Wavelength Division Multiplexing (WDM) is the most adequate solution for its transport. However, the radio technologies recommended for 5G will drastically increase the CPRI bit-rate making its transport very challenging with low-cost WDM. This thesis deals with four main topics:

- The introduction of a control channel in the CPRI enables offering the WDM infrastructure monitoring and the wavelength tunability in the transceivers. The study of this control channel integration in the fronthaul link is reported in the second chapter as well as an investigation on the wireless transmission of CPRI.
- The use of Analog Radio over Fiber (A-RoF) can significantly improve the fronthaul spectral efficiency compared to CPRI-based fronthaul enabling, potentially, the transport of 5G interfaces. A thorough investigation on the actual gain brought by this solution is stated in the third chapter.
- CPRI compression based on uniform and non-uniform quantization is also a solution to enhance the CPRI spectral efficiency. The fourth chapter describes this solution and experimentally shows the achievable compression rates.
- Finally, establishing a new functional split in the radio equipment was considered as a promising solution for 5G. Two new interfaces have been identified for high and low layer functional splits. A theoretical and experimental study of these new interfaces is reported in the fifth chapter.

Keywords : Cloud RAN, 5G, Fronthaul, WDM, CPRI, A-ROF, Compression, functional splits